

ADVANCED COMPUTING TECHNIQUES IN STRUCTURAL
EVALUATION OF FLEXIBLE PAVEMENTS USING THE
FALLING WEIGHT DEFLECTOMETER

by

Fabricio Leiva-Villacorta

A dissertation submitted to the Graduate Faculty of
Auburn University
in partial fulfillment of the
requirements for the Degree of
Doctor of Philosophy

Auburn, Alabama

August 4, 2012

Approved by

David H. Timm, Chair, Brasfield & Gorrie Professor, Civil Engineering

Randy C. West, Director, National Center for Asphalt Technology

Rod E. Turochy, Associate Professor, Civil Engineering

John Fulton, Associate Professor of Biosystems Engineering

ABSTRACT

The use of nondestructive deflection testing has become an integral part of the structural evaluation and rehabilitation process of pavements in recent years. The falling weight deflectometer (FWD) is commonly used to obtain material properties that can be used in mechanistic-empirical pavement design. These properties are currently obtained through an iterative process called backcalculation which has several limitations with one of the most notorious: the non-uniqueness of the results. The use of artificial neural networks (ANN) is currently being studied as a more reliable methodology and an advanced alternative. In addition, the loading frequency of the FWD impact loading can be considered similar to that of vehicle loading at a high speed. Hence, significant error could result between calculated from FWD and measured strain responses from traffic loads at operational speeds.

The objectives of this study were to develop neural networks capable of predicting pavement layer moduli rapidly and reliably; and to determine correction factors for the high frequency/high speed FWD pavement responses to typical operating speed responses. The deflection basin database from the 2009 structural sections at the NCAT Test Track and the FWD test results from a section of the low volume route Lee 159 were used for verification of ANN models. The software 3D-Move was used to determine pavement theoretical response correction factors that were applied to actual values.

The results indicated that the backcalculation process tended to overestimate the moduli of the asphalt concrete layer while the moduli of the subgrade were little or not affected. Besides the significant reduction in computed errors, the use of ANNs showed a clear advantage over conventional backcalculation: a couple of seconds to obtained ANN outputs versus minutes to

hours from backcalculation. The capability for ANNs to predict pavement layer moduli was validated using multiple load levels and full slip condition as a layer interaction. This presented a clear advantage over previous studies that have been focused on one load level and full bond conditions.

The analysis of measured versus predicted pavement responses indicated that significant errors can be obtained from using high speed/high frequency FWD backcalculated moduli to predict highway speed pavement responses. Therefore, correction factors should be applied on pavement responses from backcalculated moduli to represent highway speed loads. For the conditions and scenarios evaluated in this study, correction factors helped close the gap between measured and predicted pavement responses.

ACKNOWLEDGEMENTS

The author would like to thank Dr. David Timm for all of his support in this endeavor. Also the author would like to express his gratitude for all the support he received from the committee members Dr. Randy West, Dr. Rod Turochy and Dr John Fulton. Finally, to his wife Adriana, very special thanks are given for all of her patience and hard work.

The author wishes to thank the following state departments of transportation for their support of this research: Alabama, Florida, North Carolina, South Carolina, Oklahoma and Tennessee. The Federal Highway Administration also deserves recognition for their support and cooperation. Finally, Kraton Performance Polymers, Inc., Lake Asphalt of Trinidad and Tobago (1978) Ltd., and Shell Oil Products U.S.A. deserve special recognition for their support and cooperation.

TABLE OF CONTENTS

ABSTRACT	ii
ACKNOWLEDGEMENTS	iv
LIST OF TABLES.....	ix
LIST OF FIGURES	xi
LIST OF ABBREVIATIONS	xvi
CHAPTER ONE: INTRODUCTION	1
1.1 Background.....	1
1.2 Mechanistic-Empirical (M-E) Pavement Design (Rehabilitation).....	2
1.3 Backcalculation of Pavement Layer Modulus	3
1.4 Analysis of Moving Loads.....	5
1.5 Summary.....	6
1.6 Objectives.....	6
1.7 Scope of Work	7
1.8 Organization of Dissertation.....	7
CHAPTER TWO: LITERATURE REVIEW.....	9
2.1 Nondestructive Testing.....	9
2.2 Backcalculation.....	11
2.3 Layer Moduli Backcalculation Methodologies.....	13
2.3.1 Problems Encountered In Backcalculation	13
2.4.1 Neural Networks Definition.....	22
2.4.2 Benefits of Neural Networks.....	23

2.4.3 Artificial Feedforward Neural Networks	23
2.4.4 Back-Propagation Training Technique	24
2.5 Simulation of Moving Vehicle Loads and Load Pulse Durations.....	26
2.5.1 FWD Load Versus Moving Loads.....	26
2.5.2 Simulation of Moving Loads.....	28
2.5.3 Load Pulse Duration	31
2.6 Summary.....	36
CHAPTER THREE: EXPERIMENTAL DESIGN	38
3.1 Accelerated Testing Facility	38
3.2 ANN Development to Predict Pavement Material Properties.....	38
3.2.1 Analysis of Conventional Backcalculation Process.....	38
3.2.2 Analysis of ANN vs. Conventional Backcalculation.....	40
3.2.3 Analysis of Potential Use of ANN to Predict Layer Thickness.....	41
3.2.4 Verification Using Field Data from NCAT FWD Testing.....	41
3.2.5 Training Tool (MATLAB 7.10.0 – R2010a).....	41
3.3 Correction Factors for the High Frequency/High Speed FWD Pavement Responses to Typical Operating Speed Responses	45
3.3.1 Determination of FWD Loading Pulse from Instrumented Pavements	45
3.3.2 Determination of Equivalent Loading Pulse and Equivalent Loading Speed	45
3.3.3 Determination and Application of Correction Factors.....	46
3.3.4 Mechanistic Modeling Tool	46
3.4 Summary.....	50
CHAPTER FOUR: TEST FACILITY AND SECTIONS PROPERTIES	51
4.1 Test Sections.....	52
4.2 Traffic.....	55
4.3 Performance Monitoring.....	56

4.4 Pavement Instrumentation	57
4.5 Low Volume Road Section.....	60
4.6 Summary.....	61
CHAPTER FIVE: ASSESSMENT OF CONVENTIONAL BACKCALCULATION AND	
ARTIFICIAL NEURAL NETWORKS	
5.1 Effect of Tolerance Error on Backcalculated Moduli.....	62
5.2 ANN vs. conventional backcalculation process.....	66
5.3 Removing the Input Variable “Thickness”	70
5.4 Potential Use of ANNs to Predict Layer Thickness	73
5.5 Errors in Pavement Layer Moduli Backcalculation Due to Improper Modeling of the Layer Interface Condition	77
5.6 Summary.....	80
CHAPTER SIX: APPLICATION OF ANN ON ACTUAL FWD TESTING RESULTS.....	
6.1 Deflections and Backcalculated Material Properties.....	82
6.2 Indications of Weakening Bond between the AC Layer and the Granular Base Layer.....	90
6.3 Development of ANN for Selected Sections at the 2009 Test Track.....	92
6.4 General Application of ANNs.....	100
6.5 Application of ANNs on Low a Volume Roadway.....	104
6.6 Additional ANN Models	109
6.7 Summary.....	111
CHAPTER SEVEN: DETERMINATION OF EQUIVALENT LOADING PULSE AND	
STRAIN CORRECTION FACTORS.....	
7.1 Viscoelastic Properties of Asphalt Concrete (AC) Layers.....	112
7.2 FWD Loading Pulse from Instrumented Pavements.....	116
7.3 Determination of Equivalent Loading Pulse and Equivalent Loading Speed.....	119
7.4 Simulated Temperature and Speed Effects.....	121

7.5 Determination of Correction Factors.....	125
7.6 Measured Pavement Responses	130
7.7 Predicted Versus Measured Critical Responses.....	134
7.8 Application of Correction Factors.....	144
7.9 Summary.....	148
CHAPTER EIGHT: CONCLUSIONS AND RECOMMENDATIONS	150
8.1 Summary of Findings	150
8.1.1 Application of ANNs.....	150
8.1.2 Correction Factors for the High Frequency/High Speed FWD Pavement Responses to Typical Operating Speed Responses	152
8.2 Conclusions.....	153
8.3 Recommendations	155
REFERENCES.....	156

LIST OF TABLES

TABLE 4.1 Asphalt Concrete Layer Properties – As Built.....	54
TABLE 4.2 Axle Weights (lbs) for Trucking Fleet at NCAT Test Track.....	55
TABLE 5.1 Effect of tolerance error on estimated moduli	66
TABLE 5.2 Effect of number of neurons on training	69
TABLE 5.3 Comparison of backcalculated and ANN predicted parameters	70
TABLE 5.4 Paired T-test results on moduli relative error	79
TABLE 6.1 Deflections equations coefficients	84
TABLE 6.2 AC modulus equation coefficients.....	87
TABLE 6.3 Tukey-Kramer analysis of granular base modulus	88
TABLE 6.4 Tukey-Kramer analysis of subgrade modulus	89
TABLE 6.5 Artificial database variables	92
TABLE 6.6 Comparison of backcalculated and ANN Parameters for Synthetic Database	95
TABLE 6.7 Range of predicted layer moduli for all sections	96
TABLE 6.8 Analysis of RMS errors for all sections	98
TABLE 6.9 Overall changes in moduli for all sections	100
TABLE 6.10 Artificial database variables	101
TABLE 6.11 Relationship between backcalculated and ANN predicted moduli.....	104
TABLE 7.1 Pulse durations on different gauges, Section S9.....	118
TABLE 7.2 Pulse durations on different gauges, remaining sections.....	118
TABLE 7.3 Determination of moving load speed at equivalent loading pulse	121

TABLE 7.4 Equation coefficients for strain correction factors.....	127
TABLE 7.5 Equation coefficients for stress (base) correction factors.....	128
TABLE 7.6 Equation coefficients for stress (subgrade) correction factors.....	129
TABLE 7.7 Strain equation coefficients.....	131
TABLE 7.8 Base stress equation coefficients	132
TABLE 7.9 Subgrade stress equation coefficients	133
TABLE 7.10 Equation coefficients for calculated microstrain	136
TABLE 7.11 Equation coefficients for calculated stress (Base)	139
TABLE 7.12 Equation coefficients for calculated stress (Subgrade)	142
TABLE 7.13 Application of strain correction factors.....	145
TABLE 7.14 Application of base stress correction factors	147
TABLE 7.15 Application of subgrade stress correction factors	147

LIST OF FIGURES

FIGURE 1.1 M-E Design Schematic.	3
FIGURE 2.1 Diagram of the Falling Weight Deflectometer (10).....	10
FIGURE 2.2 Typical location of loading plate and deflection sensors for impulse deflection equipment (13).....	10
FIGURE 2.3 Typical force output from falling weight deflectometers (time from A to B is variable, depending on drop height): A = time at which weights are released; B = time at which weight package makes first contact; C = peak load reached (13).	11
FIGURE 2.4 Flow chart of the backcalculation of layer moduli (14).....	12
FIGURE 2.5 Air gap influence on a four-layer asphalt concrete system (18).....	15
FIGURE 2.6 Approached followed by Meier and Rix (1).....	16
FIGURE 2.7 Frequency distributions of relative error for four neural networks (2).	18
FIGURE 2.8 Performances of ANN backcalculation models for predicting layer moduli of conventional flexible pavements (3).	18
FIGURE 2.9 Performances of ANN backcalculation models for predicting layer moduli of granular bases for conventional flexible pavements (19).	20
FIGURE 2.10 Estimation of pavement layer properties using SOFTSYS (19).....	20
FIGURE 2.11 ANN AC moduli predictions compared with BAKFAA predictions (20).	21
FIGURE 2.12 Schematic of Neural Networks.....	22
FIGURE 2.13 Schematic of a feedforward neural network (6).	24
FIGURE 2.14 Flow chart of backpropagation training process (21).....	25
FIGURE 2.15 Comparison of measured and predicted strain under moving loads (22).....	26
FIGURE 2.16 Average duration of the impulses under different loading conditions (24).....	27

FIGURE 2.17 Comparison of strain responses under FWD loading and truck loading at the same level of loads (24).....	28
FIGURE 2.18 Validation of the software 3D-Move (26-27).....	29
FIGURE 2.19 Viscoelastic versus FEA analysis (28).....	30
FIGURE 2.20 Comparison between measured and calculated vertical stress at a speed of 45 mph (29).....	31
FIGURE 2.21. Moving load as a function of time (11).....	33
FIGURE 2.22 Measured compressive stress pulse (36).....	35
FIGURE 2.23 Measured load duration versus theoretical (38).....	36
FIGURE 3.1 Training of ANNs flow chart.	40
FIGURE 3.2 Matlab default desktop.....	42
FIGURE 3.3 Example of the training tool.....	43
FIGURE 3.4 Example of performance regression plots.	44
FIGURE 3.5 Main Window of <i>3D-Move</i> Analysis.	47
FIGURE 3.6 Pavement Layer Properties Window for Asphalt Materials.....	48
FIGURE 3.7 Layer Properties Window for Unbound Materials.....	49
FIGURE 3.8 Response Points Window.....	49
FIGURE 4.1 The NCAT Test Track.	51
FIGURE 4.2 Layout of test track (40).....	52
FIGURE 4.3 Structural sections at the 2009 NCAT Test Track.....	53
FIGURE 4.4 Example of the triple flat-bed trailer truck.....	55
FIGURE 4.5 Falling weight deflectometer testing at the Test Track.....	56
FIGURE 4.6 Schematic of test locations.....	57
FIGURE 4.7 Typical strain gauge array.....	58
FIGURE 4.8 Strain amplitude definition.....	59

FIGURE 4.9 Example of compressive stress signal.....	59
FIGURE 4.10 Condition of the low volume road section.	60
FIGURE 5.1 Schematic of pavement structure.....	63
FIGURE 5.2 Estimated moduli at a 0.1% tolerance level.	64
FIGURE 5.3 Estimated moduli at two different tolerance levels.....	65
FIGURE 5.4 Training performance plot.....	68
FIGURE 5.5 Predicted responses from ANN with and without thickness.	71
FIGURE 5.6 Predicted layer moduli from ANN with and without thickness.....	72
FIGURE 5.7 ANN Predicted thicknesses.	73
FIGURE 5.8 Effect of H1 on deflection.....	74
FIGURE 5.9 Effect of H2 on deflection.....	75
FIGURE 5.10 Effect of H2 on deflection-continued.....	75
FIGURE 5.11 Effect of number of deflections (sensors) on training performance.....	76
FIGURE 5.12 Modeled interface conditions.	77
FIGURE 5.13 Cumulative distributions of RMSE values.....	78
FIGURE 5.14 Cumulative distributions of moduli relative errors.	79
FIGURE 6.1 Deflection-temperature relationships.....	83
FIGURE 6.2 Backcalculated AC moduli.....	85
FIGURE 6.3 AC modulus versus temperature.....	86
FIGURE 6.4 Backcalculated moduli of the granular base for all sections.	88
FIGURE 6.5 Backcalculated moduli of the subgrade for all sections.....	89
FIGURE 6.6 Pre-traffic layer moduli versus post-traffic layer moduli.....	91
FIGURE 6.7 Schematic of ANN model and training process.....	94
FIGURE 6.8 Cumulative distribution plot for estimated moduli.....	97

FIGURE 6.9 Backcalculated vs. ANN Predicted E1 of the Control Section (S9).	99
FIGURE 6.10 Cumulative distribution of RMSE for estimated moduli.	102
FIGURE 6.11 Backcalculated vs. ANN predicted moduli.	103
FIGURE 6.12 ANN vs. backcalculated properties (BWP).	106
FIGURE 6.13 Comparison of predicted layer moduli from different models.	107
FIGURE 6.14 Comparison of layer moduli at different locations.	109
FIGURE 6.15 Predicted strain from ANN model with thickness as input versus predicted strain from ANN model without thickness as input.	110
FIGURE 6.16 ANN-predicted versus actual AC thickness.	111
FIGURE 7.1 Dynamic modulus relative differences from the control section at 10 and 33 Hz.	114
FIGURE 7.2 Relative differences between dynamic moduli at 10 and 33 Hz.	115
FIGURE 7.3 Backcalculated AC modulus versus $E_{\text{effective}}$	116
FIGURE 7.4 Measured versus simulated FWD loading pulse.	117
FIGURE 7.5 Pulse duration under different loading speeds.	119
FIGURE 7.6 Influence of vehicle speed on pulse duration – Control Section S9.	120
FIGURE 7.7 Influence of vehicle speed on simulated longitudinal microstrain – Control Section S9.	122
FIGURE 7.8 Influence of vehicle speed on simulated compressive stress – Control Section S9.	123
FIGURE 7.9 Simulated longitudinal microstrain – All sections versus S9.	124
FIGURE 7.10 Simulated compressive stress – All sections versus S9.	125
FIGURE 7.11 Relationship between strain correction factors and temperature.	126
FIGURE 7.12 Relationship between stress (base) correction factors and temperature.	128
FIGURE 7.13 Relationship between stress (subgrade) correction factors and temperature.	129
FIGURE 7.14 Measured longitudinal microstrain section S9.	130
FIGURE 7.15 Measured compressive stress on top of granular base.	132

FIGURE 7.16 Measured compressive stress on top of subgrade.....	133
FIGURE 7.17 Modeled layer interface conditions.....	134
FIGURE 7.18 Calculated microstrain versus temperature - S9.....	135
FIGURE 7.19 Comparison between measured and calculated microstrain.....	137
FIGURE 7.20 Measured versus predicted longitudinal microstrain.....	138
FIGURE 7.21 Calculated compressive stress section S9 (Base).....	139
FIGURE 7.22 Comparison between measured and calculated stress (Base).....	140
FIGURE 7.23 Measured versus predicted compressive stress (Base).....	141
FIGURE 7.24 Calculated compressive stress section S9 (Subgrade).....	142
FIGURE 7.25 Comparison between measured and calculated stress (Base).....	143
FIGURE 7.26 Measured versus predicted compressive stress (Subgrade).....	144
FIGURE 7.27 Example of the application of strain correction factors.....	145
FIGURE 7.28 Example of the application of stress correction factors.....	146

LIST OF ABBREVIATIONS

AASHTO: American Association of State Highway and Transportation Officials

AC: Asphalt Concrete

ANN: Artificial Neural Networks

APT: Accelerated Pavement Testing

ARAN: Automatic Road Analyzer

CDP: Cumulative Distribution Plot

ESAL: Equivalent Single Axle Load

FHWA: Federal Highway Administration

FWD: Falling Weight Deflectometer

IRI: International Roughness Index

LTPP: Long Term Pavement Performance

MEPDG: Mechanistic-Empirical Pavement Design Guide

MSE: Mean Square Error

MTD: Mean Texture Depth

NCAT: National Center for Asphalt Technology

NCHRP: National Cooperative Highway Research Program

NMAS: Nominal Maximum Aggregate Size

RAP: Reclaimed Asphalt Pavement

RMSE: Root-Mean-Square Error

SBS: Styrene Butadiene Styrene

WMA: Warm Mix Asphalt

CHAPTER ONE: INTRODUCTION

1.1 Background

The management and maintenance of pavements can be a complicated decision making process. In order to make decisions quickly and more efficiently, new tools and techniques are continually being introduced. Techniques such as expert systems and artificial neural networks (ANN) have been used in pavement management systems to perform structural evaluation of pavements (1-3).

The use of nondestructive deflection testing has become an integral part of the structural evaluation and rehabilitation process of pavements in recent years. The falling weight deflectometer (FWD) is commonly used by state highway agencies to apply patterns of loading and record deflection data along the pavement. Current deflection analysis procedures utilize deflections, thicknesses and load levels as the input variables to solve for layer properties. This is an iterative process that compares calculated deflections with the measured deflections. The problem with this process is the non-uniqueness of the results. A good match between the deflections does not guarantee that the backcalculated moduli are reasonable for a given cross-section. Thus, the exploration for a more accurate and reliable methodology to estimate pavement materials properties and pavement responses is still an important task of any pavement management system.

The new Mechanistic–Empirical Pavement Design Guide (MEPDG) developed by NCHRP under AASHTO sponsorship requires that structural analysis be performed more than 1,000 times for a single design simulation of a pavement structure (4). For rigid pavement design, the MEPDG already takes advantage of neural networks to reduce processing time. For flexible pavement design the process can become extremely time consuming due to its reliance on mechanistic computations throughout the analysis. This processing time can be reduced, even more, by the incorporation of artificial neural networks. Furthermore, the results obtained from FWD tests are widely used for pavement condition analysis and selection of maintenance strategies that can be also incorporated within the MEPDG. The integration of ANNs capable of

predicting pavement critical responses not only can help identify pavement distresses but also could complement existing pavement management systems.

Even though the use of more advanced techniques can provide pavement properties more accurately, caution is needed when using predicted layer moduli from either backcalculation or ANN in mechanistic analysis. The loading frequency of FWD loading is similar to that of vehicle loading at a very high speed (loading pulse from FWD is estimated to be between 0.025 to 0.035 seconds). Hence, significant error could result between calculated and measured strain responses under slower speeds when using predicted moduli in a mechanistic model. In addition, the viscoelastic nature of asphalt concrete (AC) renders its properties to be frequency-dependent. Static backcalculation of layer moduli from FWD testing does not take into account this frequency-dependence. Therefore, the exploration for a methodology to incorporate frequency-dependent material properties to estimate pavement responses similar to those applied by moving vehicles becomes another important task of any pavement management system.

1.2 Mechanistic-Empirical (M-E) Pavement Design (Rehabilitation)

Mechanistic-empirical (M-E) pavement design, for new pavements and for rehabilitation, is used to determine the appropriate materials and layer thicknesses to provide the structural capacity for the required performance period. Mechanical properties of the pavement structure along with information on traffic, climate, and observed performance are used to more accurately model the pavement structure and predict its remaining life. Most mechanistic-empirical methods for determining the remaining life of an existing pavement rely on the use of deflection-based non-destructive evaluation (NDE) devices. Figure 1.1 is a schematic of the M-E process. This process integrates the NDE results, and material properties of all the existing layers and environmental conditions into the pavement structure. The structure is then modeled using a mechanical analysis program, and the pavement response is calculated given the axle load and tire configuration. The pavement response is then used to estimate the remaining life from empirically-derived transfer

functions. Finally, if the rehabilitation technique requires the design of an overlay, an iterative process is carried out until the remaining life of the new structure matches the new design life.

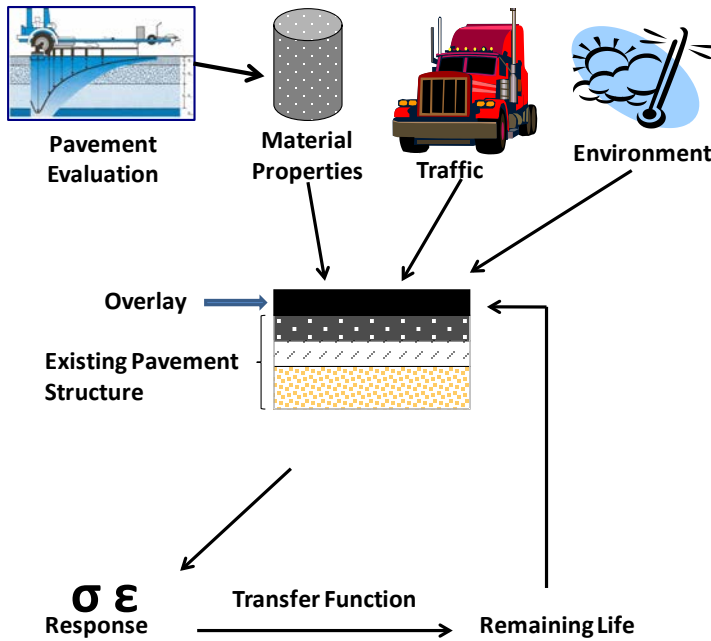


FIGURE 1.1 M-E Design Schematic.

1.3 Backcalculation of Pavement Layer Modulus

One of the most common field tests used to evaluate the structural condition of a pavement is done with an FWD. This apparatus drops a circular load on the pavement structure that is representative of a heavy vehicle tire load. With the use of deflection sensors, the resulting deflection basin of the pavement surface can be measured. Backcalculation is an inverse process that utilizes deflections, thicknesses and load levels as the input variables to solve for layer moduli. The computational procedure to solve this problem includes both a pavement response model and an optimization algorithm. Basically, it is an iterative process that compares calculated deflections with the measured deflections. If the difference between the calculated and measured deflections is acceptable, then the assumed layer moduli are treated as the actual moduli. The problem with the backcalculation process is the non-uniqueness of the results. A good match between the deflections does not guarantee that the backcalculated moduli are reasonable for a

given cross-section. However, some investigators have compared measured strains to backcalculated (theoretical) strains based on layered elastic analyses with satisfactory results (5).

Artificial neural networks (ANN) are part of the new tools also used to backcalculate pavement layer moduli and critical pavement responses from the results of FWD tests. These neural networks provide the same solutions as existing programs, only thousands of times faster (1-3). A methodology based on ANNs to compute the remaining life of flexible pavements and compare results with field data has been found to be another useful application of ANNs (3). One of the most important benefits of this approach was that the backcalculation process for determining layer moduli was not necessary.

An artificial neural network can be defined as a massively parallel distributed processor that has a natural propensity for storing experimental knowledge and making it available for use (5). Consequently, knowledge is acquired by the network through a learning (training) process; the strength of the interconnections between neurons is implemented by means of the synaptic weights used to store the knowledge. The learning process is a procedure of adapting the weights with a learning algorithm in order to most accurately capture the knowledge. In other words, the aim of the learning process is to map a given relation between inputs and outputs of the network.

One of the most common networks selected by pavement researchers uses a back-propagation algorithm to train the network (1-3). This learning algorithm is applied to multilayer feed-forward networks consisting of processing elements with continuous and differentiable activation functions. Such networks associated with the back-propagation learning algorithm are also called back-propagation networks (6). With this network, error is calculated from outputs and used to update output weights. Additionally, the error at hidden nodes is calculated and updated by back propagating the error at the outputs through the new weights. The process continues until the minimum mean square error (MSE) calculated between outputs and targets is obtained. Further explanation of neural networks can be found in chapter 2 of this document.

Pavement layer thicknesses are important elements to calculate layer properties. Accurate information of layer thicknesses is not always available due to numerous reasons: records of very old structures are missing, overlays and maintenance records not up to date, etc. Generation of this information involves additional testing at an extra cost. This testing can be performed either by using nondestructive techniques such as the ground-penetrating radar or destructive techniques such as coring. Consequently, research is needed to identify and evaluate methods for estimating pavement layer thicknesses and/or pavement responses based on deflection measurements resulting in no additional cost to the agencies.

1.4 Analysis of Moving Loads

Dynamic response of asphalt concrete (AC) pavements under moving load is a key component for accurate prediction of flexible pavement performance. The time and temperature-dependency of AC materials calls for utilizing advanced material characterization and mechanistic theories, such as viscoelasticity and stress/strain analysis. State-of-the-art load modeling is required for pavement structures subject to dynamic loads. One example is the application of finite element methodology or FEM. In finite element modeling, viscoelastic behavior of AC materials can be characterized through relaxation moduli and dynamic loads can be modeled in terms of duration of the load and velocity. Another example is the implementation of the layered elastic theory in the Mechanistic-Empirical Pavement Design Guide (MEPDG). In this guide, the time dependency is accounted for by calculating the loading times at different AC layer depths. Loading times or frequencies are matched to material frequencies to compute the response. However, this procedure has been significantly criticized and its applicability to model dynamic responses is still questionable (4).

More recently, the application of finite layer methodology has gained popularity and one example of this can be found in the newly developed software *3D-Move*. The analytical software *3D-Move* was created by the Asphalt Research Consortium and it is currently on its version 1.2

(7). This tool accounts for moving traffic loads with complex contact stress distributions of any shape, vehicle speed, and viscoelastic properties of asphalt concrete layers to calculate pavement responses using a continuum-based finite-layer approach. The finite-layer approach treats each pavement layer as a continuum and uses the Fourier transform technique (8). Since pavements are horizontally layered and pavement responses are required only at a few selected locations *3D-Move* takes advantage of the finite layer approach (8). Asphalt concrete layers can be modeled using dynamic complex modulus master curves allowing the computation of pavement response as a function of vehicle speed and temperature.

1.5 Summary

Assessment of pavement layer properties, pavement responses and prediction of layer thicknesses using ANN's has been performed previously. However, these evaluations were limited to the use of one load level and the assumption of full bond interaction between layers. Therefore, the development of ANNs that can predict pavement layer moduli rapidly and reliably for multiple load levels and for layer interface other than fully bonded was necessary. The literature also suggested that the frequency of FWD loading can be similar to that of vehicle loading at a very high speed. Therefore, it was necessary to find the speed to which the FWD can be compared with and to evaluate the potential error that could result from the use of backcalculated high frequency pavement responses compared to operational speed/frequency responses.

1.6 Objectives

The main objectives of this research study were to:

- Develop neural networks capable of predicting pavement layer moduli rapidly and reliably.
- Determine correction factors for converting the high frequency/high speed FWD pavement responses to typical operating speed responses.

Secondary objectives of this study were to evaluate the effect of tolerance levels in the conventional backcalculation process, to assess the potential use of ANN's to predict layer

thickness, to examine the use of ANNs to predict layer moduli under full slip layer interaction and to analyze differences between measured and predicted pavement responses.

1.7 Scope of Work

To accomplish the above objectives, several Artificial Neural Networks were created to perform forward calculations of pavement layer moduli and critical responses from non-destructive testing information. Synthetic databases were created using a modified version of the software PerRoad (developed uniquely for this study) for a three layer flexible pavement. These databases consisted of layer moduli, deflection basins, critical pavement responses and layer thicknesses. The software MATLAB 7.1 was utilized to train and develop ANN's. These networks were created, first, with deflection basins and thicknesses to estimate layer moduli and responses. In later cases, deflections were set as the only inputs used to calculate the remaining variables. The deflection basin database from the 2009 structural sections at the NCAT Test Track was used for verification purposes where ANN estimated results were compared against backcalculated results. Backcalculated results were obtained using the software EVERCALC. Finally, the software *3D-Move* was used to first determine the loading pulse produced by a moving load equivalent to the loading pulse produce by the FWD and second to determine correction factors to be applied on pavement responses using backcalculated modulus.

1.8 Organization of Dissertation

This dissertation contains a literature review of the current backcalculation technique used for characterization of material properties and the use of Artificial Neural Networks (ANNs) for similar purposes (chapter 2). The effects of time- and temperature-dependency properties of asphalt concrete mixtures on pavement responses within a non-destructive testing perspective were also reviewed. Following the literature review is a basic overview of the pavement structures (test sections) used to conduct this research (chapter 3). Chapter 4 describes the methodologies to develop ANNs and the analysis of FWD loading versus traffic loading. The

body of this investigation included two main studies related to advance material characterization techniques. The first one was focused on the application of ANNs as an alternative procedure to conventional backcalculation (chapters 5 and 6). Chapter 5 discusses the results of ANN analyses performed with synthetic databases its comparison with backcalculated results while chapter 6 has to do with the verification of ANNs using actual data. The second study, also related to non-destructive testing, was focused on the correction of predicted responses from high frequency/speed FWD loading to represent typical operational vehicle speeds. The conclusions and recommendations for future work are discussed in the last chapter.

CHAPTER TWO: LITERATURE REVIEW

In the mechanistic-empirical framework, accurate material characterization from non-destructive testing is imperative in successfully predicting pavement responses and pavement performance. On this topic, a literature review of the conventional backcalculation process and the application of artificial neural networks used to predict pavement layer moduli was performed. The effects of time and temperature dependency properties of asphalt concrete mixtures on pavement responses and load pulse durations were also investigated. The literature review on this topic included not only theoretical analyses but also findings from actual results.

2.1 Nondestructive Testing

Nondestructive testing (NDT) of pavements involves applying a known load to the pavement structure and measuring the resulting surface deflection basin. With respect to flexible pavements, NDT deflection measurements can be used to determine the following:

- Modulus of each of the structural layers.
- Pavement structural adequacy,
- Overlay thickness design,
- Remaining structural life.

In NDT, the pavement structure is evaluated without any material disturbance or modification and the tests are relatively quick and inexpensive. This allows a large number of tests to be completed with limited disruption to traffic (9). Figure 2.1 illustrates the Falling Weight Deflectometer (FWD). The FWD contains up to nine high speed velocity transducers that measure pavement deflections. These transducers are lowered hydraulically to the pavement surface where the deflection data are to be obtained. Locations of the sensors can be adjusted depending upon the purpose of the study (Figure 2.2).

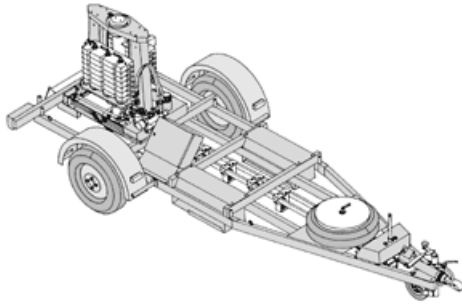


FIGURE 2.1 Diagram of the Falling Weight Deflectometer (10).

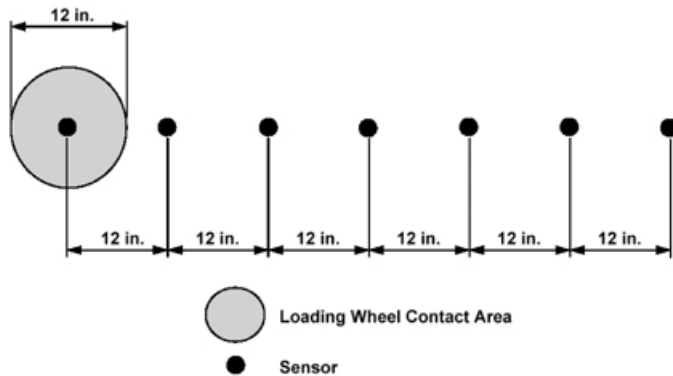


FIGURE 2.2 Typical location of loading plate and deflection sensors for impulse deflection equipment (13).

The FWD utilizes a transient impulse loading which simulates the impact of a moving wheel load. The loads produced are normally between 2,000 lb and 25,000 lb depending on the traffic type and weight to be simulated (11). The load pulse duration is between 25 and 30 milliseconds (Figure 2.3). The force is typically applied to the pavement structure through a 5.91 in. radius steel plate underlain by a rubber pad. A transducer within the loading plate measures the actual time history of the load applied to the pavement. The FWD impulse load duration is considered to approximate the same load duration of a vehicle traveling at 40 to 50 mph (12).

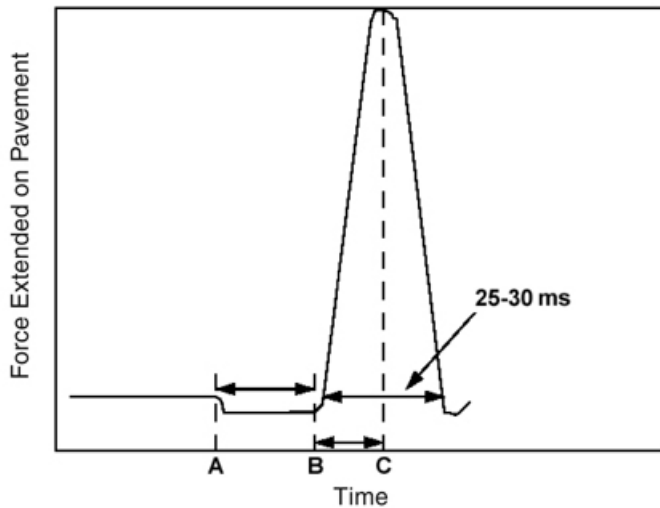


FIGURE 2.3 Typical force output from falling weight deflectometers (time from A to B is variable, depending on drop height): A = time at which weights are released; B = time at which weight package makes first contact; C = peak load reached (13).

2.2 Backcalculation

Backcalculation is the process of computing pavement layer moduli and the subgrade resilient modulus based on pavement deflection basins generated by FWD (14). To conduct a backcalculation, the initial moduli of pavement layers should be first assumed, the values are usually estimated base on an engineer's experience or equations. After assuming the initial layer moduli, pavement surface deflections can be calculated using pavement response models. The calculated deflections are then compared to the measured values. By adjusting the pavement layer moduli, a good match (within some tolerable error) between the measured and theoretical deflections can be reached. The process of backcalculation is iterative. Many programs were developed for backcalculation such as Modulus 6.0, Elmod 6.0, and EVERCALC 5.0. Figure 2.4 presents a basic flowchart of backcalculation procedure utilized in EVERCALC 5.0.

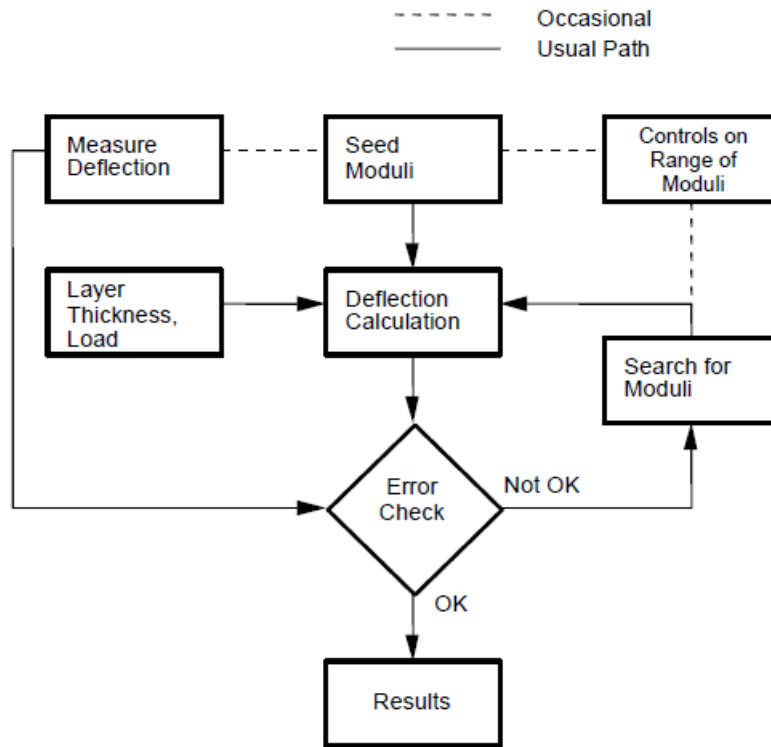


FIGURE 2.4 Flow chart of the backcalculation of layer moduli (14).

The main components in a backcalculation process include:

- *Layer thicknesses and loads*: Thickness of each pavement layer and load levels applied on the pavement surface.
- *Measured deflections*: Surface deflections measured during FWD tests.
- *Seed moduli*: Initial moduli used to compute theoretical surface deflections.
- *Deflection calculation*: Use pavement response models to calculate theoretical surface deflections.
- *Error check*: Compare the calculated and measured deflections.
- *Search for new moduli*: Iteratively search for the new moduli of pavement layers until the calculated and measured deflection are matched (within acceptable error).

- *Controls on the range of moduli:* The backcalculation programs usually can define a range of modulus for each pavement layer to prevent unreasonable pavement layer moduli.

2.3 Layer Moduli Backcalculation Methodologies

Different methodologies exist to obtain pavement layer moduli. In general, methodologies of backcalculation involve an application of elastic theory and the application of finite element methodology.

- Traditional elastic programs. These are based on numerical integration (i.e. *ELSYM5*, *CHEVRON*, *BISAR*, *WESDEF*, *EVERCALC*). The analytical models and the material parameters used are the elastic parameters (Young's modulus and Poisson's ratio).
- Finite element (FE) programs. These programs use a Finite Element Method that consists of dividing a structure into multiple elements, describing the behavior of each element in a simple way, and reconnecting elements at "nodes". In stress analysis, the equations on the program are equilibrium equations of the "nodes". Some backcalculation programs that use FE are *ILLIPAVE* and *MICHPAVE*.
- General structural analysis. Some general structural programs such as *ANSYS*, *ABACUS* and *ADINA* apply Finite Element Methods.

2.3.1 Problems Encountered In Backcalculation

Traditional elastic programs use an iterative backcalculation process. The iterative process stops when measured and predicted deflections match within tolerance levels or when the maximum number of iterations set by the user is reached. Ullidtz (16) described some limitations about this procedure:

1. It requires the user to enter starting values and ranges for the moduli. Then, unless appropriate starting values are selected, the program will never converge to a solution within the selected ranges.

2. The solution depends on the initial “seed modulus” values selected. Thus, the values of boundaries must be selected judiciously.
 - 2.1 If the limits were too narrow, they would prevent the program from converging to the correct solution.
 - 2.2 If the limits were too broad, they would allow the program to converge to an incorrect solution.
3. As the layers of a pavement structure increase, the time consumed by the software during backcalculation will increase.
4. Reliability of the results decreases as the layers of a pavement increase due to the limited degrees of freedom.

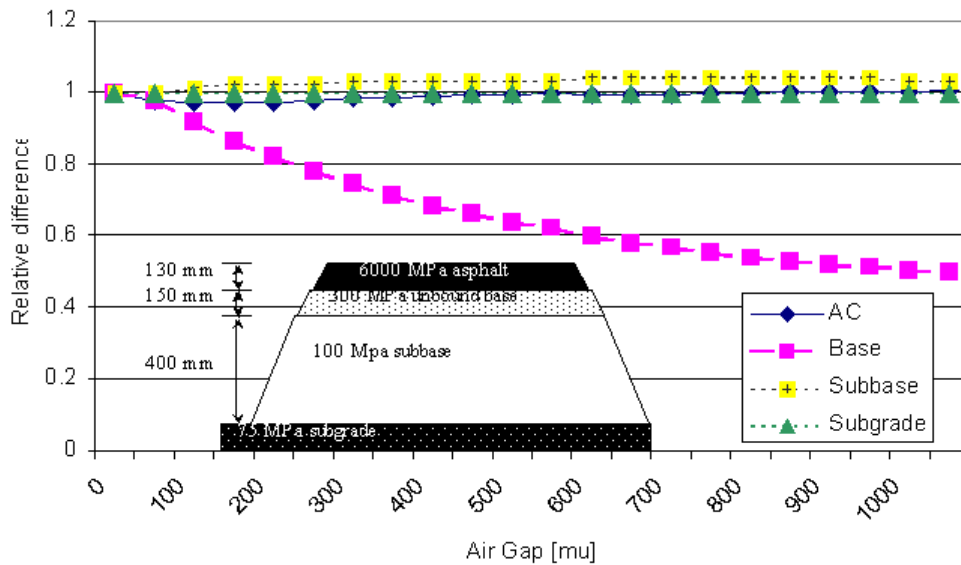
Differences between the theoretical deflections and the FWD measured deflections are due to some problems encountered in the real pavement structure such as the following:

- Pavement distress.
- Variations in layer thickness.
- Nonlinear material response.
- Presence of bedrock or other stiff layer.
- The effects of moisture and temperature (the weather, the presence of cloud cover, water table depth, effect of trees, and the effects of vegetation near the paved surface) (15).

In 2002 Romanoschi and Metcalf (16) evaluated the potential error in pavement layer moduli backcalculation due to improper modeling of the layer interface condition. The finite element program ABAQUS was used to simulate different interface conditions and then obtain deflections for typical flexible and semirigid road structures. The layer moduli were backcalculated from the deflection data using the MODULUS backcalculation software, and the values obtained were compared to the initial moduli values. It was found that the condition of the wearing-binder layer interface leads to an error in backcalculated moduli for the granular base layers, for both flexible and the semirigid structures. The asphalt surface layer moduli were

overestimated, up to 120 percent of the initial values, while the modulus of the stabilized base was underestimated (up to six times smaller than the original values). The backcalculated subgrade modulus was the least influenced by the simulated layer interface condition.

Lenngren and Olsson (17) studied the effect of performing conventional backcalculation on a four-layer system with full slip (air gap) condition between layers. Their results indicated that the backcalculated modulus of the unbound base was most affected by adding friction between layers (Figure 2.5). The effect on the unbound base is considerable and may explain a lot of underestimated modulus on base courses. The modulus of the base course was found to be about 50% lower than the actual modulus when the full bond condition was used in the backcalculation process. The asphalt layer modulus was little or not affected; however, the horizontal strain at the bottom of the layer was somewhat underestimated. The subgrade and subbase moduli were only marginally affected.



Air Gap = 0 means full slip, Air Gap > 1000 means full bond.

FIGURE 2.5 Air gap influence on a four-layer asphalt concrete system (18).

2.4 Advanced Approaches to Backcalculation

Artificial neural networks (ANN) are part of the new tools also used to predict pavement layer moduli and critical pavement responses from the results of FWD tests. Meier and Rix (1) were first to introduce neural network methodology for pavement backcalculations. This is an advanced approach that achieves a real-time backcalculation with higher precision. Figure 2.6 is the flow chart of the approach followed by Meier and Rix in 1994. In their study, a mechanistic pavement analysis model was used to calculate a synthetic deflection basin for a presumed set of pavement layer properties. The artificial neural network was then trained to perform the inverse operation of mapping the synthetic deflection basin (input layer) back onto the presumed set of properties (output layer). Training of the network was an iterative process. At the beginning, the neural network generated higher differences (errors) between actual or measured values and computed values. The inverse function was reached (training process stops) when a minimum error was achieved.

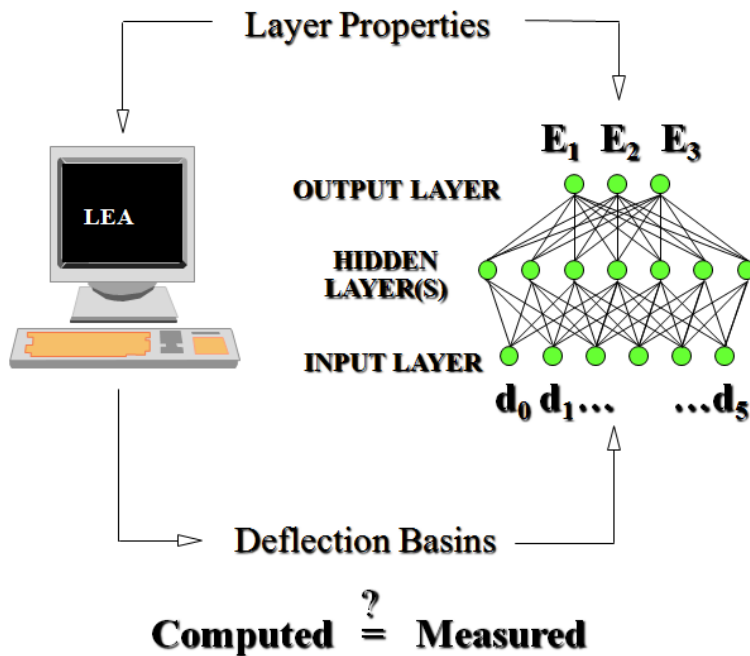


FIGURE 2.6 Approach followed by Meier and Rix (1).

Trained ANN models need to be tested based on an independent dataset within the ranges that they were trained. A sufficiently wide dataset obtained from the pavement analysis can be chosen independently considering the given ranges of material and geometry properties and used as the testing dataset for the verification of proper ANN learning (6). The remaining data are then used for the training and learning procedure. Although training takes a long computation time, testing is often much faster (on the order of micro seconds). Meier et al. (1-2) developed an ANN as a complement of the layered elastic analysis software WESDEF. With the addition of the neural networks, WESDEF was able to backcalculate pavement layer moduli 42 times faster, on average, than it did through conventional methods.

An optimal ANN, trained to achieve the minimum possible error, should also produce outputs with low errors when applied on an independent dataset. Figure 2.7 shows the cumulative frequency distributions of the relative output errors (i.e., output error divided by target output) for a 10,000 deflection basin database for four different pavement scenarios studied by Meier et al. (2). In every case, 99 percent of the calculated deflections were in error by 5 percent or less. Ferregut et al. (3) developed a methodology based on ANNs to compute the remaining life of flexible pavements and compare results with field data from the Texas Mobile Load Simulator. In this study the inputs of the network were layer thickness and deflection basins. The outputs were the best estimate of the remaining life (or critical responses needed to calculate it) and the pavement performance curve. One of the most important benefits of their approach was that the backcalculation process for determining layer moduli was not necessary. Figure 2.8 is a plot of the predicted (ANN output) versus desired (synthetic) remaining life in millions of equivalent single axle loads (ESALS). This plot shows that the error between predicted and desired values was not constant and in fact, the error increased as the number of ESALS increased. The authors considered an interval of $\pm 20\%$ error acceptable for predicting the remaining life of flexible pavements.

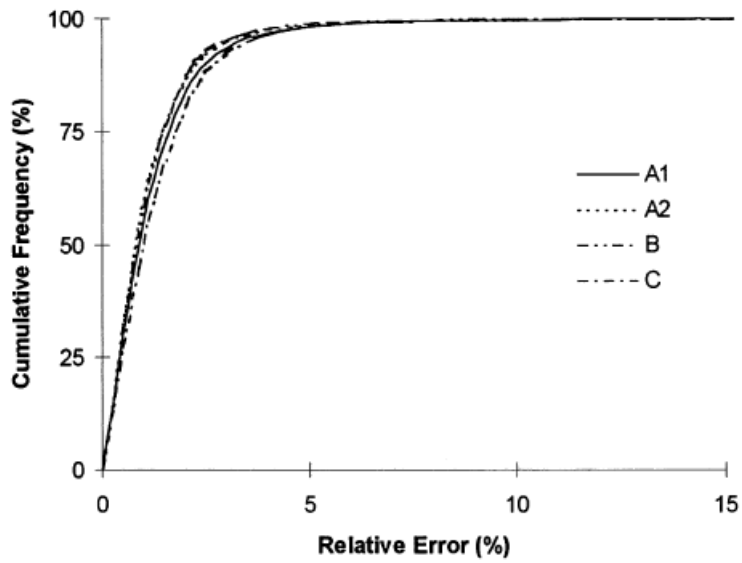


FIGURE 2.7 Frequency distributions of relative error for four neural networks (2).

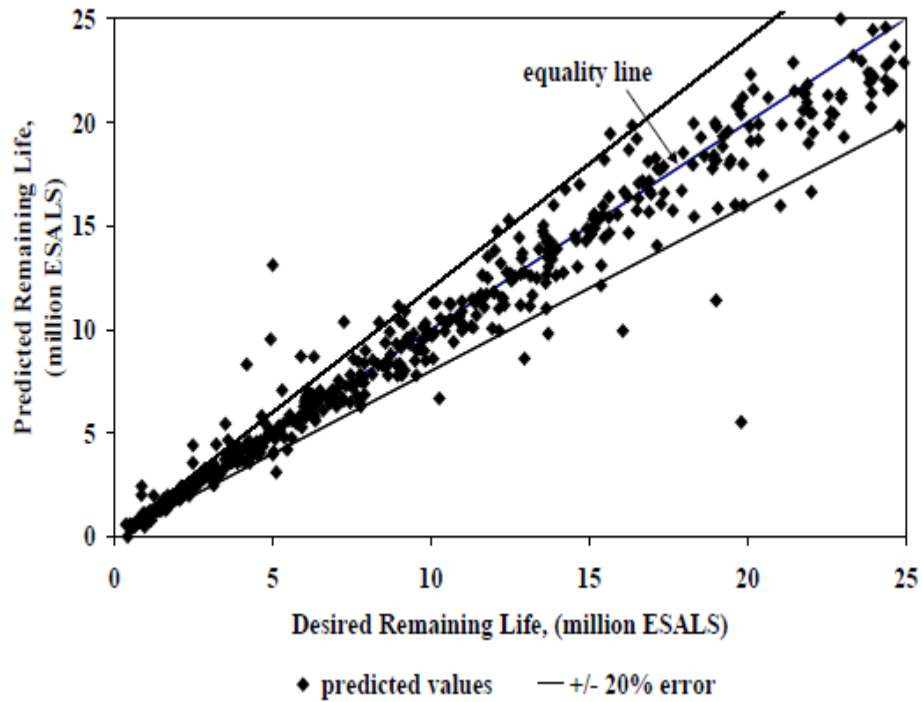


FIGURE 2.8 Performances of ANN backcalculation models for predicting layer moduli of conventional flexible pavements (3).

Ceylan et al. (18) focused on the development of ANN-based forward and backcalculation type flexible pavement analysis models to predict critical pavement responses and layer moduli. The ILLI-PAVE finite element program, which considers the nonlinear stress-dependent geomaterial characterization, was utilized to generate a solution database for developing ANN-based structural models to accurately predict pavement deflection basins, and pavement layer moduli from realistic FWD deflection profiles.

Tutumluer et al. (19) developed a Soft Computing Based Pavement and Geomaterial System Analyzer (SOFTSYS) framework as a software tool to backcalculate nonlinear stress-dependent geomaterial properties for conventional flexible pavements and the total AC thicknesses of full-depth asphalt pavements. Artificial neural network pavement structural models were developed using the results of the synthetic data obtained from ILLI-PAVE FE solutions. Their results indicated that performance of ANN backcalculation models for predicting layer moduli of granular bases for conventional flexible pavements provided the highest average absolute errors (AAEs) on the order of 6% (Figure 2.9). Their results also indicated that AAEs on the order of 6% and 9% were obtained for the HMA thickness estimation for full depth pavements and full depth pavements built on lime stabilized soil layers (Figure 2.10). In addition, the thickness data obtained from GPR testing matched reasonably well with the SOFTSYS results. However, in some locations the maximum difference between the two methodologies reached 3 inches.

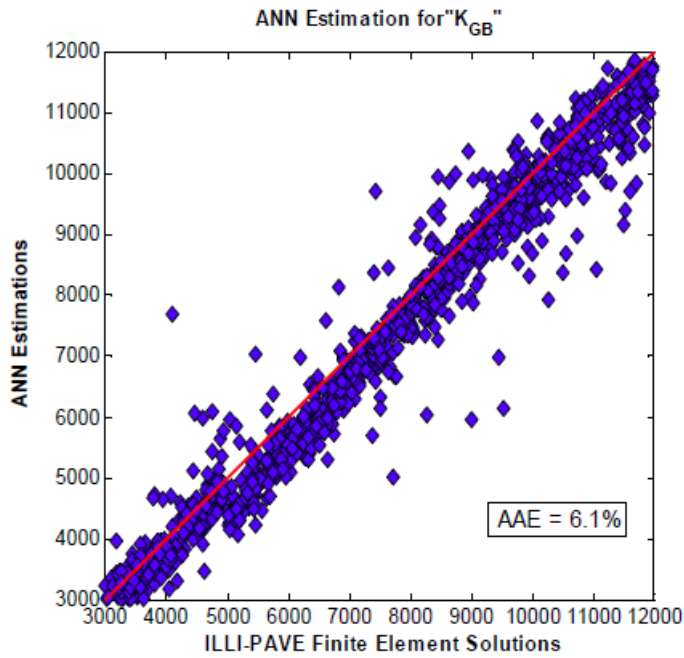


FIGURE 2.9 Performances of ANN backcalculation models for predicting layer moduli of granular bases for conventional flexible pavements (19).

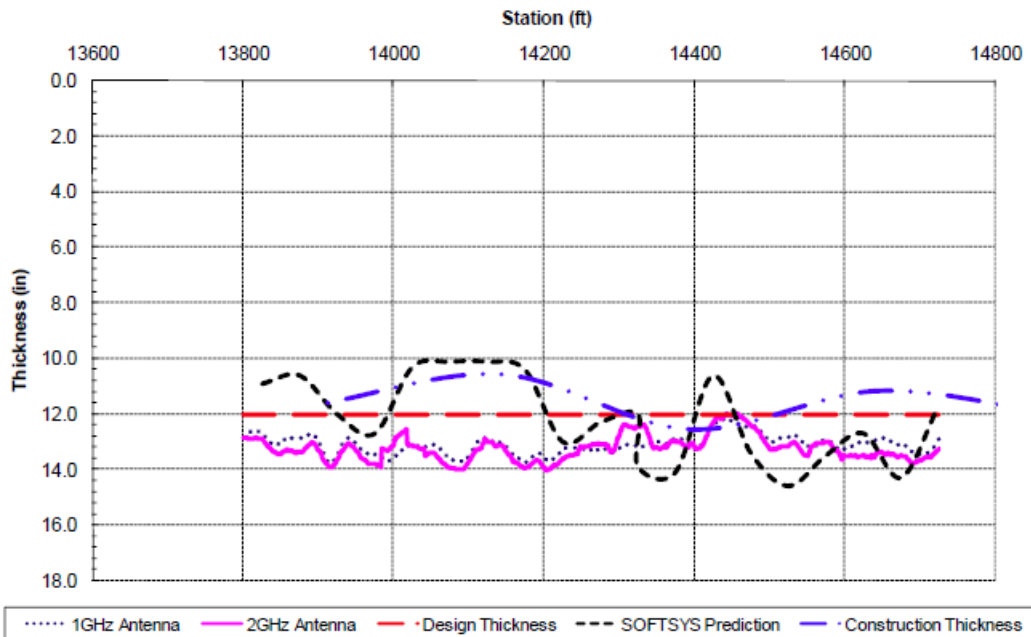


FIGURE 2.10 Estimation of pavement layer properties using SOFTSYS (19).

In 2007, Gopalakrishnan (20) used artificial neural networks for predicting non-linear layer moduli of flexible airfield pavements subjected to new generation aircraft (NGA). This study was based on the deflection basins obtained from heavy weight deflectometer (HWD) data. HWD tests were performed the Federal Aviation Administration's National Airport Pavement Test Facility (NAPTF) to monitor the effect of Boeing 777 (B777) and Boeing 747 (B747) test gear trafficking on the structural condition of flexible pavement sections. The pavement sections at NAPTF were modeled in ILLI-PAVE and a synthetic database was generated for a range of moduli values. A multi-layer, feed-forward network with error-back propagation algorithm was trained to approximate the HWD backcalculation function using that database. The ILLI-PAVE synthetic database was used in the ANN training to account for the stress-hardening behavior of unbound granular materials and stress-softening behavior of fine-grained subgrade soil. The model was able to predict the asphalt concrete (AC) and subgrade non-linear moduli from actual HWD field test data. Figure 2.11 shows the plot of predicted ANN modulus of the AC layer versus backcalculated modulus using the software BAKFAA. It was noted that the rut depths in the NAPTF flexible test sections reached significant levels (3 in to 4 in) towards the end of traffic testing and that explained not only the significant difference in results but also the significant variability during the final stages of traffic testing.

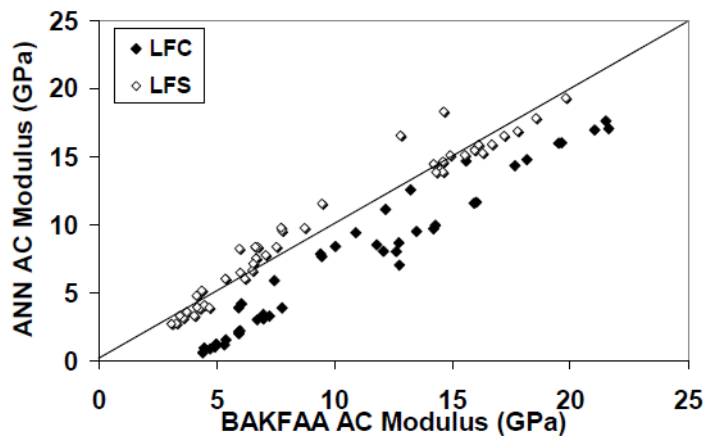


FIGURE 2.11 ANN AC moduli predictions compared with BAKFAA predictions (20).

On a more elaborate scale, the new Mechanistic–Empirical Pavement Design Guide (MEPDG) procedure, developed by NCHRP under AASHTO sponsorship, requires that structural analysis be performed more than 1,000 times for a single design simulation of a pavement structure (4). For rigid pavement design, the MEPDG already takes advantage of the neural networks to reduce processing time. The MEPDG uses a stress prediction neural network in conjunction with a fatigue transfer function, originally derived from field slab test results of the U.S. Army Corps of Engineers, to predict either bottom-up or top-down transverse fatigue cracking near the mid-slab edge.

2.4.1 Neural Networks Definition

A neural network is an information processing system that is nonalgorithmic, nondigital, and intensely parallel (21). It consists of a number of very simple and highly interconnected processors called neurons, which are the analogs of the biological neurons, in the brain (Figure 2.12). The neurons are connected by a large number of weighted links, over which signals can pass. Each neuron typically receives many signals over its incoming connections (dendrites).

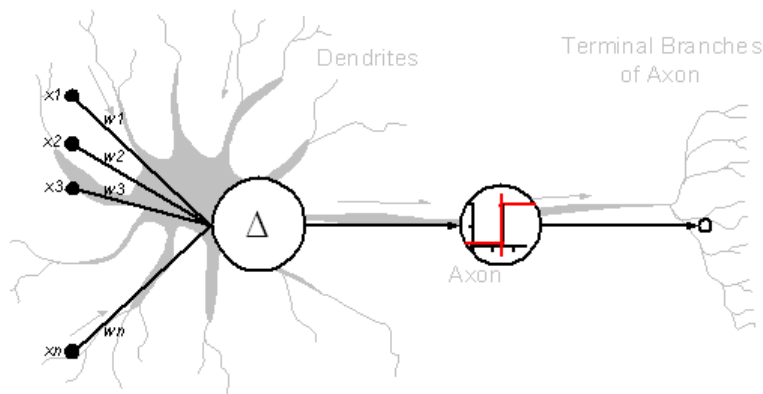


FIGURE 2.12 Schematic of Neural Networks.

The neuron usually has many incoming signal connections; however, it never produces more than single outgoing signals. That output signal transmits over the neuron's outgoing

connection (corresponding to the biological axon of a neuron), which usually splits into a very large number of smaller connections, each of which terminates at a different destination.

2.4.2 Benefits of Neural Networks

The use of neural networks offers the following useful capabilities:

1. Neural networks are capable to adapt themselves (the synapses connections between units) to special environmental conditions by changing their structure or strength of connections.
2. Every new state of a neuron is a nonlinear function of the input pattern created by the firing nonlinear activity of the other neurons.
3. Their different states are characterized by high robustness or insensitivity to noisy and fuzzy of input data due to use of a highly redundant distributed structure (6, 21).

2.4.3 Artificial Feedforward Neural Networks

This type of ANN is also a massively parallel distributed processor that has a propensity for storing experimental knowledge and making it available for use. It means that knowledge is acquired by the network through a learning (training) process (6). The strength of the interconnections between neurons is implemented by means of the synaptic weights used to store the knowledge. The learning process is a procedure of the adapting the weights with a learning algorithm in order to capture the knowledge. In other words, the goal of the learning process is to map a given relation between inputs and outputs of the network.

Figure 2.13 shows an example of feedforward ANNs. In this case, the neurons are grouped into layers. The input layer consists of neurons that receive input from the external environment. The output layer consists of neurons that communicate the output of the system to the user or external environment. There are usually a number of hidden layers between these two layers. This is also a simple structure with only one hidden layer. An ANN is of the feedforward type as depicted in Figure 2.13 if a neuron's output is never dependent on the output of

subsequent neurons. Signals only go forward through the network with no loops. When the input layer receives the input its neurons produce output, which becomes input to the other layers of the system. The process continues until a certain condition is satisfied or until the output layer is invoked and fires their output to the external environment (21).

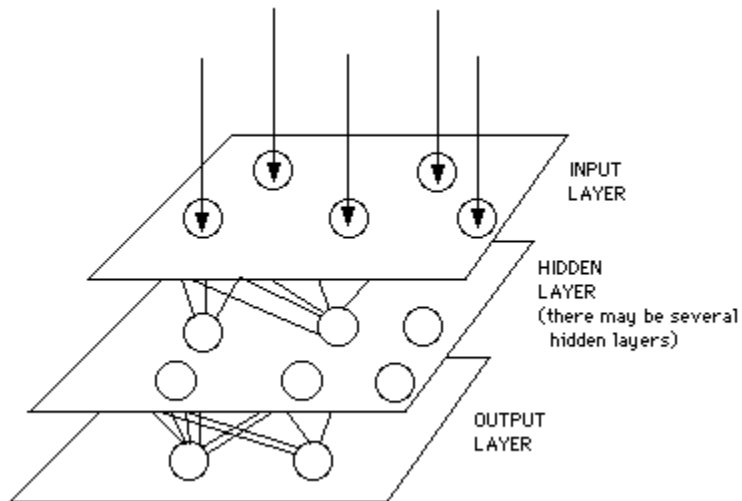


FIGURE 2.13 Schematic of a feedforward neural network (6).

The main advantages of utilizing feedforward ANN models are the speed to compute the outputs; they are easy to use, and capable to process large amounts of data. The two main limitations that the model does not have the ability to extrapolate beyond the range of parameters used in training (it can be overcome by carefully selecting the training set), and the developing time is very long (it affects the model developers). ANNs are also considered black boxes. They cannot explain why a given pattern has been classified as x rather than y.

2.4.4 Back-Propagation Training Technique

Back-propagation is often used in conjunction with feedforward networks and it provides a way of using examples of a target function to find the weights that make the mapping function approximate the target function as closely as possible (6). Figure 2.14 shows a flow chart of this training process. Training begins with an arbitrary set of weights. Series of computations

(iterations) are done in which the calculated output is compared with the known values, adjusting the weights in such a way that the difference between the calculated values and the target function is minimized (21). With each iteration, the hidden layer passes information through based on values of the weights in memory and the output values are calculated. The output nodes are then informed of the difference between the actual and target values. Each output neuron determines in which direction its weights must be adjusted to reduce the error and propagates the information to the hidden layer, which in turn determines in which direction its weights must be changed. At the hidden layer level the weights are adjusted in such a way as to reduce the error across the full set of output neurons thus minimizing the error in the network. For each iteration, there is a forward pass followed by a backward pass during which error information is propagated backward from the output neurons to the hidden neurons.

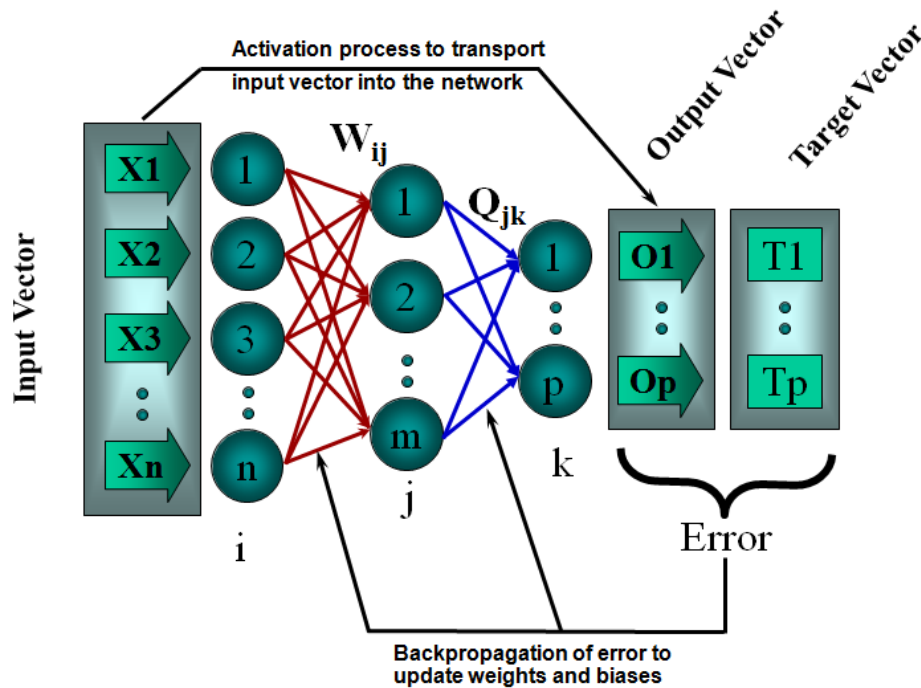


FIGURE 2.14 Flow chart of backpropagation training process (21).

2.5 Simulation of Moving Vehicle Loads and Load Pulse Durations

2.5.1 FWD Load Versus Moving Loads

The viscoelastic nature of asphalt concrete (AC) renders its properties to be frequency-dependent. Static backcalculation of layer moduli from falling weight deflectometer (FWD) testing does not take into account this frequency-dependence. In 1999, Chatti and Kim (22) evaluated the effect of frequency-dependent AC properties on the horizontal strain and vertical deflection using the computer program SAPSI-M and field results. The analysis showed that the decrease in horizontal strain with increasing truck speed can be duplicated only by using frequency-dependent properties for the asphalt concrete layer (Figure 2.15). However, using a constant backcalculated AC surface layer modulus and static analysis seemed to be sufficient for giving a prediction that is reasonably close to the actual tensile strain under moving loads at high speeds. They also mentioned that backcalculated modulus for the AC layer was generally higher than the creep modulus, and the horizontal tensile strain was not affected by speed when using a constant AC layer modulus.

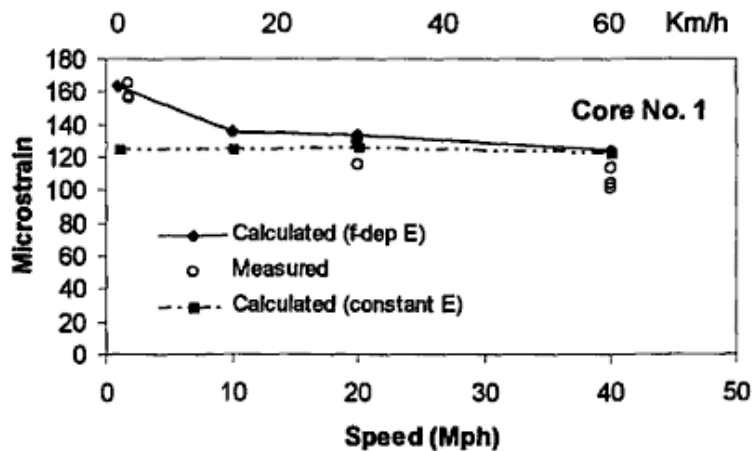


FIGURE 2.15 Comparison of measured and predicted strain under moving loads (22).

The response of pavements to FWD tests has been examined by Hoffman and Thompson (23) as part of an investigation on a range of nondestructive testing devices. Their results showed

that FWD pulse durations were of the order of 30 msec, in contrast to typical truck pulse durations at 50 mph that were estimated at 120 msec. In addition, neither the deflection pulse duration nor the accelerations imposed by the FWD agree well with those measured for moving wheel loads. It was indicated in this study that a fixed-in-place nondestructive testing device cannot simulate the loading effect of a moving load. However, they point out that FWD and moving truck deflections measured in their study compare very favorably.

In a more recent study by Jianfeng Q. (24), the impulse durations caused by moving vehicles were found to be about two to seventeen times longer than the pulse duration caused by the FWD. For a truck driven at a speed of 45-55 mph, the pulse duration of the truck was about two to three times longer than the FWD loading (Figure 2.16). On the other hand, the author indicated that for the same level of loading (single wheel), strains under FWD loading were close to the strain caused by a controlled load vehicle (CVL) driving at 55 mph (Figure 2.17). This study was performed on perpetual pavements with average AC layer thickness of 16.0 inches and maximum recorded strain responses of 75 microns.

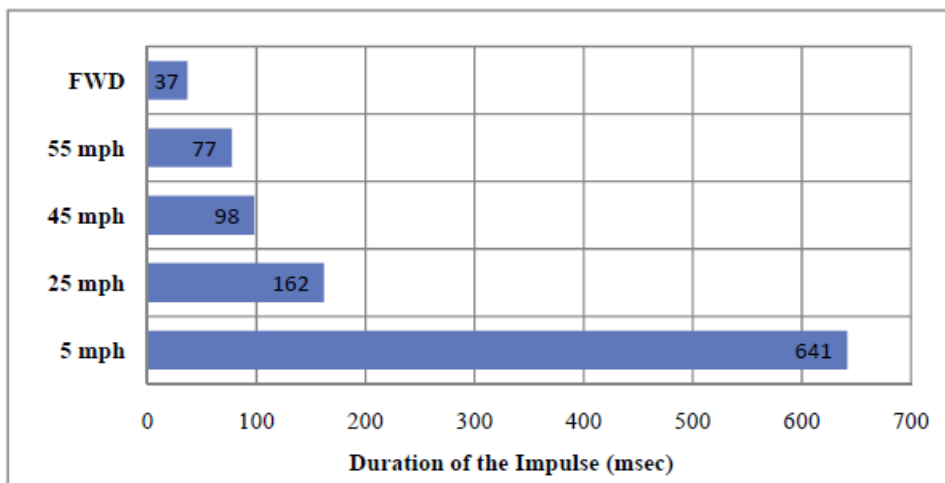


FIGURE 2.16 Average duration of the impulses under different loading conditions (24).

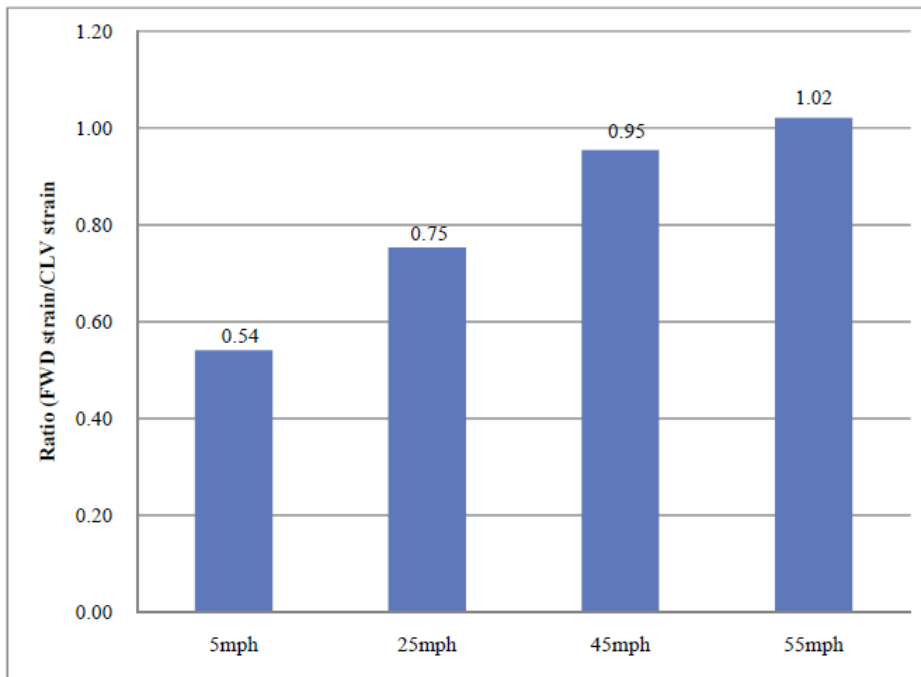


FIGURE 2.17 Comparison of strain responses under FWD loading and truck loading at the same level of loads (24).

2.5.2 Simulation of Moving Loads

The finite element methodology (FEM) along with a simplified version such as finite layer methodology has been widely accepted as a methodology to simulate moving loads. In finite element modeling, viscoelastic behavior of AC materials can be characterized through relaxation moduli and dynamic loads can be modeled in terms of duration of the load and velocity. One example of this can be found in the newly developed software 3D-Move and several verification studies have been conducted to validate the applicability and versatility of it (8, 25-27). This tool accounts for moving traffic loads with complex contact stress distributions of any shape, vehicle speed, and viscoelastic properties of asphalt concrete layers to calculate pavement responses using a continuum-based finite-layer approach. The finite-layer approach treats each pavement layer as a continuum and uses the Fourier transform technique (8). Since pavements are horizontally layered and pavement responses are required only at a few selected

locations *3D-Move* takes advantage of the finite layer approach (8). Some of these efforts included field calibrations from the Penn State University test track, MN/Road and an UNR off-road vehicle study. These studies compared a variety of independently-measured pavement responses (stresses, strains, and displacements) with those computed. For instance, Siddharthan et al. (26-27) studied the capability of 3D-Move to predict pavement response and compared the results to full-scale field-measurements at the bottom of the asphalt concrete (AC) layer. The results indicated good agreement between predicted and field-measured strain responses, with the difference between them less than 14 percent (Figure 2.18). In addition, tensile microstrain decreased by as much as 50 percent when the speed of the vehicle increased from 20 to 50 mph.

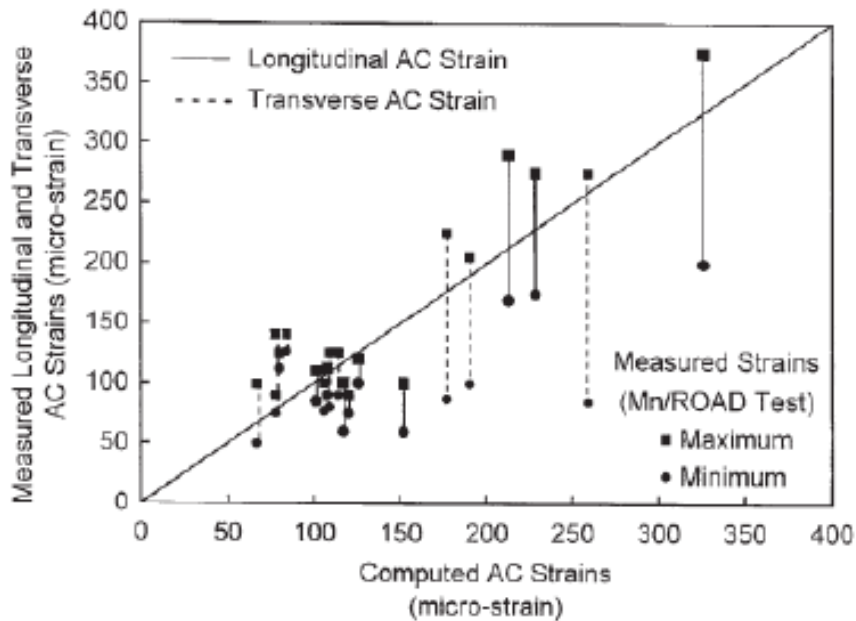


FIGURE 2.18 Validation of the software 3D-Move (26-27).

In 2010, Kim (28), showed the results of a study related to analysis of moving loads. In this paper, a linear viscoelastic solution for the multilayered system subjected to a cylindrical unit step (static) load was derived from the elastic solution by using the principle of elastic-viscoelastic correspondence and the numerical inversion of Laplace transforms. The solution was then extended to simulating pavement responses subjected to a moving load by employing the

Boltzmann's superposition principle. The soundness of output from the viscoelastic solution was confirmed by comparing them to those of the finite-element analysis (FEA). Compared to the time and effort required in FEA, the analysis based on the viscoelastic solution was much faster. Figure 2.19 shows a verification of Kim's approach (viscoelastic V-Layer) using the finite-element method. For this figure, the horizontal stress calculated at the bottom of the AC layer obtained from the viscoelastic solution matched the results obtained from finite-element analysis.

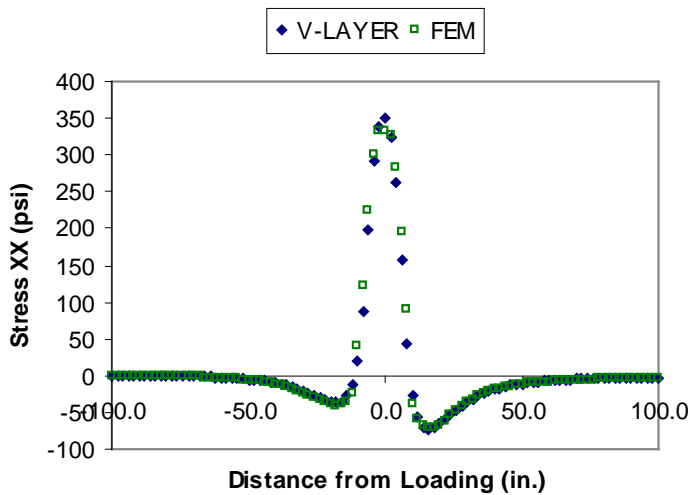


FIGURE 2.19 Viscoelastic versus FEA analysis (28).

A study by Elsefi et al. (29) was meant to characterize hot-mix asphalt (HMA) viscoelastic properties at intermediate and high temperatures and to incorporate laboratory-determined parameters into a three-dimensional finite element (FE) model to accurately simulate pavement responses to vehicular loading at different temperatures and speeds. Results of the developed FE model were compared against field-measured pavement responses from the Virginia Smart Road. Results of this analysis indicated that FE viscoelastic model were in better agreement with field measurements than the layered elastic theory. Figure 2.20 shows that the vertical stress calculated at the bottom of the AC layer obtained from the viscoelastic solution were reasonably close to stresses measured at 45 mph.

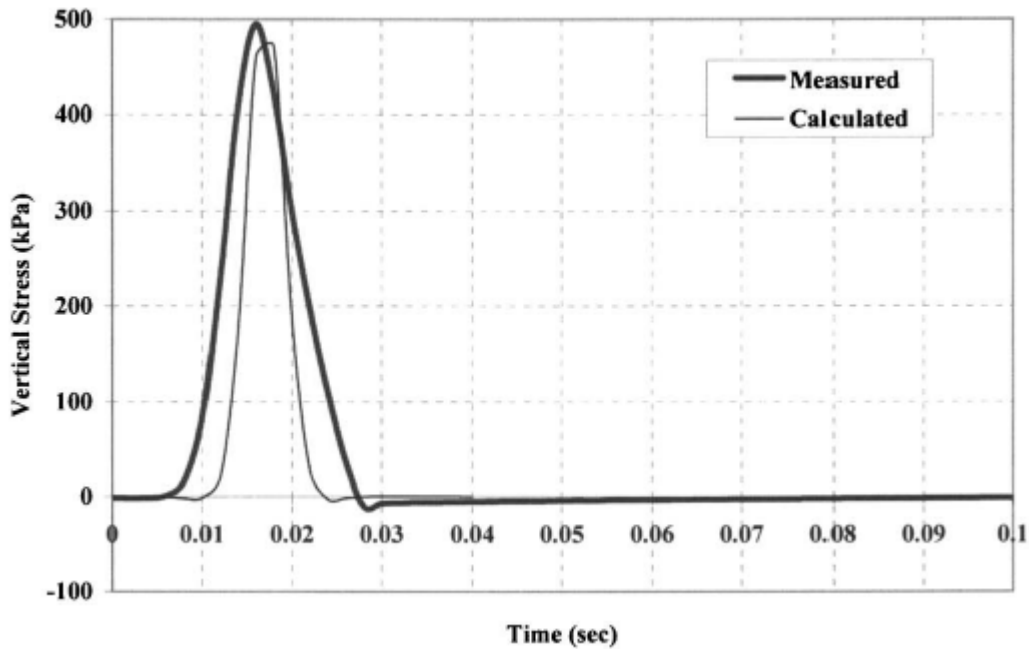


FIGURE 2.20 Comparison between measured and calculated vertical stress at a speed of 45 mph (29).

2.5.3 Load Pulse Duration

In the NCHRP Project 1-37A Mechanistic–Empirical Pavement Design Guide (MEPDG), the dynamic modulus master curve is constructed as a function of loading time, t (4). Because dynamic modulus results are obtained as a function of frequency, a conversion from frequency to loading time is needed. The MEPDG uses an iterative procedure to compute the load duration under dynamic loading. The MEPDG assumes the load duration as the length of time for one complete haversine stress pulse in the longitudinal direction for an applied load (4). A simplified procedure based on a 45 degree influence zone was adopted to calculate the frequency of the applied load as a function of the vehicle speed and the cross-section of the pavement structure. Through the use of the complex modulus master curve, the MEPDG software internally selects the applicable complex modulus depending on the pertinent temperature and loading frequency.

Concerns were raised that the current MEPDG methodology may be overestimating the frequency resulting in under prediction of distress levels (30). In addition, the current frequency

calculation procedure was also reported to override the effect of temperature compared with the effects in other mechanistic–empirical design procedures. To quantify the level of inaccuracy in MEPDG to account for load frequency, Al-qadi et al. (31), evaluated the MEPDG methodology for calculation of the loading time, the results of the MEPDG procedure were compared with those of an advanced three-dimensional (3-D) finite element (FE) approach that simulates the approaching-leaving rolling wheel at a specific speed. Comparison of these two methods showed that the frequencies calculated on the basis of the MEPDG procedure were greater than the ones determined by the 3-D FE method. Ultimately, this would result in underestimation of the pavement response to a load and, therefore, greater errors in calibrations of the pavement response to field distress. Correction factors were presented to ensure the correctness of the loading time calculation in MEPDG.

The elastic—viscoelastic correspondence principle can be applied directly to moving loads, as indicated by Huang (11) in a multilayer system. The complexities of the analysis and the large amount of computer time required make these methods unsuited for practical use. Therefore, a simplified method has been used in KENLAYER. In this method, it is assumed that the intensity of load varies with time according to a haversine function, as shown in Figure 2.21. With $t = 0$ at the peak, the load function is expressed in equation 2.1.

$$L(t) = q \sin^2 \left(\frac{\pi}{2} + \frac{\mu t}{d} \right) \quad \text{Eq. 2.1}$$

Where;

d = the duration of load

q = peak load

t = time

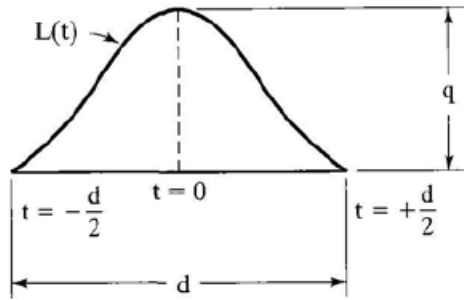


FIGURE 2.21. Moving load as a function of time (11).

When the load is at a considerable distance from a given point, or $t = \pm d/2$, the load above the point is zero, or $L(t) = 0$. When the load is directly above the given point, or $t = 0$, the load intensity is q . The duration of load depends on the vehicle speed (s) and the tire contact radius (a). A reasonable assumption is that the load has practically no effect when it is at a distance of $6a$ from the point, or

$$d = \frac{12a}{s} \quad \text{Eq. 2.1}$$

Where;

d = the duration of load,

a = the tire contact radius,

s = the moving load speed

If $a = 6$ in and $s = 40$ mph (58.7 ft/s), then $d = 0.1$ s. On the other hand, if $d = 0.03$ s (FWD load pulse duration) and $a = 5.91$ in (FWD plate radius), $s = 134$ mph (197 ft/s). Therefore, it would be necessary to simulate a moving load with a speed of 134 mph to make it comparable to the FWD impact load.

The relationship between frequency and loading time for asphalt concrete mixtures was defined by Jacobs et al. (32) as the dynamic modulus frequency equals the inverse of loading time t ($1/t$). Jacobs et al. also suggested that a loading frequency of 8 hz corresponded to a vehicular speed of 37 mph. On the other hand, Kim and Lee (33) compared the uniaxial dynamic modulus

results with the resilient modulus results obtained by the indirect tensile test at a frequency of 10 Hz, assuming that the loading time in the resilient modulus test is inversely related to the dynamic modulus test frequency (in hertz), such that $t = 1/f$. The same relationship was used to convert a falling weight deflectometer loading time of 0.03 s to a dynamic modulus test frequency of 33 Hz. To convert the dynamic modulus as a function of frequency to the dynamic modulus as a function of loading time for input in MEPDG, Bonaquist and Christensen (34) and Witzczak et al. (35) suggested that a frequency of 10 Hz be used to represent highway speeds and, therefore, that the dynamic modulus result at 10 Hz be used.

Loulizi et al. (36) at the Virginia Smart Road facility characterized the effects of speed, depth and temperature on measured vertical compressive stress pulse times (2002). Pulse durations were measured for truck speeds ranging from 5 mph to 45 mph at various pavement depths. Similar testing conducted at a later date was used for temperature comparisons, resulting in maximum in-situ temperature differences between test dates of 55.8°F and 44.2°F for the two pavement types investigated. Due to the lack of symmetry in the stress pulses, the loading time was taken to be twice the time of the rising normalized vertical compressive stress pulse beginning at a normalized stress of 0.01 psi. The results led to the conclusion that normalized compressive stress pulse durations generally increased with depth and were related to vehicle speed by a power function. Figure 2.22 shows the effect of vehicle speed on the normalized vertical stress pulse duration. The influence of the load and the duration of the pulse decreased as the speed of the vehicle increased.

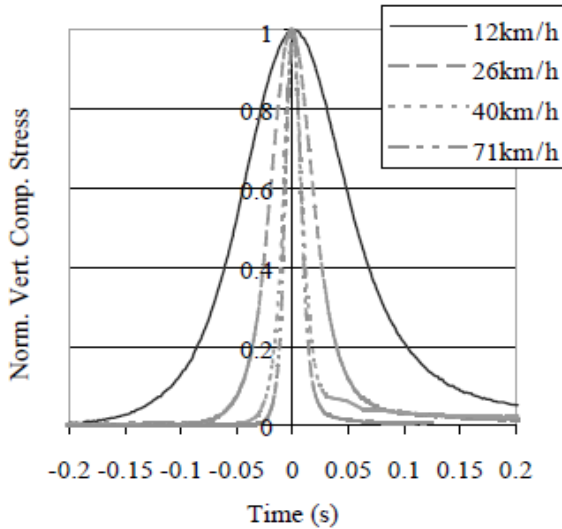


FIGURE 2.22 Measured compressive stress pulse (36).

In 2008, Garcia and Thompson (37) utilized strain signals to measure the loading pulse duration. A traffic load simulator, the Advanced Transportation Loading Assembly (ATLAS), was employed to apply loads with no lateral displacement under a single tire inflated to 110 psi. ATLAS testing was conducted at very low speeds, 2 mph, 6 mph, and 10 mph for loads ranging from 5-11 kips. Load duration measurements were taken at various depths in the pavement and were compared with computed load pulse durations from Equations 2.1 and 2.2. These results showed that measured longitudinal strain pulse durations were overestimated by only 2.21%

$$L_{eff} = 200 + 2z \quad \text{Eq. 2.1}$$

Where:

L_{eff} = effective length of load pulse (mm)

z = actual depth (mm)

$$t = L_{eff} / v \quad \text{Eq. 2.2}$$

Where:

t = time of loading (s)

v = vehicle speed (mm/s)

In 2009, Robbins (38) studied the effects of speed, depth and temperature on measured strain pulse duration. From the individual relationships, the combined effect of these three factors on load duration was then characterized to provide a means to predict the load duration for any set of conditions. The load durations computed by the MEPDG procedure were compared with the strain pulse durations measured during the field investigation. The results showed that the MEPDG procedure consistently over-predicts the load durations (Figure 2.23). Over-prediction of load duration would be expected to result in lower modulus of the AC layer and consequently an over-prediction of pavement responses.

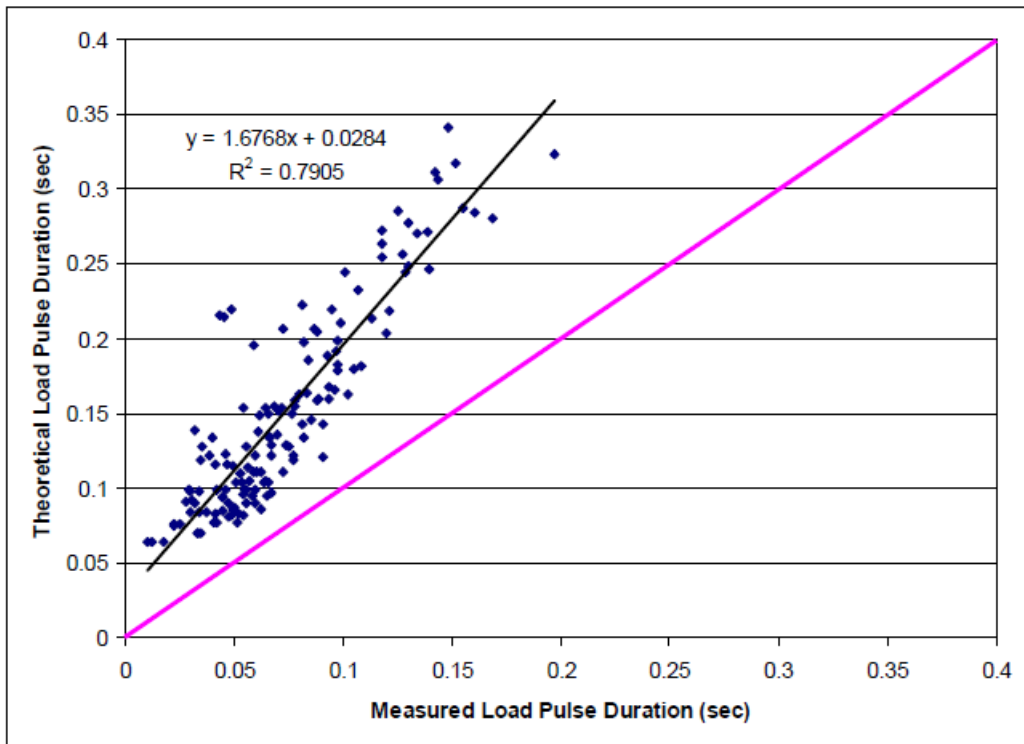


FIGURE 2.23 Measured load duration versus theoretical (38).

2.6 Summary

The literature suggests that the current backcalculation process is highly dependent on initial seed values. Therefore, the starting values and ranges for the moduli must be selected judiciously. The number of layers of a pavement structure, the selected level of tolerance, the number of deflection

basins to be analyzed and starting values can significantly affect the time consumed and reliability during backcalculation. On the contrary, the results obtained from ANNs are unique, will be the same no matter the times the ANN is applied and time consumed is minimal. The literature also suggests that there is a potential error in pavement layer moduli backcalculation due to improper modeling of the layer interface condition. The granular base modulus is more likely to be the most affected by considering a full bond layer interface condition when the actual conditions tend to be full slip layer interface.

Regarding the capability to the FWD to simulate moving loads, the literature suggests that significant differences were observed when the load pulse duration of the FWD was compared to vehicles moving at operational speeds. A frequency of 10 Hz has been recommended for laboratory dynamic modulus tests and to simulate operational moving loads. However, a 33 Hz frequency has been acknowledged to represent the FWD load frequency. Finally, the literature proposes that the proper determination of the loading pulse duration is not only essential to deal with frequency dependent materials such as asphalt concrete but also to properly predict pavement responses and ultimately performance.

CHAPTER THREE: EXPERIMENTAL DESIGN

To accomplish the objectives of this study, two main experimental designs were created. The first one had to do with creation and implementation of artificial neural networks as an alternative to conventional backcalculation. The second design pertained to the capability for the falling weight deflectometer to represent moving loads and the determination of correction factors applied to backcalculated pavement properties to obtain more accurate pavement responses. An overview of the different tasks followed to complete each experimental design are described in the following subsections. The following chapters present the results and discussion of these tasks.

3.1 Accelerated Testing Facility

FWD test results and measured pavement responses from the NCAT Test Track were used in this study. Therefore, in the following chapter, a brief description of the test facility and tests sections was necessary to provide background concerning the available information.

3.2 ANN Development to Predict Pavement Material Properties

Artificial Neural Networks were created to perform forward calculations of pavement layer moduli and critical responses from non-destructive testing information. Synthetic databases were created using a modified version of the software PerRoad (WESLEA-based software) for a three layer flexible pavement. These databases included layer moduli, deflection basins, critical pavement responses and layer thicknesses.

3.2.1 Analysis of Conventional Backcalculation Process

This analysis was performed to investigate the non-uniqueness of backcalculated results when setting different initial conditions. The software EVERCALC 5.0 was used to analyze the effect of the level of tolerance, calculated by means of the root mean square error (RMSE), on estimated pavement layer moduli. EVERCALC uses WESLEA as the mechanistic engine to perform the forward analysis. The forward analysis involves the calculation of surface deflections at the

specified radial offsets using different combinations of initially assumed layer moduli. The calculated surface deflections are then compared to the field-measured deflections. For each combination of layer moduli, the error between these calculated and measured moduli is determined. This step is repeated several times until the error is minimized. This process is known as the error minimization or optimization of solution. A modified Gauss-Newton algorithm is used for error minimization. FWD data from a maximum of ten sensors can be used and it can analyze twelve drops at each station. During the error minimization process, a trial is stopped whenever one of the following conditions is satisfied first (14):

- Moduli tolerance is based on the modulus difference between two consecutive iterations.
- Deflection tolerance calculates the deflection error between the field measured and the calculated deflections using the following formula:

$$RMSE = \sqrt{\frac{1}{n_d} \sum \left(\frac{d_{ci} - d_{mi}}{d_{mi}} \right)^2} \times 100\% \quad \text{Eq. 3.1}$$

Where;

RMSE = root mean square of the error,

d_{ci} = calculated pavement surface deflection at sensor i,

d_{mi} = measured pavement surface deflection at sensor i, and

n_d = number of deflection sensors used in the backcalculation process.

The effect of the root mean square error (RMSE) on estimated pavement layer moduli and pavement responses was evaluated by setting three different levels of tolerance: 0.1%, 1.0% and 3.0%. A forward-calculated synthetic dataset was created using layered elastic analysis (WESLEA) which is the same mechanistic engine used to perform backcalculation. All the deflection basins were introduced in EVERCALC and a conventional backcalculation process was performed.

3.2.2 Analysis of ANN vs. Conventional Backcalculation

The back-propagation algorithm was used as a learning algorithm to be applied on multilayer feed-forward networks. A synthetic database was generated using LEA for a three-layered flexible pavement structure. Inputs for the ANN's were deflection basins, layer thicknesses and load. The targets were layer moduli and critical pavement responses. An additional dataset was used to test the accuracy of the ANN and the results were compared to the outcomes obtained using EVERCALC. Figure 3.1 shows the flow chart followed to create and train ANNs [step 1]. This process was repeated three times and the network with the lower error was selected as the optimal ANN to be used for predicting a new deflection data set and compared with the results from EVERCALC [step 2].

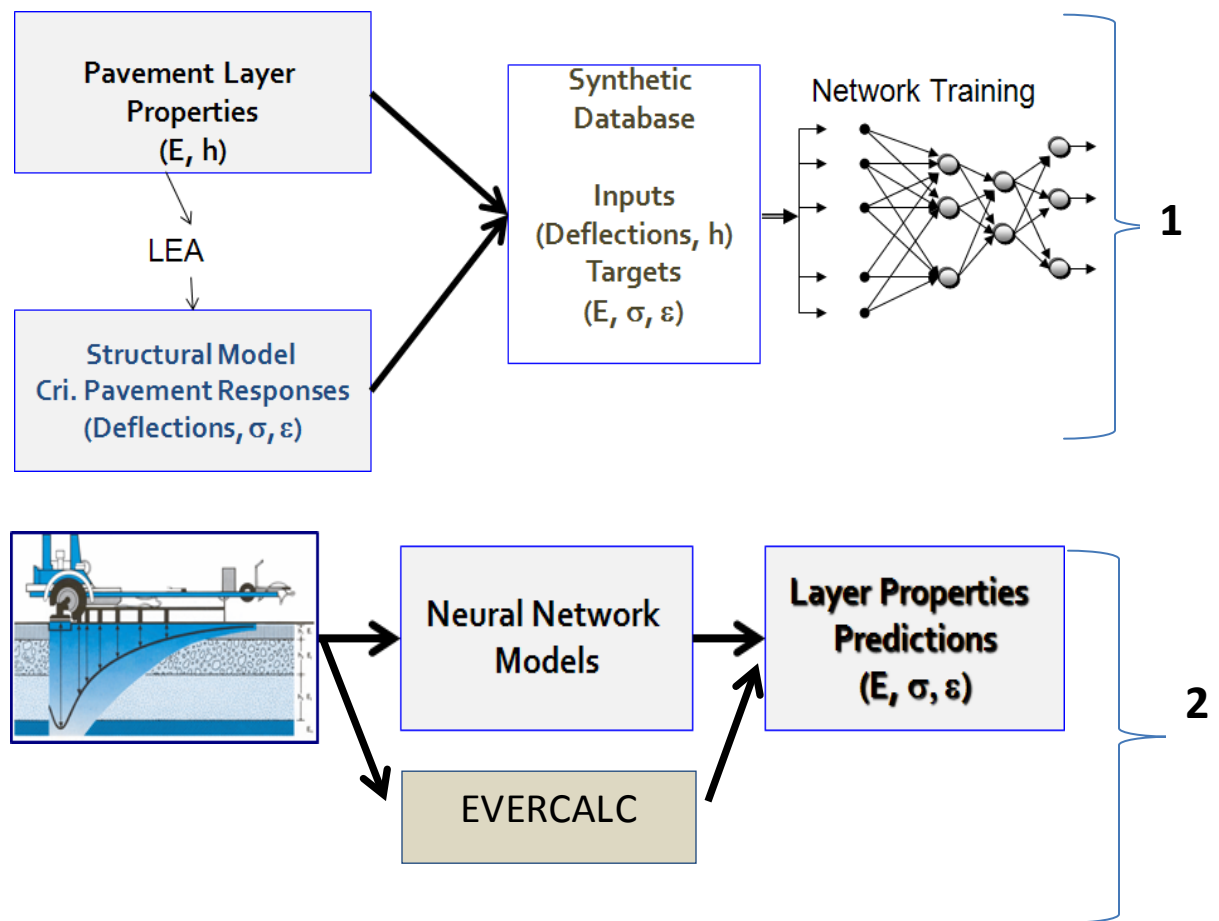


FIGURE 3.1 Training of ANNs flow chart.

3.2.3 Analysis of Potential Use of ANN to Predict Layer Thickness

A back-propagation algorithm was used to obtain ANNs capable of determining the layer thickness of pavement structures using synthetic deflection data. A sensitivity of the deflection data due to thickness variation also helped determine the predictability of layer thicknesses using the ANN approach. A typical FWD sensor configuration requires the use of seven geophones to generate a deflection basin with seven deflection points. At the NCAT Test Track, the FWD sensor configuration utilizes nine geophones to provide a more detailed deflection basin. For this study, the number of input deflections (7, 9 and higher) was tested to evaluate the accuracy of thickness prediction.

3.2.4 Verification Using Field Data from NCAT FWD Testing

The quality of the existing databases was important to minimize variation in the results simply due to testing, and construction practices. The NCAT Test Track database was used as the source of data for this study. Non-destructive testing using the FWD was performed several times per month at the Test Track and pavement temperature at different depths was also collected during testing. Backcalculated moduli and critical pavement responses were compared against the predicted moduli and critical responses obtained using ANN.

3.2.5 Training Tool (MATLAB 7.10.0 – R2010a)

The following illustrations show some of the elements found in MATLAB used to create and train ANNs. Figure 3.2 shows MATLAB's default desktop. Here the Command Window is used to enter variables and to run MATLAB functions and scripts. Statements entered in the Command Window are logged with a timestamp in the Command History. In the MATLAB workspace the set of variables and data are entered and stored in memory (39).

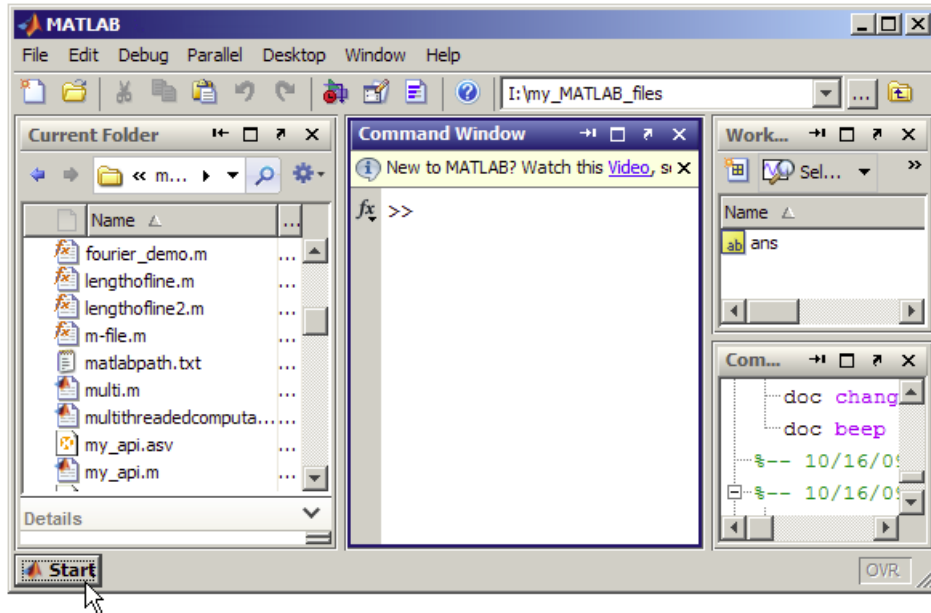


FIGURE 3.2 Matlab default desktop.

Figure 3.3 shows an example of the training tool (window) used with MATLAB. During training, the progress is constantly updated in the training window. Of most interest are the performance, the magnitude of the gradient of performance and the number of validation checks. The magnitude of the gradient and the number of validation checks are used to terminate the training. The gradient will become very small as the training reaches a minimum performance level. The number of validation checks represents the number of successive iterations when the validation performance value fails to decrease. If this number reaches 6 (the default value), the training will stop. In this example, the training did stop because of the number of validation checks. For this example, training stops when any of these conditions occurs:

- The maximum number of epochs (repetitions) is reached.
- The maximum amount of time is exceeded.
- Performance is minimized to the goal.

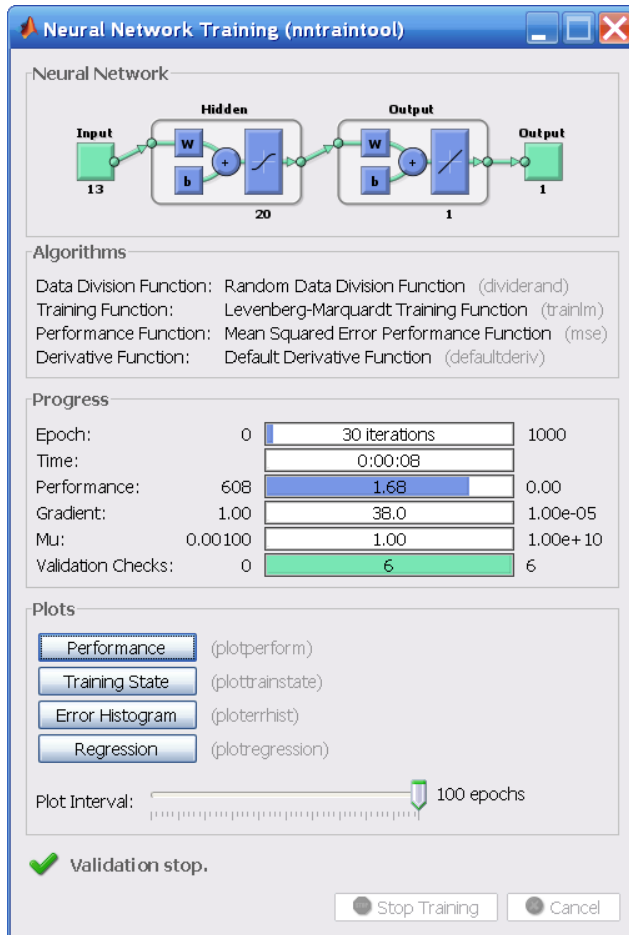


FIGURE 3.3 Example of the training tool.

The training process for this type of ANN can be explained as follows: In general, under-fitted models will have a high bias and over-fitted models will have a high variance. To avoid either of these, the network is normally divided into two main sets: training and validation, and sometimes a testing set is included. The network is trained using only the training data. The training process is continuously tested for performance using the independent validation set. The testing data set is used to check the applicability of the network on a completely independent dataset. While the performance of the training data will continue improving and leading to over-fitting, performance on the validation set will stop improving, and will typically get worse. The typical performance function used for training feedforward neural networks is the mean sum of squares of the network errors as shown in Equation 3.2.

$$MSE = \frac{1}{N} \sum_{i=1}^N (t_i - o_i)^2 \quad \text{Eq. 3.2}$$

Where;

MSE = Mean square error

N = total number of target values,

t_i = target values,

o_i = output values.

A linear regression between the network outputs and the corresponding targets can be also obtained at any point of the training process (Figure 3.4). Single correlation (R-value) is also used to check the performance of the network by targeting values close to 1.0.

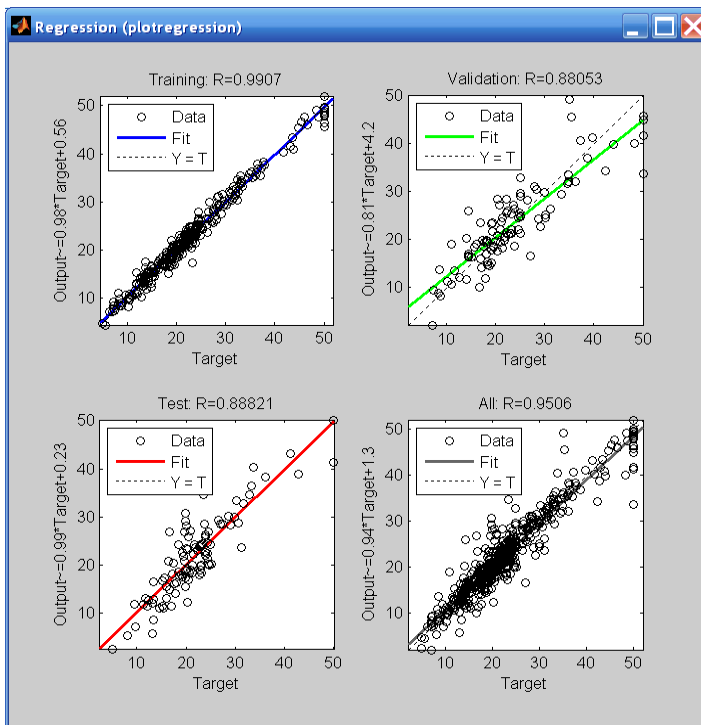


FIGURE 3.4 Example of performance regression plots.

3.3 Correction Factors for the High Frequency/High Speed FWD Pavement Responses to Typical Operating Speed Responses

The mechanistic analysis software *3D-Move* was used to determine the speed of a moving load that produces a load pulse duration equivalent to the loading pulse produced by the FWD. Pavement responses were calculated at that equivalent FWD speed and at the NCAT Test Track operating speed of 45 mph. Correction factors were calculated as the difference between these responses at different temperatures. Finally, these factors were applied to pavement responses from actual backcalculated moduli and compared against measured pavement responses.

3.3.1 Determination of FWD Loading Pulse from Instrumented Pavements

The FWD loading pulse was obtained from measured pavement response signals. FWD tests were performed on nine structural sections built in 2009 at the Test Track. The signal measured from a pressure plate was used to calculate the loading pulse. FWD stress and strain pulses followed a haversine waveform with distinguishable termination points. Stress pulses due to moving loads produced a waveform very similar to the FWD one and therefore it was used in the analysis. An example of a FWD wave form can be seen in Figure 2.3 and an example of stress pulse can be seen in Figure 2.20.

3.3.2 Determination of Equivalent Loading Pulse and Equivalent Loading Speed

The *3D-Move* software was used to estimate the speed which produced an equivalent pulse to the pulse obtained in the previous task. A single uniform load of 9000 lb with radius of 5.91 inches was modeled in *3D-Move* to simulate the dynamic load applied by the FWD. Backcalculated moduli were used to model base and subgrade layer properties, while dynamic moduli and frequencies were calculated at the mid-depth temperature measured during field testing. The loading speed was varied until the target loading pulse was obtained.

3.3.3 Determination and Application of Correction Factors

Pavement responses were calculated at 5 different temperatures (40, 70, 100, 115 and 130°F) and at 5 different operating speeds (15, 25, 35, 45 and 60 mph). These responses were compared to those responses calculated at the “equivalent speed”. Correction factors were applied to backcalculated pavement responses and then compared to actual responses measured at 45 mph.

3.3.4 Mechanistic Modeling Tool

The analytical software *3D-Move* was created by the Asphalt Research Consortium at the University of Nevada in Reno and it is currently on version 1.2. This tool accounts for moving traffic loads with complex contact stress distributions of any shape, vehicle speed, and viscoelastic properties of asphalt concrete layers to calculate pavement responses using a continuum-based finite-layer approach. 3D-Move has the following features:

- SI / US units
- Static / Dynamic analysis
- Uniform contact pressure distribution (Circle, Ellipse and Rectangle)
- Non-Uniform contact pressure distribution from database
- Semi-Trailer truck including vehicle dynamics (uniform / non-uniform contact pressure distribution)
- Special non-highway vehicle loading (e.g., End-Dump Truck, Forklift)
- Braking/Non-Braking condition (Interface Shear Stresses)
- Dynamic variation of tire load (Dynamic Loading Coefficient, DLC)
- Dynamic Modulus, $|E^*|$, from laboratory data or using the Witczak model for asphalt materials (34)
- Response computations at an array of points
- Text output (Text files and Microsoft Excel files)
- Graphical output

Figure 3.5 shows the main window of *3D-Move*. In the top left corner, a user needs to define the unit system to be used for the scenario under consideration. Also the user is prompted to input the project details and to define the analysis type: Static or Dynamic. At the bottom left corner the user starts specifying the vehicle loading condition followed by details of the pavement structures such as thickness and material type (viscoelastic or linear elastic).

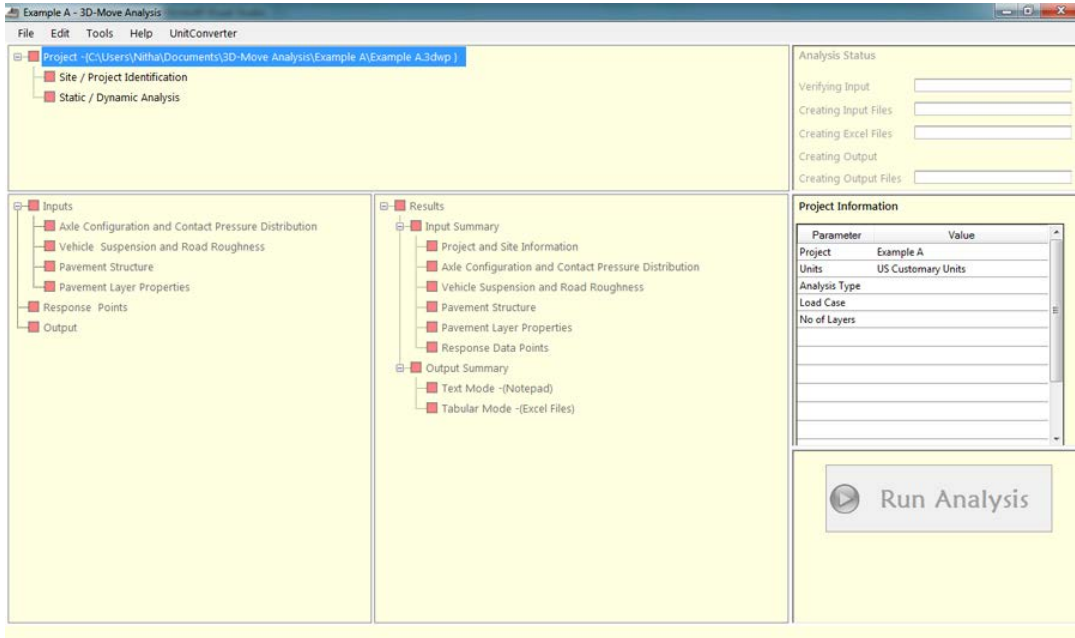


FIGURE 3.5 Main Window of *3D-Move* Analysis.

Figure 3.6 shows the pavement layers properties window for asphalt materials. Here, the asphalt layer material can be characterized as a linear elastic material or as a viscoelastic material. The dynamic modulus, $|E^*|$, is required for the viscoelastic analysis. $|E^*|$ can be input in three different ways:

Dynamic Modulus Lab Data

Asphalt materials properties can be specified using the dynamic modulus lab data. The *3D-Move Analysis* incorporates the master curve, which enables the input of dynamic modulus at any selected pavement temperature in the analysis. It uses an optimization tool which is independent of Microsoft Excel to construct the master curve from the lab data.

Witczak Model

In this version of *3D-Move Analysis*, the Witczak model (35) is included to calculate the frequency-dependent dynamic modulus based on the gradation and binder properties of the mixture.

User Defined Materials Properties

A set of data of $|E^*|$ as function of frequency can be specified by the user. Other input variables (Poisson's and Damping ratios) can be either specified as constants or as a function of frequency.

Pavement Layer Properties - Layer 1

Type of Material

Linear Elastic Material

Viscoelastic Material

Layer Thickness: 6 in

Note:

Dynamic Modulus Data

Witczak Model

User Defined Properties

Asphalt Mixture Properties | Asphalt Binder Properties | **|E*| Master Curve** | Asphalt General

Dynamic Modulus, |E*| | Damping Ratio and Poisson's Ratio

No of Temperatures: 3 | No of Frequencies: 3 | Reference Temperature: °F

Temperature (°F)	Dynamic Modulus E* , (psi)		
	0.1 Hz	0.5 Hz	1 Hz

Unit Weight: lb/in³

Cancel Previous Next OK

FIGURE 3.6 Pavement Layer Properties Window for Asphalt Materials.

The required properties for unbound materials are Young's modulus, Poisson's ratio, damping ratio and unit weight. Figure 3.7 shows the input window for unbound materials. Finally, response points can be defined as individual points or as an array of data points located in a vertical plane. Figure 3.8 shows the response points window.

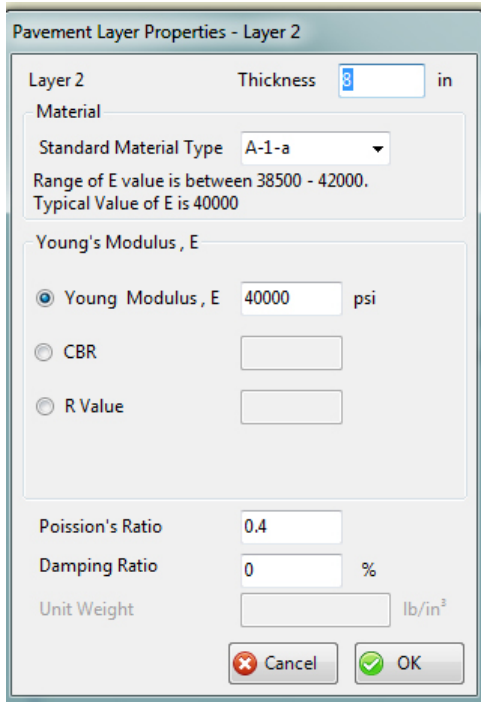


FIGURE 3.7 Layer Properties Window for Unbound Materials.

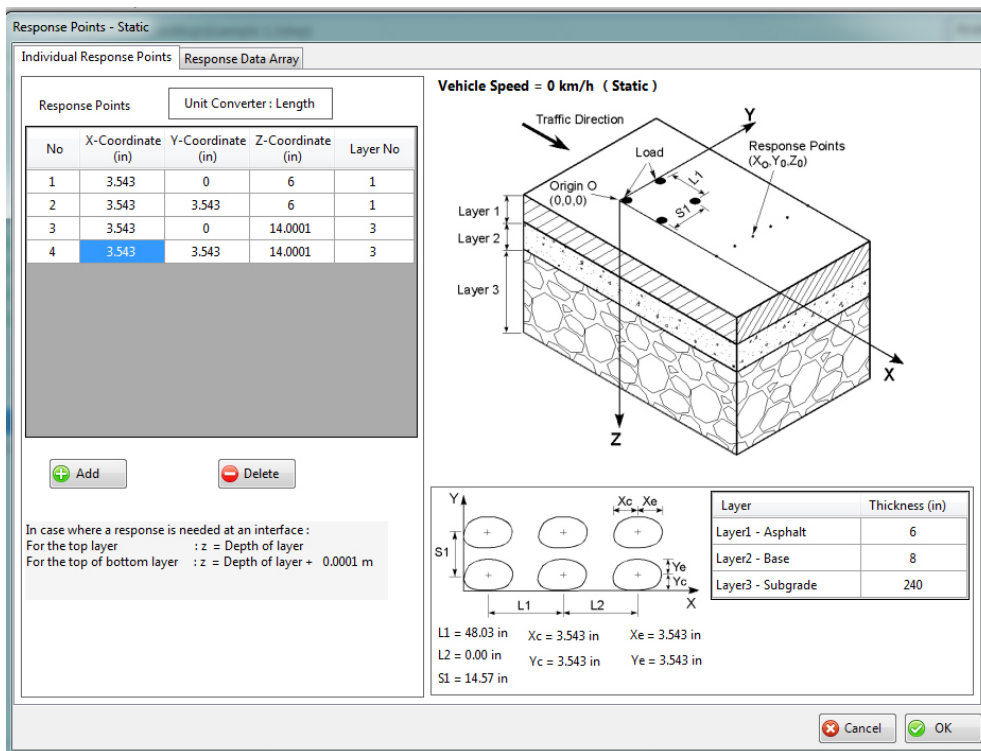


FIGURE 3.8 Response Points Window.

3.4 Summary

Two main experimental designs were created to accomplish the objectives of this study. In the first one, different ANN models used to predict layer moduli were trained using the software MatLab 7.10. Synthetic databases were created using a unique version of the software PerRoad. These ANN models were implemented and compared with backcalculated results. Backcalculated moduli were obtained from the NCAT test track FWD testing database. For the second design, the mechanistic analysis software *3D-Move* was used to determine the speed of a moving load that will produce a loading pulse equivalent to the loading pulse produce by the FWD. Pavement responses were calculated at that equivalent FWD speed and at different vehicle operational speeds. Correction factors were applied on predicted pavement responses obtained from backcalculated layer moduli to account for the difference between loading pulse durations. Finally, these corrected responses were compared with measured pavement responses from the NCAT test track.

The following chapter provides an overview of the tests sections from which the field information was acquired. Chapters five and six show the results related to ANNs and chapter seven the results from the moving loads/FWD analyses. A summary of findings, conclusions and recommendations are shown in the final chapters.

CHAPTER FOUR: TEST FACILITY AND SECTIONS PROPERTIES

Field information used in this study such as deflection basins, measured pavement responses and performance were obtained from the structural sections built at the National Center for Asphalt Technology Test Track in 2009. Such information was used for verification of ANN models and application of dynamic (moving loads) analyses aimed to achieve accurate pavement responses.

The NCAT Test Track is a facility where instrumentation is used to study many issues pertaining to mechanistic-empirical (M-E) design. The Test Track (FIGURE 4.1) is a 1.7 mile pavement test facility and consists of 46 test sections with various asphalt mixtures (FIGURE 4.2). Ten million equivalent single axle loads are applied over a two-year period with field performance documented weekly (40). It has been in operation for ten years and the construction of the fourth experiment cycle took place in 2009. Inclusion of instrumented sections started in 2003 (second cycle) where only eight sections were utilized for a structural experiment. Currently, that number has been doubled to sixteen sections.



FIGURE 4.1 The NCAT Test Track.

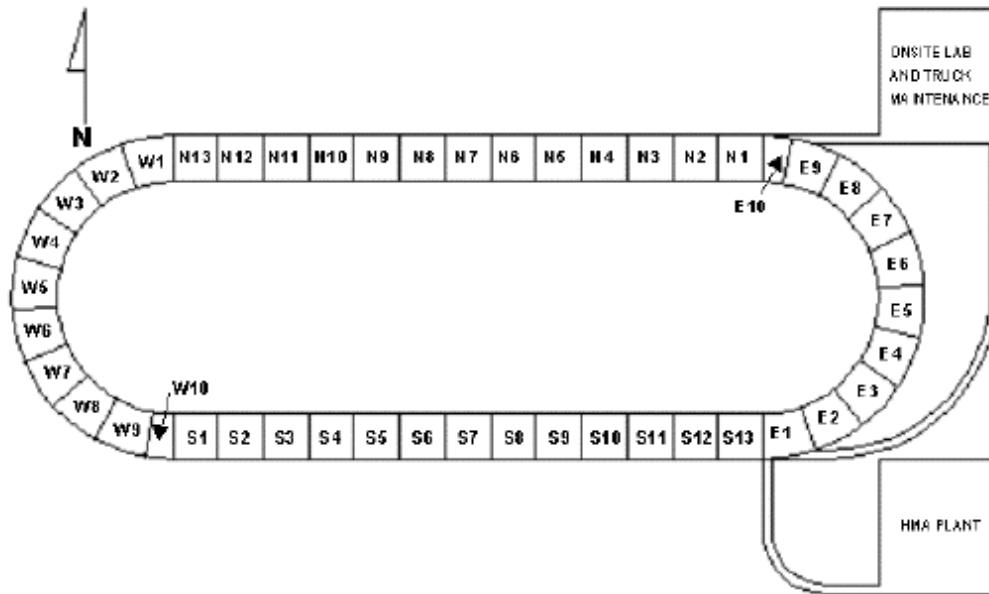


FIGURE 4.2 Layout of test track (40).

4.1 Test Sections

Two design gradations were used in this study. The surface layers utilized a 9.5 mm nominal maximum aggregate size (NMAS) while the intermediate and base mixtures used a 19 mm NMAS gradation. The aggregate gradations were a blend of granite, limestone and sand using locally available materials. These gradations were developed for each mixture (surface, intermediate and base) to achieve the necessary volumetric targets as the binder grade and nominal maximum aggregate size (NMAS) changed between layers. Figure 4.3 contains as-built thickness for each lift in each section. The primary differences between S9 (the control section) and the other eight sections were the mixture technology and overall AC thickness.

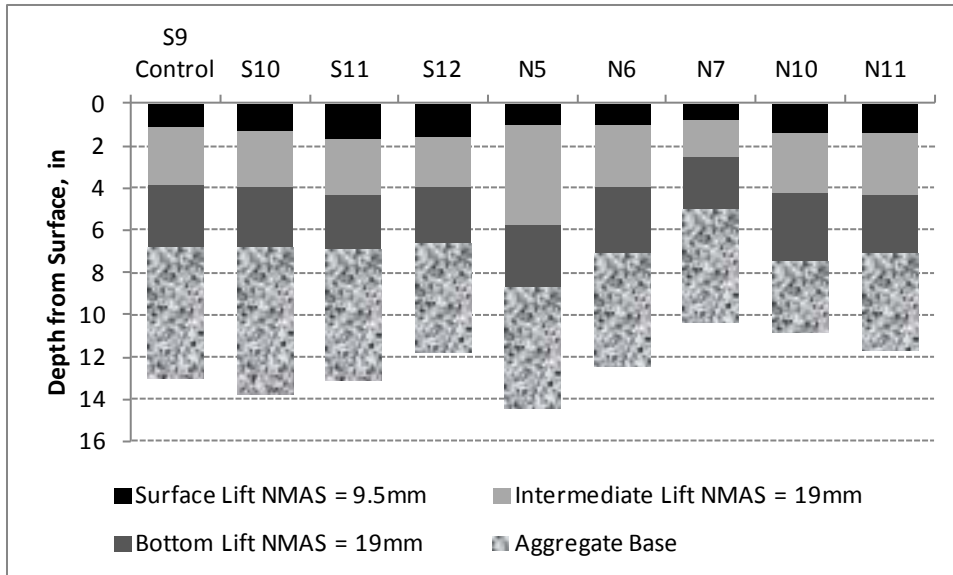


FIGURE 4.3 Structural sections at the 2009 NCAT Test Track.

Table 4.1 contains pertinent as-built information for each lift in all the studied sections. The primary difference between S9 (control) and sections S10 and S11 was the technology used to create the mixture at the plant. This technology allows production of asphalt mixtures at lower temperatures compared to conventional mixtures. This technology is known as warm mix asphalt (WMA). Each lift of S10 was produced with a foam-based WMA technology and each lift of S11 was produced with an additive. Further details of these types of mixtures can be seen elsewhere (41). The primary difference between S9 (control) and S12 was the 25% asphalt modifier used in S12 compared to conventional polymer modification used in the upper lifts of the control section. The virgin binder PG grade of the S12 mixtures was 67-28 which after modification resulted in a PG 76-16. The primary differences between S9 and N7 were the amount of polymer and overall AC thickness. Section N7 contained 7.5% styrene butadiene styrene (SBS) polymer in each lift while S9 utilized 2.8% SBS in the upper two lifts with no polymer in the bottom lift. The nominal binder PG grade of the modified mixtures in N7 was PG 88-22.

The surface layers in sections N5 and N6 were the same as in S9 (surface control mixtures). The intermediate lifts in N5 and lift 2 in N6 were designed to have 40% of a sulfur-

based modifier, while the bottom lifts in N5 and N6 were intended to have 30% modifier. Higher total asphalt contents in the lower lifts of N5 and N6 relative to the control resulted from designing these mixes with the expectation of better fatigue cracking performance. The primary difference between S9 (control) and sections N10 and N11 was amount of reclaimed asphalt concrete (RAP), the asphalt modifier and the technology used to create the mixture at the plant. Mixes in N10 and N11 were used without asphalt modifier and each lift was design to incorporate 50% RAP in the mixture. In addition, N11 was produced as a WMA mixture at the plant. The effect of the aged binder contained in the RAP resulted in the highest Superpave performance grade for the intermediate and bottom lifts of N10 (PG 94-10). Overall, all sections and lifts met or exceeded 92% of maximum theoretical density (less than 8.0% air voids).

TABLE 4.1 Asphalt Concrete Layer Properties – As Built

Lift	1-Surface								
Section	S9	S10	S11	S12	N5	N6	N7	N10	N11
%Modifier	2.8	2.8	2.8	25	2.8	2.8	7.5	0.0	0.0
PG Grade ^a	76-22	76-22	76-22	76-16	76-22	76-22	88-22	82-10	80-16
RAP ^b , %	0.0	0.0	0.0	0.0	0.0	0.0	0.0	50	50
Asphalt, %	6.1	6.1	6.4	6.1	6.1	6.1	6.3	6.0	6.1
Air Voids, %	6.9	7.5	6.4	5.5	5.9	6.2	6.3	7.4	8.0
Lift	2-Intermediate								
Section	S9	S10	S11	S12	N5	N6	N7	N10	N11
%Modifier	2.8	2.8	2.8	7.5	40	40	7.5	0.0	0.0
PG Grade ^a	76-22	76-22	76-22	88-22	67-22	67-22	88-22	94-10	88-10
RAP ^b , %	0.0	0.0	0.0	0.0	0.0	0.0	0.0	50	50
Asphalt, %	4.4	4.7	4.6	4.6	5.7	5.7	4.6	4.4	4.7
Air Voids, %	7.2	7.0	7.2	7.3	7.0	7.1	7.3	7.1	6.8
Lift	3-Base								
Section	S9	S10	S11	S12	N5	N6	N7	N10	N11
%Modifier	0.0	0.0	0.0	25	30	30	7.5	0.0	0.0
PG Grade ^a	67-22	67-22	67-22	76-16	67-22	67-22	88-22	94-10	88-10
RAP ^b , %	0.0	0.0	0.0	0.0	0.0	0.0	0.0	50	50
Asphalt, %	4.7	4.7	5.0	4.9	6.2	6.1	4.6	4.7	4.6
Air Voids, %	7.4	7.9	6.2	6.1	6.4	6.3	7.2	5.0	5.8

^aSuperpave Asphalt Performance Grade

^b Reclaimed asphalt pavement

4.2 Traffic

Trafficking at the 2009 Test Track was conducted using four triple flat-bed trailer trucks (Figure 4.4) and one triple box trailer which loaded the pavement five days per week. Trafficking began in August, 2009 and ended in September, 2011 after approximately 10 million ESALs had been applied to the pavement structures. Table 4.2 provides the axle weights for each of the five trucks under normal loading conditions. The trucks were normally operated at 45 mph.



FIGURE 4.4 Example of the triple flat-bed trailer truck.

TABLE 4.2 Axle weights (lbs) for trucking fleet at NCAT Test Track

Truck #	Steer	Front Drive Tandem	Rear Drive Tandem	Single # 1	Single # 2	Single # 3	Single # 4	Single # 5
1	9,400	20,850	20,200	20,500	20,850	20,950	21,000	20,200
2	11,200	20,100	19,700	20,650	20,800	20,650	20,750	21,250
3	11,300	20,500	19,900	20,500	20,500	21,000	20,650	21,100
4	11,550	21,200	19,300	21,000	21,050	21,000	20,750	20,800
5	11,450	20,900	19,400	20,100	20,450	21,000	20,050	20,650
Average	10,980	20,710	19,700	20,550	20,730	20,920	20,640	20,800

4.3 Performance Monitoring

Surface condition studies were conducted every Monday to document performance of all experimental sections. Field performance evaluations focused on the middle 150 feet of each 200-foot test section to eliminate the effects of transitions near section ends. The ARAN (Automated Road Analyzer) van was used to capture rutting measurements and texture while driving at highway speeds. Rutting was quantified by determine the depth of the permanent deformation at the wheel paths; texture was quantified using the mean texture depth (MTD) and the international roughness index (IRI) was used to quantify the amount of roughness. Cracking was determined by manually inspecting the surface of the test sections.

During the two-year research cycle, the control section was subjected to FWD testing three Mondays per month. The remaining sections were tested several Mondays per month (Figure 4.5). Within each section, twelve locations were tested with three replicates at four drop heights (6, 9, 12 and 16 kip loads). The three repetitions of each loading scenario were recorded in the inside wheelpath, outside wheelpath, and between the wheelpaths at three random locations over the length of the test section. A fourth location, the middle of the gauge array, was also part of the regular FWD testing scheme (Figure 4.6).



FIGURE 4.5 Falling weight deflectometer testing at the Test Track.

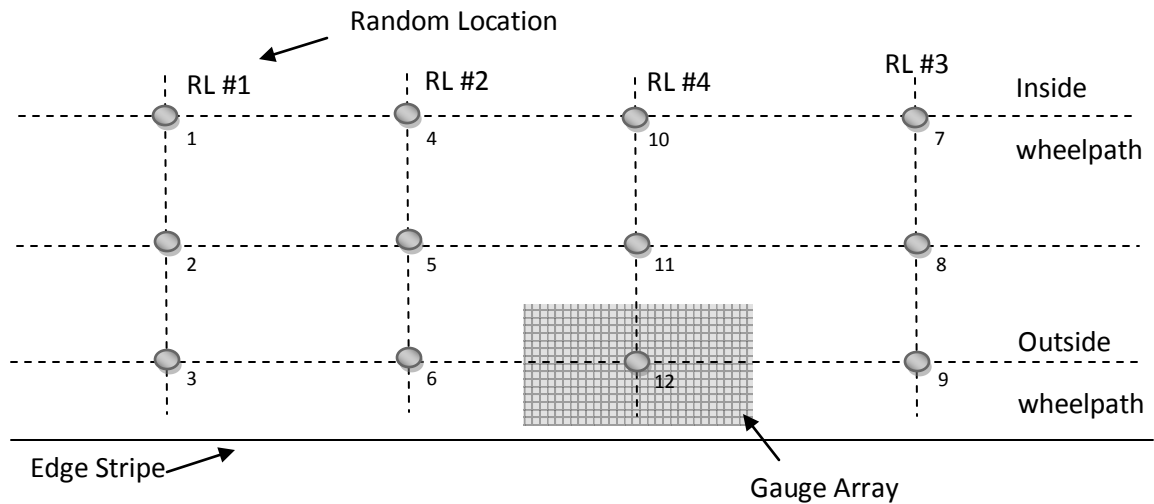


FIGURE 4.6 Schematic of test locations.

4.4 Pavement Instrumentation

Information obtained from the last two Test Track research cycles that is related to the installation of gauges, methodology for data collection and data analysis has been well documented (41-43). A typical structural section at the Test Track contained 12 strain gauges and two pressure cells (Figure 4.7). One earth pressure cell was placed at the top of the base material layer and the other on top of the subgrade material layer. The strain gauge array was centered along the outside wheel path of the pavement structure. The array consisted of two rows of three longitudinal gauges and two rows of three transverse gauges. Each asphalt gauge had an offset of 2 ft from each other (43). All these devices were connected to a data acquisition unit. During gauge installation, trenches for the conduits containing the cables and cavities for pressure cells were excavated. Prior to the placement of the next layer these elements were hand-backfilled and hand-compacted. Finally, all the asphalt strain gauges were covered with the respective mix sieved through the No. 4 sieve prior to compaction by rollers. Temperature probes were also installed in each structural section. Probe bundles were designed on a per-section basis where the tips of the

temperature probes measured the surface temperature, mid-depth temperature, full-depth temperature, and the temperature three inches into the aggregate base material.

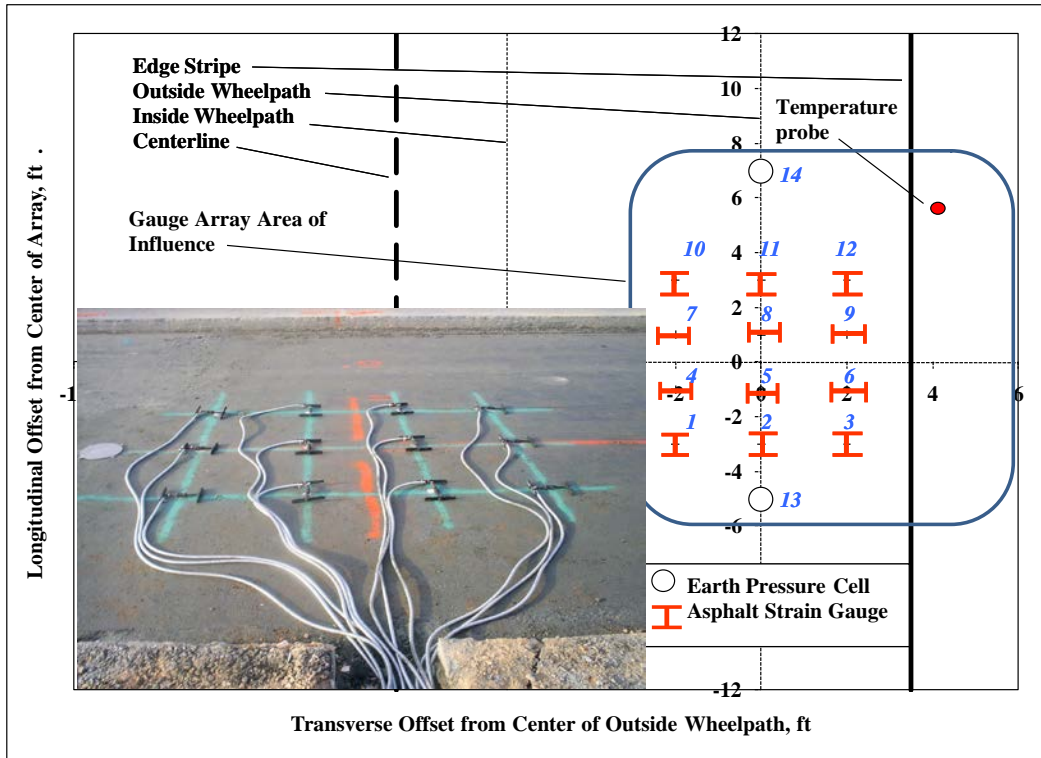


FIGURE 4.7 Typical strain gauge array.

Dynamic pavement responses were measured weekly at the Test Track. During the collection process, strain and pressure were measured for three passes of the five test vehicles on each test section. Further details regarding data processing are documented elsewhere (44). These measurements were then compiled into a database where a representative strain response (95th percentile strain) was calculated for a given axle type each day of testing. Each strain response was defined as an amplitude (Figure 4.8) while a maximum value (peak) was used to define stress (Figure 4.9). The amplitude was taken as the difference between the preceding inflection point and the peak reading.

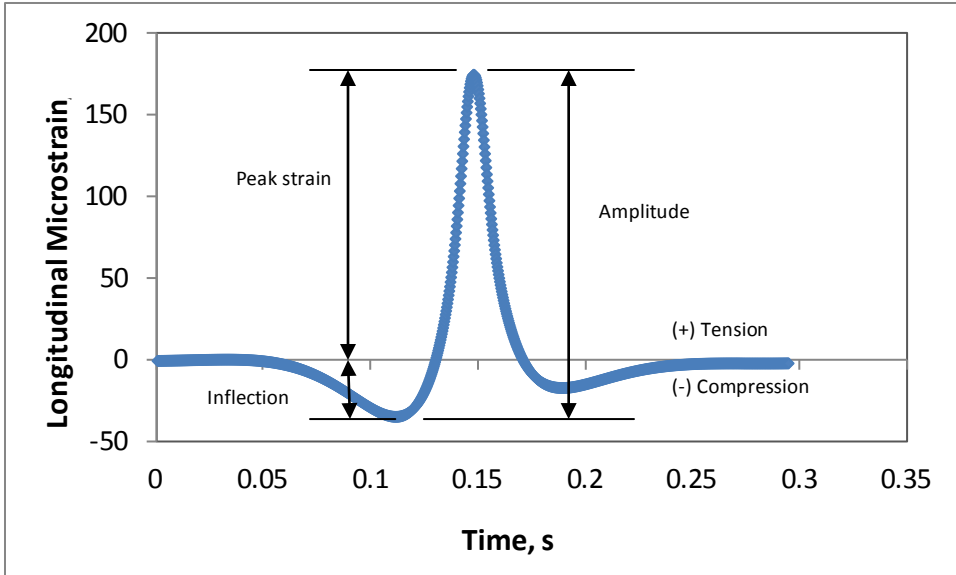


FIGURE 4.8 Strain amplitude definition.

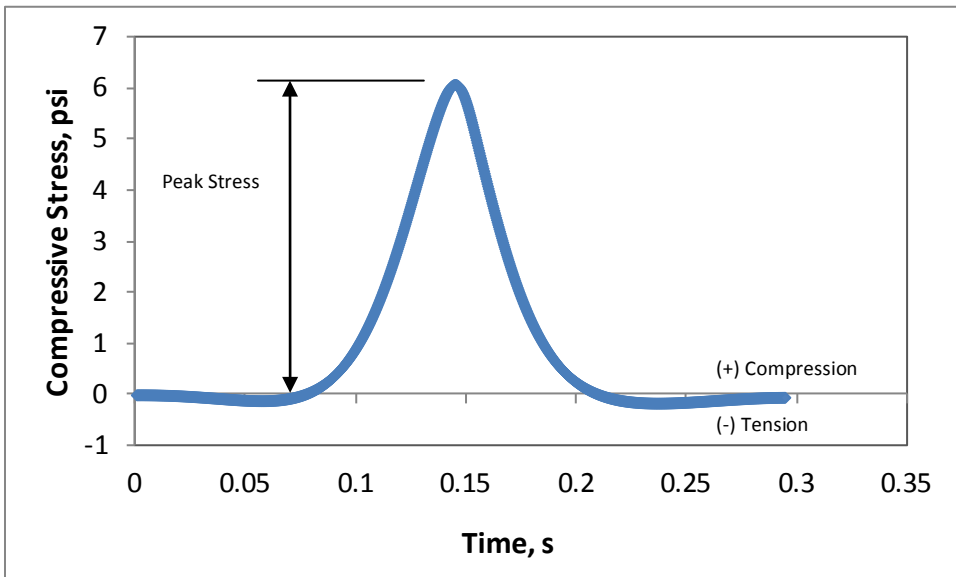


FIGURE 4.9 Example of compressive stress signal.

4.5 Low Volume Road Section

FWD testing was performed in 2012 on a small segment of Lee Road 159 in Auburn, AL. This section was selected by NCAT as an experimental project to investigate different pavement preservation strategies. For this study, this section was selected to further validate the results obtained from a highly controlled facility such as the NCAT Test Track and apply these results to typical roadways found in Alabama. Contrary to the highly characterized sections at the Test Track, the only known fact about this roadway is that the foundation (subgrade material) is similar to the one found at the Test Track. The thickness of the asphalt concrete layer was calculated to be 5.75 inches and the thickness of the granular base was estimated to be 6.0 inches. The length of the section was 2500 ft and FWD testing was performed at 51 stations equally distance from each other (every 50 ft). Figure 4.10 shows an overview of the condition of this section.



FIGURE 4.10 Condition of the low volume road section.

4.6 Summary

All the field information used in this study was collected mainly at the Test Track. A brief description of the test facility and test sections was necessary to provide a background concerning the available information and to help explain observed trends. Information such as FWD tests results and backcalculated layer moduli was used for verification of ANN models. On the other hand, information regarding measured pavement responses was used in dynamic (moving loads) analyses aimed to incorporate viscoelastic properties of asphalt concrete mixtures and to help obtain accurate pavement responses. Results from FWD testing and measured pavement responses are shown in chapters 6 and 7, respectively.

CHAPTER FIVE: ASSESSMENT OF CONVENTIONAL BACKCALCULATION AND ARTIFICIAL NEURAL NETWORKS

The analysis of conventional backcalculation was performed to investigate the non-uniqueness of the results when setting different initial conditions. The software EVERCALC 5.0 was used to analyze the effect of the level of tolerance, calculated by means of the root mean square error (RMSE), on estimated pavement layer moduli. Artificial Neural Networks were created to perform forward calculations of pavement layer moduli and critical responses from non-destructive synthetic information. Synthetic databases were created using a modified version of the software PerRoad for a three-layer flexible pavement. Other analyses performed in this chapter included the potential use of ANNs to predict layer thickness and the potential errors in pavement layer moduli backcalculation due to improper modeling of the layer interface condition.

5.1 Effect of Tolerance Error on Backcalculated Moduli

The backcalculation of pavement layer moduli is commonly carried out by assuming a set of pavement-layer moduli (seed moduli) that can produce a deflection basin similar to the measured one from the FWD test. To minimize the error between the measured and calculated deflections, the relative root-mean-square error (RMSE) is used to control the convergence of the backcalculated deflections and to assess the acceptance or rejection of the final set of pavement moduli. To study the effect of the RMSE on the moduli and strains in flexible pavements, a three-layer pavement section was selected. The flexible pavement section containing a range of thicknesses and moduli for a total of 2000 combinations is shown in Figure 5.1. Responses were forward-calculated for a circular load with a radius of 5.91 in and a load of 9,000 lb using a modified version of the software PerRoad. The backcalculated moduli, pavement responses and the associated error were determined using EVERCALC for three different levels of RMSE tolerance (0.1%, 1.0% and 3.0%). The range of moduli was first kept similar to the ones shown in Figure 5.1 and then expanded by 50%. The seed moduli were set in all cases as the midpoint of the range.

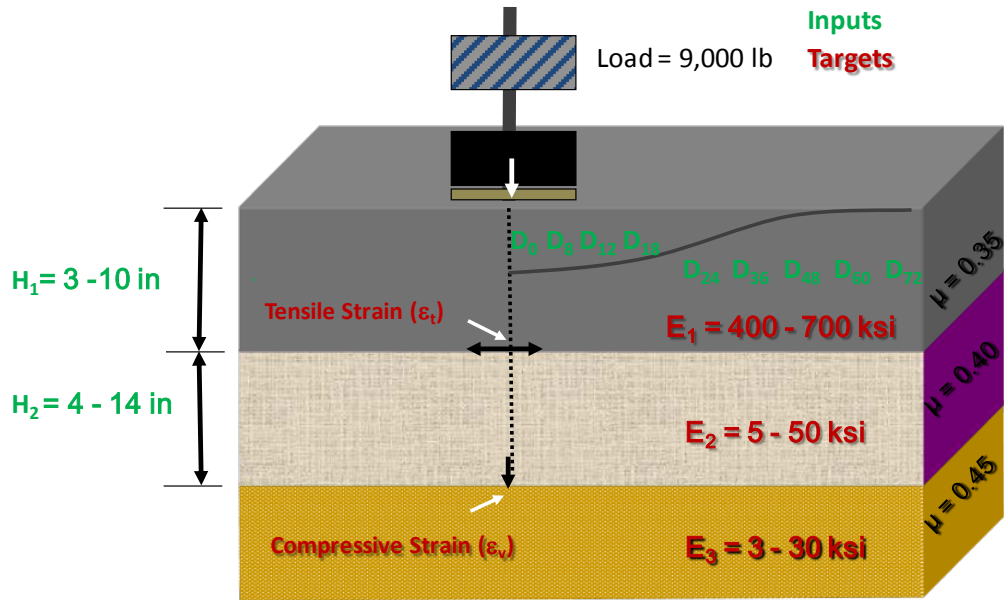


FIGURE 5.1 Schematic of pavement structure.

The effect of RMSE tolerance error on estimated moduli can be observed in Figures 5.2 and 5.3. Since the dataset used for this exercise was synthetic, it was expected to have backcalculated moduli highly correlated to the actual values when the tolerance level was set to 0.1% and applied on synthetic deflection basins. This behavior was achieved at a tolerance level of 0.1% which showed the highest R^2 values (above 0.9) and the lowest standard error of the estimate/standard deviation (Se/Sy) values (below 0.35) as shown in Figure 5.2.

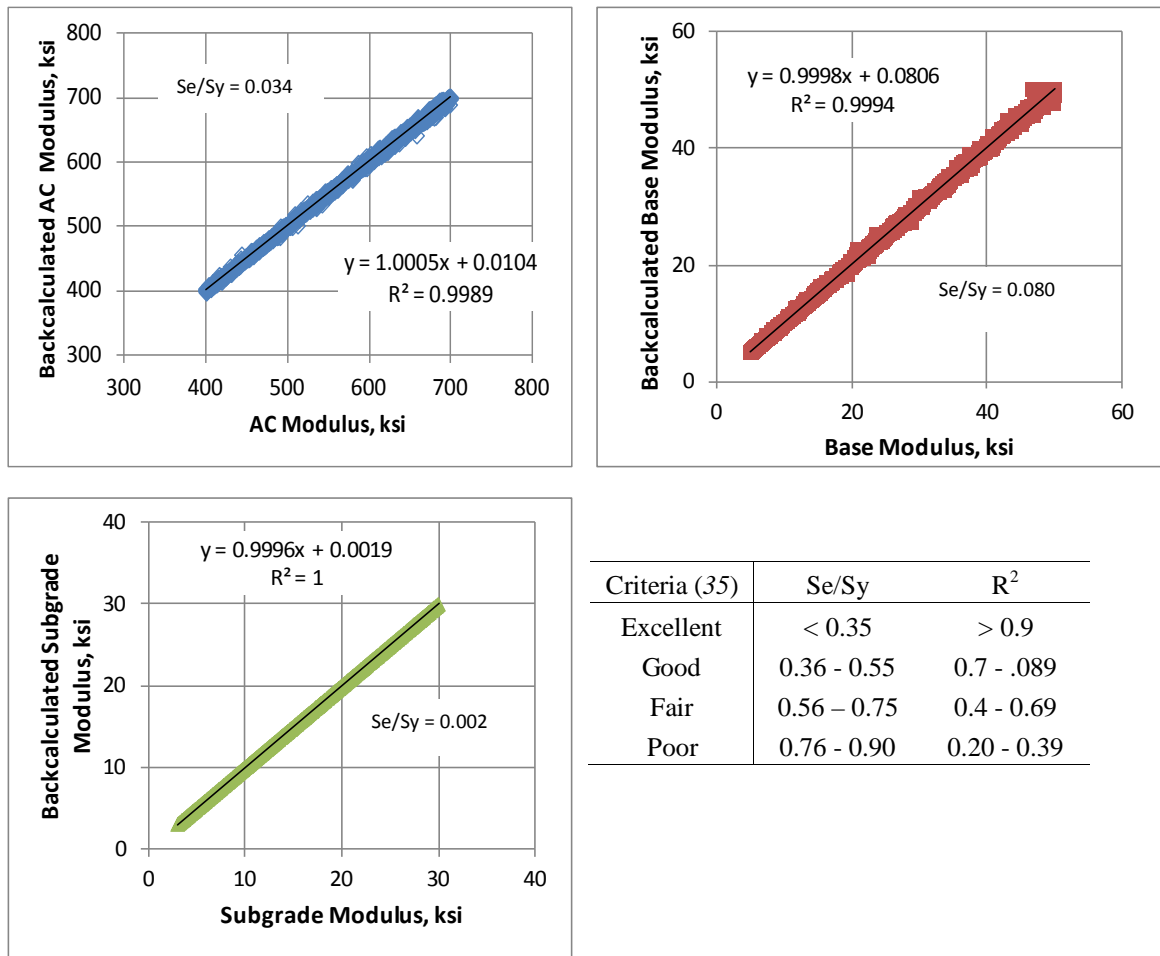


FIGURE 5.2 Estimated moduli at a 0.1% tolerance level.

As can be seen in Figure 5.3, at a tolerance level of 1.0%, the data seemed to be slightly scattered with strong correlations (high R^2 values) for the asphalt concrete layer (top layer) and base layer moduli. In the case of subgrade moduli the results still met the excellent criteria. When the level of tolerance was increased to 3.0% the data became highly scattered and the correlation had a significant decrease especially in the case of the top layer. It can be seen that some data points tended to reach the upper limit of the moduli range which could be an indication that the process tended to overestimate the moduli of the top layer. Even at a set tolerance level of 3.0% the results in terms of subgrade modulus were little or not affected.

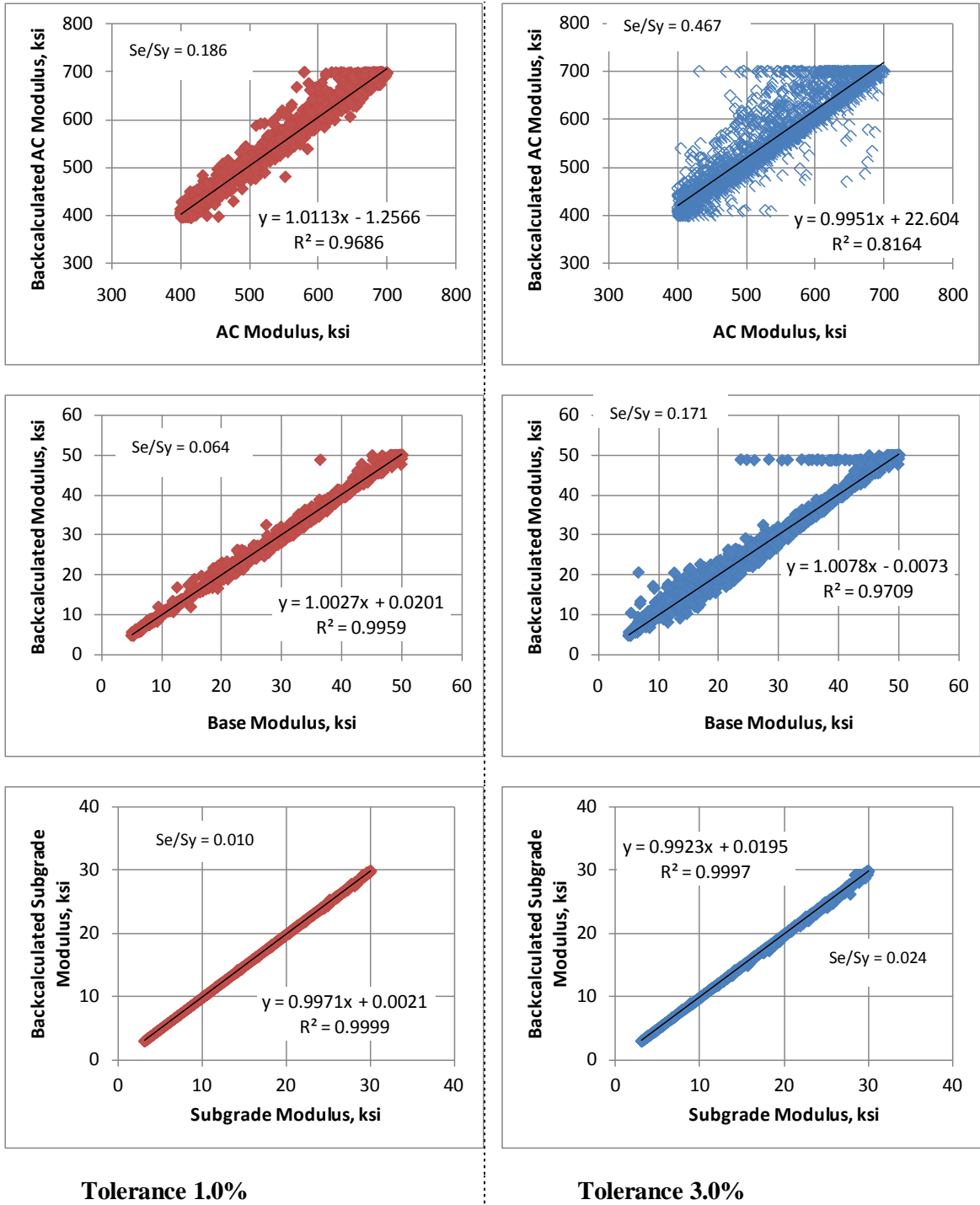


FIGURE 5.3 Estimated moduli at two different tolerance levels.

Overall, as the tolerance level was increased the R^2 values decreased and the Se/Sy values increased for the top and base layer moduli. The top layer modulus was the most affected by the

increase on the level of tolerance. As mentioned in the literature review, if the limits were too broad, these would allow the program to converge to an incorrect solution. The highlighted values on Table 5.1 represent backcalculated moduli using wider seed ranges to make sure the process could not reach the upper or lower limits. This action decreased even more the R^2 values and increased Se/Sy values with the top layer moduli being the most affected (the program converged to an incorrect solution).

TABLE 5.1 Effect of tolerance error on estimated moduli

Tolerance	RMSE	Modulus	R^2	Se/Sy	R^2 (E)	Se/Sy (E)
0.1	0.01 - 0.21	E1	0.999	0.034	0.999	0.039
		E2	0.999	0.026	0.999	0.026
		E3	1.000	0.002	1.000	0.002
1.0	0.01 - 1.0	E1	0.969	0.186	0.959	0.202
		E2	0.996	0.064	0.995	0.076
		E3	1.000	0.010	0.999	0.011
3.0	0.01 - 2.98	E1	0.816	0.476	0.738	0.589
		E2	0.971	0.171	0.979	0.145
		E3	1.000	0.024	0.999	0.027

(E) Expanded moduli range
 E1 Modulus of the AC layer
 E2 Modulus of the granular base
 E3 Modulus of the subgrade

5.2 ANN vs. conventional backcalculation process

Figure 5.4 is an example of performance curves normally applied for training ANN. For this exercise, the same flexible pavement section shown in Figure 5.1 was used. The database consisted of 10,000 combinations of thicknesses and moduli. Deflection basins and critical pavement responses were forward calculated using a modified version of the software PerRoad. Layer thicknesses H1 and H2 along with nine deflections were used as inputs for this network. Layer moduli and pavement responses were used as targets.

In an analogy to the brain, an entity made up of interconnected neurons, neural networks are made up of interconnected processing elements called “units”, which respond in parallel to a set of input signals given to each. This “unit” is the equivalent of its brain counterpart, the neuron.

To make the connection between inputs and targets an intermediate layer containing the neurons has to be defined. This intermediate layer is also called hidden layer. The ANN for this exercise had one hidden layer with 20 neurons and the network was trained using the neural network application of the software MATLAB 7.1. The selection on the appropriate number of neurons is a trial and error process. Under-fitted models with high bias can be obtained with the use of too few neurons in the hidden layer. On the other hand a model too difficult to train (too complex) can be produced when too many neurons are used in the hidden layer. This difficulty to train a network also had to do with memory and time constraints. In this case, the best result was obtained with the use of 20 neurons.

The training process for this type of ANN can be explained as follows: In general, under-fitted models will have a high bias and over-fitted models will have a high variance. To avoid either of these, the network is normally divided into two main sets: training and validation, and sometimes a testing set is included. The network is trained using only the training data. The training process is continuously tested for performance using the independent validation set. The testing data set is used to check the applicability of the network on a completely independent dataset. While the performance of the training data will continue improving and leading to over-fitting, performance on the validation set will stop improving, and will typically get worse. Therefore, training stops where performance on the validation set is optimal. For this example, the network had a typical setting of 80/10/10 which means that the input vectors and target vectors were randomly divided, with 80% used for training, 10% for validation and 10% for testing.

To determine when to stop training the network for this exercise, the performance measure “Mean Square Error” (MSE) was used. This training stopped when the validation error increased for six iterations, which occurred at iteration 507 as can be seen in Figure 5.4. The result seemed to be reasonable because 1) the final mean-square error was small, 2) the test set error and the validation set error had similar characteristics and 3) no significant over-fitting (the

model does not have a high variance) has occurred by iteration 507 (where the best validation performance occurred).

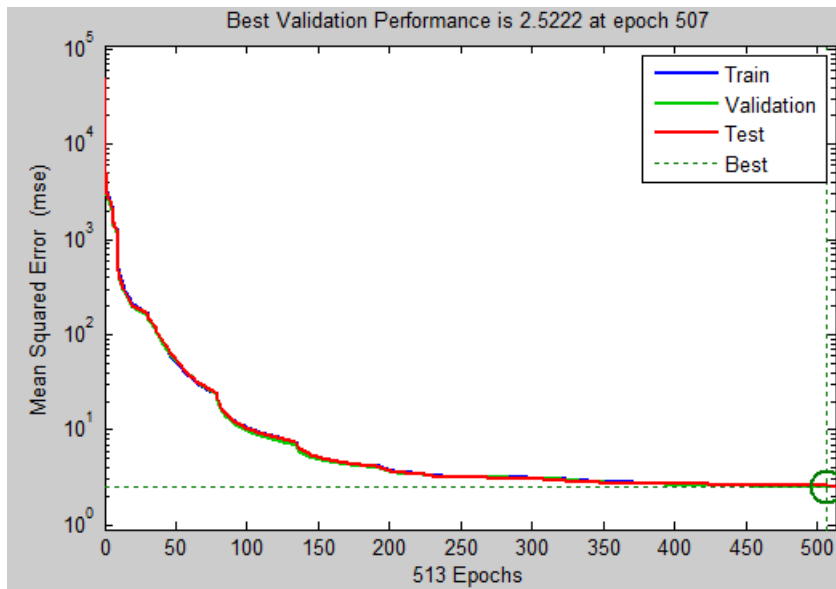


FIGURE 5.4 Training performance plot.

Table 5.2 shows the effect of the number of neurons in the hidden layer on the training of two networks: layer moduli and strain responses. In general, as the number of neurons increased, the number of iterations (epochs) and training time increased, especially for predicted strain responses. On the other hand, the mean square error decreased as the number of neurons increased, especially for predicted layer moduli. Though the R^2 values slightly increased, these could be considered insensitive to the change in number of neurons. This result indicated that R^2 values cannot be used solely as indicators of performance and a combination of parameters, MSE values and R^2 values, are needed to evaluate performance.

While training a network could take several hours, calculating results from a trained network only takes several seconds. For instance, it took about 4 hours, on average, to train the networks in this chapter; however, it only took about 2 seconds to obtain the outputs from the synthetic input dataset. On the other hand, obtaining the backcalculated moduli can be time consuming. For example, it took about 5 minutes to backcalculate 2000 deflection basins (the

results shown in Table 5.1) at a level of tolerance of 3.0% and about 10 minutes at 0.1% tolerance level. This is important for agencies and researchers that may be dealing with relatively large data sets spanning years of testing.

TABLE 5.2 Effect of number of neurons on training

Parameter/Range	Neurons	Epochs	Time, s	MSE	R ²
E1, E2, E3 3 - 700 ksi	2	200	165	92	0.9982
	6	250	277	18	0.9994
	12	420	1092	5.17	0.9998
	20	490	2204	2.38	0.9998
	30	765	5436	1.43	0.9998
ε_t and ε_v 100 - 3000 μ	2	200	178	4210	0.9628
	6	300	440	675	0.9940
	12	684	1833	78.5	0.9992
	20	710	3155	27.4	0.9996
	30	897	6473	9.7	0.9998

As mentioned above, the learning method used to develop these ANN models was a feed-forward back propagation with the sigmoidal function, equation 5.1, as the transfer function. It was found that the two-layer network with 20 nodes in the hidden layer was the most appropriate for this dataset. The basic form of the ANN is given by equations 5.1 through 5.3. For these equations, a single index indicates an array; dual indices represent a matrix with the first letter indicating the values in the row and the second letter indicating the values in the column. The index i represents the input parameters and the index k represents the hidden layer.

$$f(T) = \frac{2}{1+e^{-2T}} - 1 \quad \text{Eq. 5.1}$$

$$H_k^1 = B_k^1 + \sum_{i=1}^m W_{ik} P_i \quad \text{Eq. 5.2}$$

$$\text{Output} = f(B_o + \sum_{j=1}^m H_k^1 W_k) \quad \text{Eq. 5.3}$$

Where;

T = placeholder variable,

H_k^1 = transferred value of nodes at the hidden layer,

P_i = input variables,

W_{ik} = weight factors for the hidden layer,

W_k = weight factors for the output layer,

B_k^1 = bias factors for first layer,

B_0 = bias factor for outer layer,

m = number of nodes in hidden layer,

Output = layer moduli or pavement responses.

Table 5.3 shows a comparison between backcalculated and ANN-predicted layer moduli along with critical pavement responses. Backcalculated results were obtained using EVERCALC for a level of tolerance of 0.1%, as previously shown in Table 5.1. When comparing the results using simple correlation, both methodologies seemed to have similar R^2 values for all the parameters. On the other hand, ANN-predicted values seemed to have slightly higher Se/Sy values. The results also suggested that ANN-predicted parameters can be equivalent to backcalculated parameters calculated at a level of tolerance as low as 0.1%.

TABLE 5.3 Comparison of backcalculated and ANN predicted parameters

Parameter	Range	Backcalculated		ANN Predicted	
		R^2	Se/Sy	R^2	Se/Sy
E1	400 - 700 ksi	0.999	0.034	0.999	0.034
E2	5 - 50 ksi	0.999	0.026	0.996	0.064
E3	3 - 30 ksi	1.000	0.002	1.000	0.004
ϵ_t AC	300 - 650	1.000	0.005	1.000	0.014
ϵ_v Sub	100 - 2100	1.000	0.006	1.000	0.022

5.3 Removing the Input Variable “Thickness”

In conventional backcalculation, the thickness of the structure is an indispensable input variable and without knowing the thickness the process cannot be performed. In ANNs adding or removing input variables can be performed without completely interrupting the prediction process. Therefore, several ANNs were trained with and without the inputs H1 (asphalt concrete

thickness) and H2 (granular base thickness). Figures 5.5 and 5.6 show the effect of predicting strain responses and layer moduli, respectively, when thicknesses are removed from the analysis. In terms of strain responses (Figure 5.5), removing the thicknesses produced more scattered results and higher variability (higher Se/Sy values). The compressive microstrain (ϵ_v) located at the top of the subgrade was more affected than the tensile microstrain calculated at the bottom of the top layer. Data were more scattered with a significantly higher Se/Sy value and a lower R^2 value was obtained for ϵ_v .

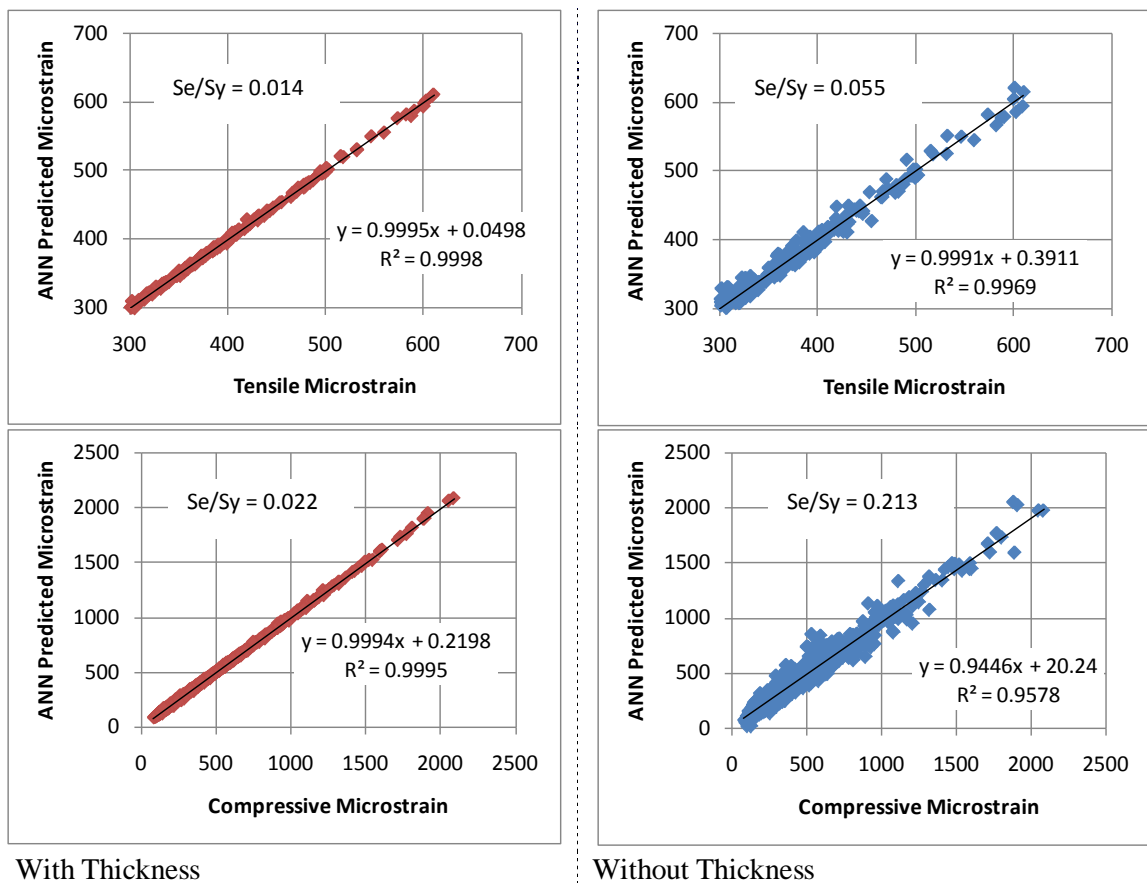
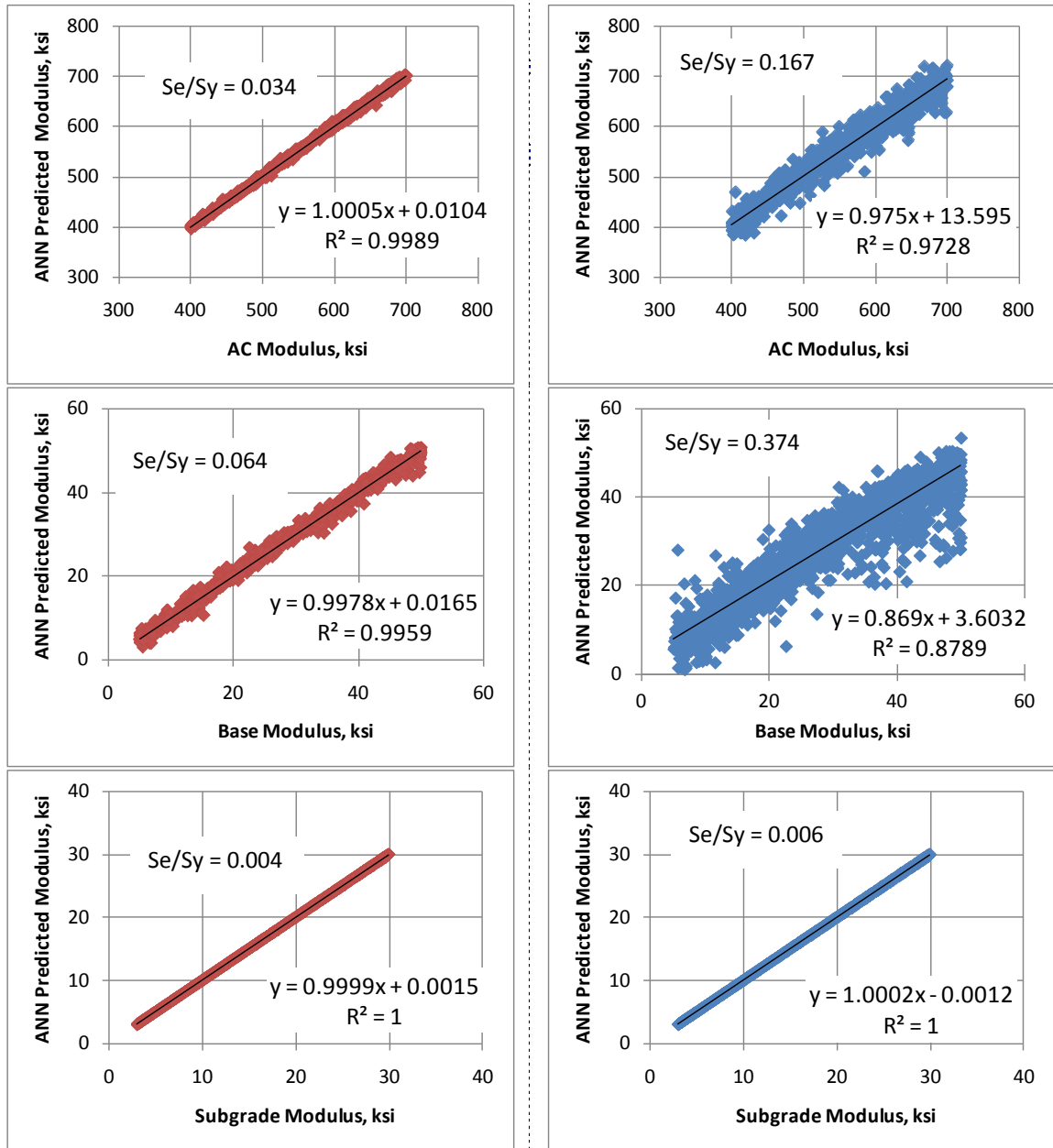


FIGURE 5.5 Predicted responses from ANN with and without thickness.

In terms of predicted layer moduli, the results showed that the most affected parameter was the base modulus with the lowest R^2 value and the highest relative increase in the Se/Sy value. This was followed by the top layer modulus and finally the subgrade modulus which was

not sensitive to the input variables H1 and H2. In general, ANNs without the thicknesses H1 and H2 as inputs tended to produce more scattered results with higher relative errors. However, material properties and pavement responses can still be estimated at a fair level of accuracy given the scenario that thicknesses are unknown.



With Thickness

Without Thickness

FIGURE 5.6 Predicted layer moduli from ANN with and without thickness.

5.4 Potential Use of ANNs to Predict Layer Thickness

The same synthetic dataset previously mentioned in this chapter was used to evaluate the possibility to predict pavement layer thickness from deflections only. Different ANNs were trained to predict the thickness of the AC layer (H1), the base thickness (H2) and the total thickness placed over the subgrade (H1+H2). Figure 5.7 shows the results obtained from this analysis using ANN. The results indicated that H1 can be easily predicted from synthetic deflection basins. On the other hand, prediction of H2 was difficult and highly scattered results were obtained in this process (Figure 5.7.b). Determination of the total pavement structure (H1+H2) also produced highly scattered results (Fig. 5.7.c) and a different attempt to predict H2 from deflections and H1 as input variables (Fig. 5.7.d) reflected the poor capability for ANNs to predict the thickness of the base layer.

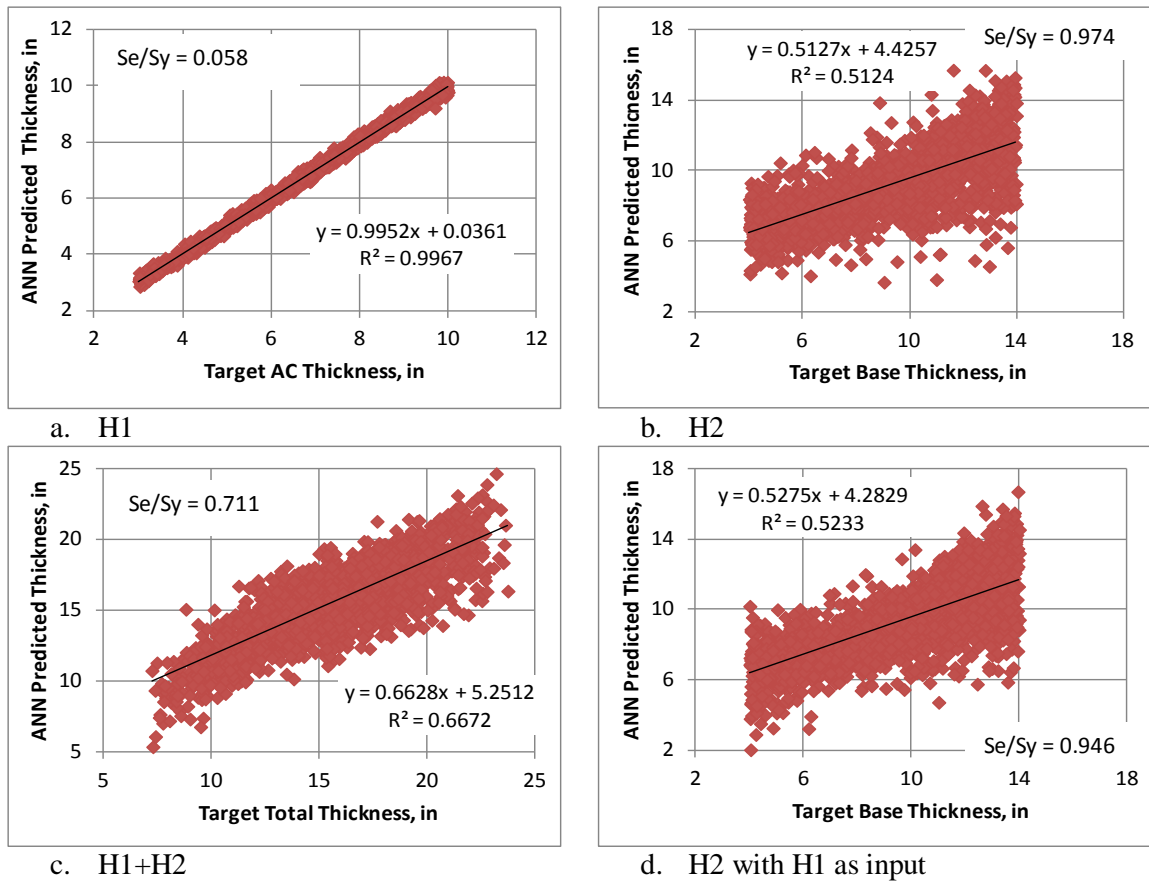


FIGURE 5.7 ANN Predicted thicknesses.

A three layer flexible pavement structure was modeled using the software WESLEA to evaluate the relationship between deflection and thickness. A baseline structure had the following properties: H1=7 in, H2 = 8 in, E1= 500 ksi, E2 = 30 ksi, E3 = 10 ksi. Seven more structures were generated by changing some of these properties. The center deflection (D0) was forward calculated for a circular load with a radius of 5.91 in and a load of 9,000 lb. To evaluate the effect of H1 on D0, H1 was varied while the remaining properties were kept constant for the different scenarios. Figure 5.8 shows a strong relationship (logarithmic type) between H1 and D0 for all the cases. This strong relationship indicates that H1 can be considered as good predictor of D0 and vice versa. Therefore, this can be used to explain the theoretically high predictability of H1 when using ANNs.

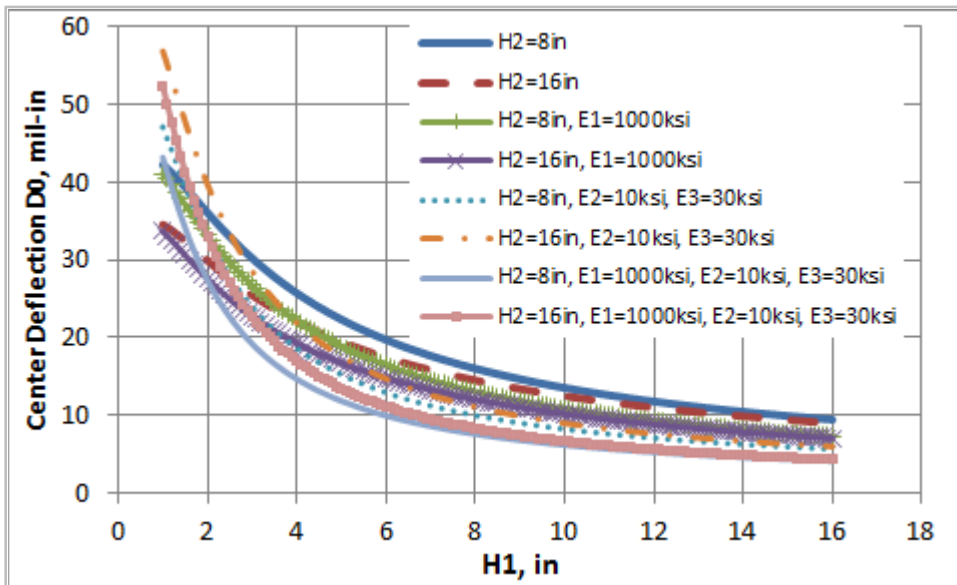


FIGURE 5.8 Effect of H1 on deflection.

To evaluate the effect of H2 on D0, H2 was varied while the remaining properties were kept constant for the different scenarios. Figures 5.9 and 5.10 show a great variability in relationships between H2 and D0 contrary to the unique trend for H1. The change in the observed trend not only led to poor relationships but also indicates that a wide variety of H2 values can be

associated with the same or similar deflection. This indicates that H2 can be considered as poor predictor of D0 and vice versa explaining the poor predictability of H2 when using ANNs.

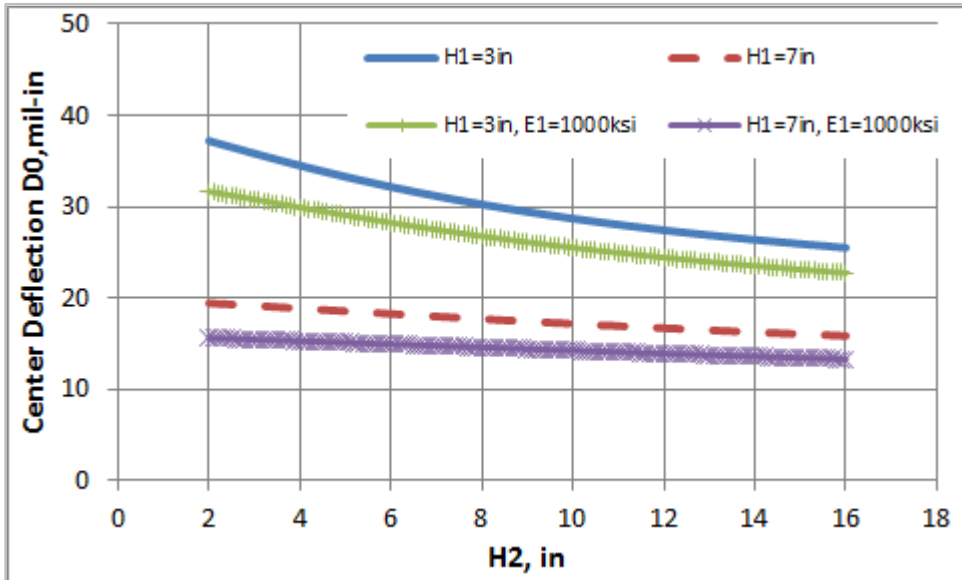


FIGURE 5.9 Effect of H2 on deflection.

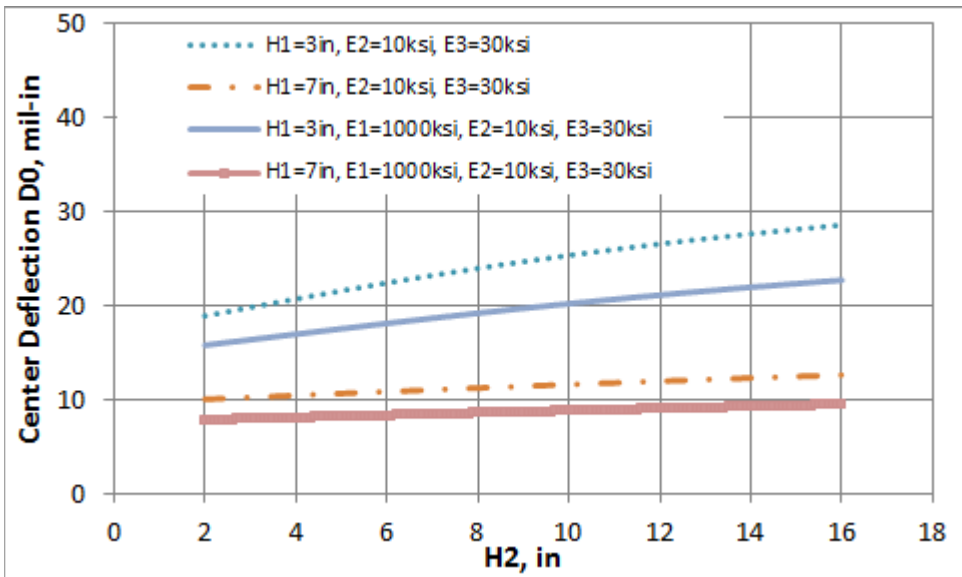


FIGURE 5.10 Effect of H2 on deflection-continued.

Further investigation was performed to evaluate the use of different number of input variables on ANNs as another attempt to predict pavement layer thickness. The effect of number

of deflections (sensors) on the ANN used to estimate the total thickness of a three-layer pavement structure (H1+H2) is shown in Figure 5.11. Four different networks were trained using 4, 7, 9, 11 and 13 deflection sensors as inputs. The 7 and 9 sensor configurations are typical in FWD testing (45-46). An increase in the number of sensors between 4 and 7 showed a significant reduction in error and significant increase in R^2 values. Increasing from 9 to 11 sensors had very little effect on the calculated error and the use of more than 11 sensors had no effect on the ANN performance. A configuration of 13 sensors where not only the number of variables was increased but the sensor spacing was changed did not have a significant effect in reducing the error. Therefore, little or no gain was obtained in the attempt to improve the predictability of the total thickness. In general, the results showed that the minimum recommended sensor configuration should be 7.

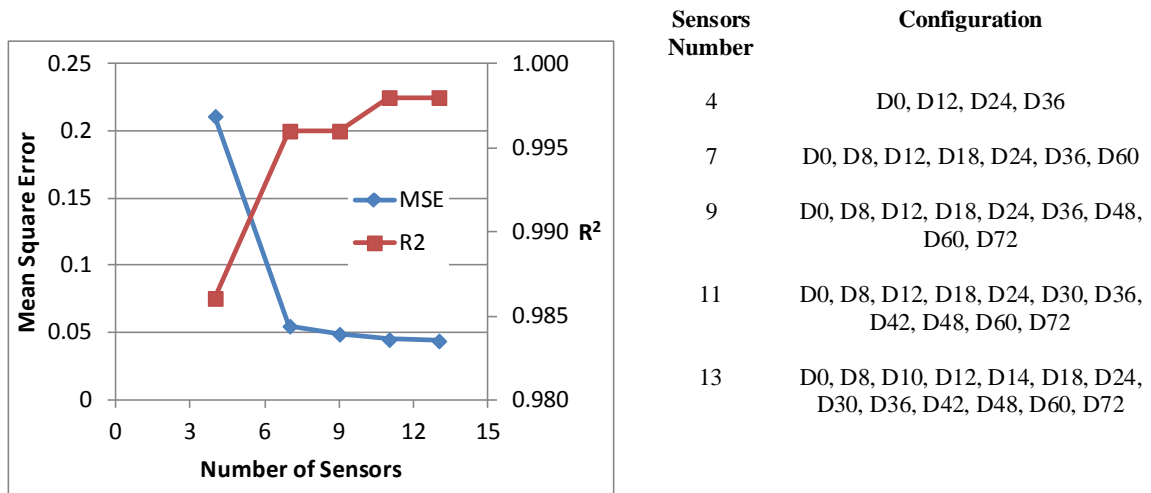


FIGURE 5.11 Effect of number of deflections (sensors) on training performance.

The analyses performed up to this point, regarding the layer thickness determination, indicated that ANNs may be used to predict the thickness of asphalt concrete layers. However, these analyses were performed using synthetic data based on layered-elastic theory. On the other hand, results indicated that ANNs cannot be used to predict the thickness of the granular base. Therefore, efforts need to be focused on evaluating the applicability of ANNs to predict AC layer thickness on actual data.

5.5 Errors in Pavement Layer Moduli Backcalculation Due to Improper Modeling of the Layer Interface Condition

The layer moduli and thicknesses of the synthetic database were finally used to compute deflections under a full slip layer interface condition (Figure 5.12) and then to perform conventional backcalculation which considers full bond conditions. An increase in the root mean square error of the backcalculation process was expected due to the inability of the software EVERCALC to simulate full slip layer interface conditions during the backcalculation process. Figure 5.13 shows the cumulative distribution plots of the RMSE values obtained from this analysis. Given that synthetic data were used, the expected RMSE values under these conditions should be close or equal to zero. Such significant errors indicated that significant differences can be obtained between actual and predicted layer moduli when the actual condition of the layer interface is full slip between layers and the simulated conditions are full bond between layers.

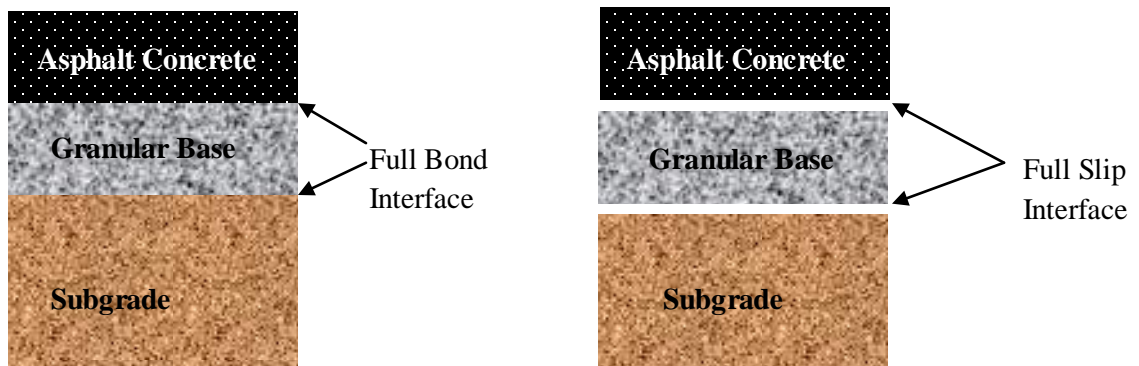


FIGURE 5.12 Modeled interface conditions.

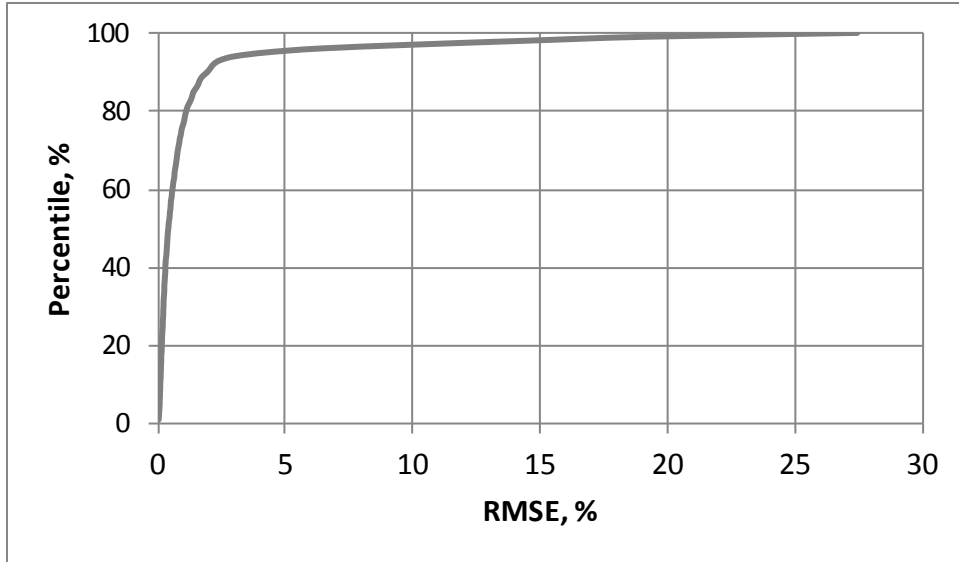


FIGURE 5.13 Cumulative distributions of RMSE values.

Figure 5.14 exhibits the cumulative distribution plots of the errors due to the improper modeling of the layer interface condition. In terms of the modulus of the asphalt concrete layer, the tendency was to significantly overestimate the modulus. On average, the AC (E1) modulus was overestimated by 30%. The modulus of the granular base (E2) was the most affected and the tendency was to underestimate the modulus, on average, by 74%. The modulus of the subgrade (E3) was the least affected with an average difference below 3%. Paired t-tests were performed to evaluate the significance of the relative differences and the results are shown in Table 5.4. As expected, statistically significant differences were obtained for the AC modulus and the granular base modulus at $\alpha = 0.05$. On the other hand there was no evidence to conclude that the moduli of the subgrade were different. These results not only served as evidence to the limitations of conventional backcalculation but also indicated a need for proper modeling of the layer interface condition. In the following chapter there are proposed ANN models capable of overcoming the limitations mentioned in this chapter.

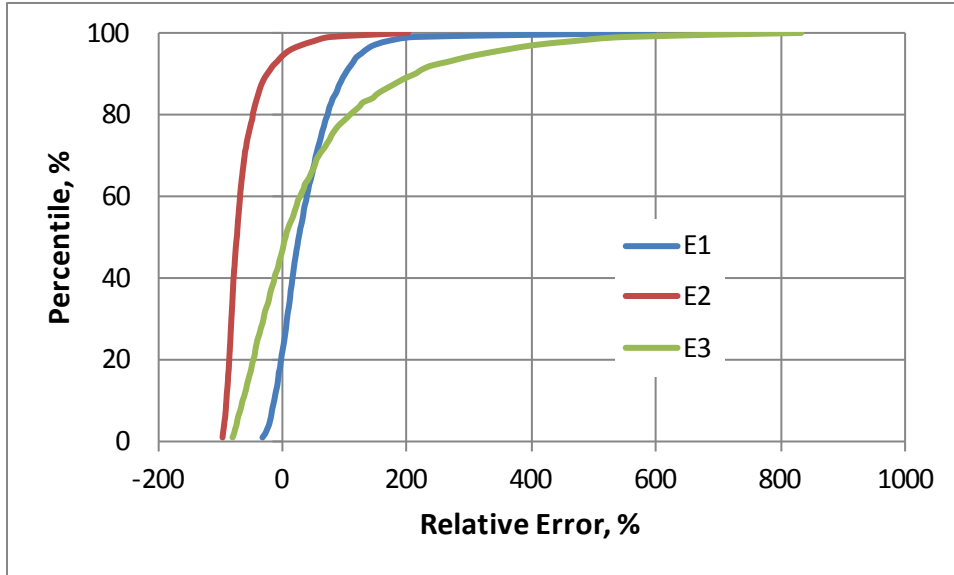


FIGURE 5.14 Cumulative distributions of moduli relative errors.

TABLE 5.4 Paired t-test results on moduli relative error

Parameter	Mean	St. Dev.	t-value	p-value
E1 Actual	498.3	113.5	28.46	<<0.05
E1 Back	647.1	190.2		
Difference	148.6	222.3		
E2 Actual	27.7	13.1	-64.85	<<0.05
E2 Back	7.1	3.61		
Difference	-20.5	13.4		
E3 Actual	16.2	7.82	1.63	0.104
E3 Back	16.6	7.62		
Difference	0.42	10.9		

Paired t-tests were also performed to evaluate the significance of the relative differences between pavement responses from full bond and full slip layer interface conditions. As shown in Table 5.5, statistically significant differences (at $\alpha = 0.05$) were obtained for the maximum deflection located at the center of the load plate (D0), for the horizontal tensile strain calculated at the bottom of the AC layer (ϵ_t), for the compressive stress calculated at the top of the granular base (σ_{base}) and for the compressive stress at the top of the subgrade ($\sigma_{subgrade}$). On average, deflections increased by 15%, tensile strains increased by 21%, compressive stresses of the granular base increased by 20% and the least affected were the compressive stresses of the

subgrade by 5.6%. Overall, these results indicated that pavement responses can be significantly under predicted when modeling pavement structures considering full bond layer interaction instead of full slip interaction. In addition, these results could also help explain differences between predicted or simulated pavement responses and measured or field pavement responses.

TABLE 5.5 Paired t-test results on pavement responses relative errors

Parameter	Mean	St. Dev.	t-value	p-value
D0 Full Bond	16.5	6.84	-40.87	<<0.05
D0 Full Slip	19.5	8.42		
Difference	-3.03	1.83		
ϵ_t Full Bond	216.6	93.8	-33.19	<<0.05
ϵ_t Full Slip	274.4	123.5		
Difference	-57.8	42.9		
σ_{base} FB	16.2	10.4	-42.47	<<0.05
σ_{base} FS	19.6	10.9		
Difference	-3.35	0.78		
$\sigma_{subgrade}$ FB	8.96	3.72	-25.64	<<0.05
$\sigma_{subgrade}$ FS	9.50	5.20		
Difference	-0.53	1.75		

5.6 Summary

Up to this point, the conventional backcalculation process used to estimate layer moduli can be considered sensitive to seed values such as setting the level of tolerance. Since a set synthetic deflection basins was used to backcalculate layer moduli it was expected to obtain minimum error no matter what the seed values were. In other words, a perfect match between actual values and backcalculated ones was expected when using synthetic values at not only the 0.1% level of tolerance. On the other hand, ANN-predicted layer moduli can be equivalent to backcalculated parameters calculated at a level of tolerance as low as 0.1%. In theory, layer moduli and pavement responses can still be estimated with the application of ANN when only deflections are used as inputs. More scattered results with higher relative errors can be expected for this type of analysis. The results also suggest that the thickness of the asphalt concrete layer could be estimated with an acceptable level of accuracy given that similar conditions used for this analysis

were found with field measurements. Finally, significant differences can be obtained between actual and predicted layer moduli when the actual condition of the layer interface is full slip between layer and the simulated conditions are full bond between layers.

CHAPTER SIX: APPLICATION OF ANN ON ACTUAL FWD TESTING RESULTS

FWD deflection testing results serve as the beginning to this chapter to examine trends and differences/similarities among test sections. Validation of the ANN approach was performed using the Test Track FWD database and a selected section of the Lee Road 159 deflection dataset. The capability for ANNs to predict pavement layer moduli was first analyzed on a very specific situation: pavement structures with similar thicknesses, but with multiple load levels. In order to incorporate a typical range of thicknesses the ANN models was limited to one load of 9,000 lb. Further implementation of ANN models was performed on a low volume roadway section (Lee Road 159, Auburn, AL).

6.1 Deflections and Backcalculated Material Properties

Figure 6.1 shows the strong relationship between mid-depth asphalt concrete (AC) temperature and the deflection at the center of the FWD load plate (D0). The deflection-temperature relationships for all sections exhibited in Figure 6.1 represent the results at the 9,000 lb load level. An exponential function has been found in the past to serve as the best fit for these datasets and therefore its used was continued in this study (47-49). For each test section, the measured deflection was expressed as a function of mid-depth temperature using Equation 6.1. A positive relationship between temperature and deflection was expected because as the temperature in a pavement structure increases higher deflections are expected under the application of FWD load (11).

$$D = k_1 e^{k_2 T} \quad \text{Eq. 6.1}$$

Where:

D = Measured deflection, mills

T = Mid-depth AC temperature, °F

k₁, k₂ = Regression coefficients.

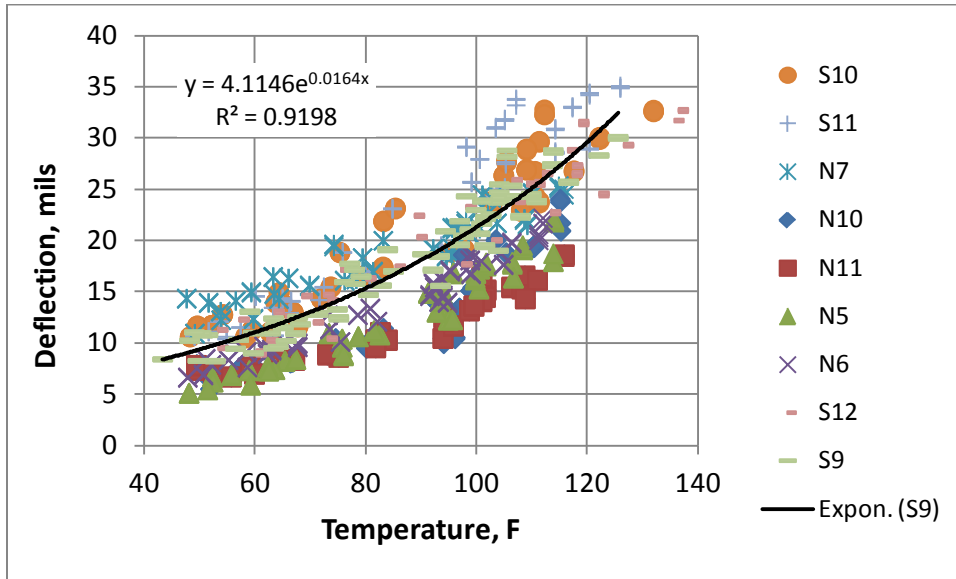


FIGURE 6.1 Deflection-temperature relationships.

Table 6.1 shows regression coefficients and R^2 values for all sections. The coefficient k_1 is related to the overall deflection magnitude while k_2 has to do with the sensitivity to changes in temperature. To determine if the deflection-temperature relationships were statistically different among the sections, 95% confidence intervals (CI) were obtained for the intercepts (k_1) and slopes (k_2). If the intervals overlapped, it could be concluded that the differences in the regression coefficients were not statistically significant. Therefore, at a 95% confidence level, all the sections had statistically different k_1 values from the control with the exception of S11 and S12. Therefore, sections S10 and N7 should exhibit higher stress and strain levels than S9. Conversely, sections N5, N6, N10 and N11 should exhibit lower stress and strain levels. In terms of the slope of the curve k_2 , only sections N5, N7 and N11 were statistically different from S9. However, N5 can be considered more temperature susceptible than S9 and N7 less susceptible than S9.

TABLE 6.1 Deflections equations coefficients

Section	k₁	<i>k₁ Lower</i> 95%	<i>k₁ Upper</i> 95%	k₂	<i>k₂ Lower</i> 95%	<i>k₂ Upper</i> 95%	R²
S9	4.411	3.883	4.360	0.0164	0.0158	0.0171	0.920
S10	5.281	4.865	5.731	0.0146	0.0137	0.0155	0.907
S11	4.603	4.236	5.000	0.0169	0.0160	0.0178	0.931
S12	4.689	4.293	5.122	0.0150	0.0140	0.0159	0.904
N5	2.158	2.013	2.312	0.0199	0.0191	0.0207	0.956
N6	3.196	3.026	3.376	0.0169	0.0163	0.0176	0.960
N7	7.818	7.376	8.287	0.0101	0.0094	0.0108	0.884
N10	2.439	2.211	2.692	0.0186	0.0174	0.0197	0.906
N11	3.27	3.050	3.506	0.0143	0.0135	0.0151	0.934

Conventional backcalculation of actual deflection basins collected at the Test Track was performed using the software EVERCALC 5.0. The backcalculated layer moduli presented below only represent the results at the 9,000 lb load level with RMSE errors less than 3%. These results will be later used to compare with ANN-predicted moduli; therefore, not only similar results are expected from ANN models but also similar trends/behavior.

Figure 6.2 shows the backcalculated AC layer moduli over the entire 2009 Test Track cycle (2 years). This figure shows the expected behavior (seasonal variation) of viscoelastic material sensitive to changes in temperature. During the cold season, the modulus of the AC mixture is higher and during the warm season the modulus is lower.

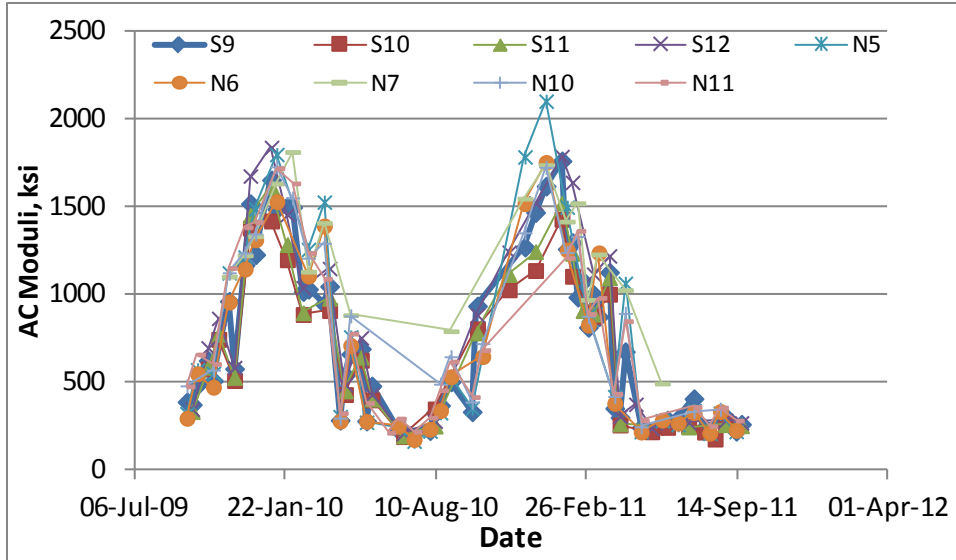


FIGURE 6.2 Backcalculated AC moduli.

During FWD testing, temperatures were recorded at the mid-depth of the AC layer. Figure 6.3 illustrates the strong relationship between mid-depth asphalt concrete (AC) temperature and backcalculated AC modulus (control section). An exponential function has been used in past research cycles at the NCAT Test Track (50-51) and it was also found to be the best fit to represent this strong relationship in this study. For each test section, the AC modulus was expressed as a function of mid-depth temperature using Equation 6.2. A negative relationship between temperature and AC modulus was expected because as the temperature in a pavement structure increases its modulus decreases (11).

$$E1 = k_1 e^{k_2 T} \quad \text{Eq. 6.2}$$

Where:

E1 = Backcalculated AC modulus, ksi

T = Mid-depth AC temperature, °F

k_1, k_2 = Regression coefficients.

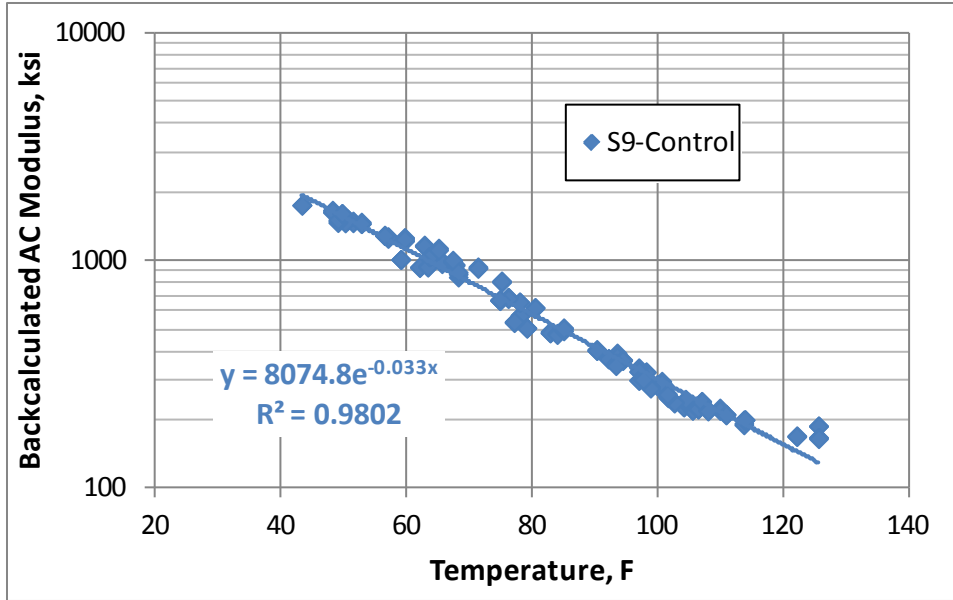


FIGURE 6.3 AC modulus versus temperature.

Table 6.2 shows regression coefficients and R^2 values for all sections. The coefficient k_1 is related to the overall modulus magnitude while k_2 has to do with the sensitivity to changes in temperature. To determine if the modulus-temperature relationships were statistically different among the sections, 95% confidence intervals (CI) were obtained for the intercepts (k_1) and slopes (k_2). If the intervals overlapped, it could be concluded that the differences in the regression coefficients were not statistically significant. At 95% confidence level, all the sections had statistically different k_1 values from the control with the exception of S11, S12 and N11. Therefore, sections S10, N11 and N7 can be considered to have lower backcalculated AC moduli than S9 while the remaining statistically different sections can be considered to have higher modulus levels. On the other hand, only the slope of section S11 cannot be considered was statistically different from S9. In this case, sections S10, S12, N7 and N11 were less sensitive to temperature changes than S9 while N5, N6 and N10 were more susceptible to changes in temperature than S9.

Further investigation showed that the best-fit exponential regression lines for S9 and N7 crossed at approximately 77°F with section N7 exhibiting lower moduli than S9 at cooler

temperatures and higher moduli at higher temperatures. This analysis was extended to sections N5 and N6 which had slightly higher k_2 coefficients than S9. It was found that the best-fit exponential regression lines crossed at approximately 70°F with sections N5 and N6 exhibiting slightly higher moduli at cooler temperatures and slightly lower moduli at higher temperatures.

TABLE 6.2 AC modulus equation coefficients

Section	k_1	k_1 Lower 95%	k_1 Upper 95%	k_2	k_2 Lower 95%	k_2 Upper 95%	R^2
S9	8074.8	7637	8538	-0.033	-0.0336	-0.0322	0.980
S10	5854.5	5432	6310	-0.029	-0.0299	-0.0282	0.979
S11	7700.6	6943	8541	-0.033	-0.0343	-0.0318	0.971
S12	8310.7	7660	9016	-0.030	-0.0311	-0.0294	0.977
N5	13953	12621	15427	-0.039	-0.0407	-0.0382	0.983
N6	10723	10023	11472	-0.037	-0.0380	-0.0364	0.988
N7	5655.6	5392	5932	-0.024	-0.0250	-0.0239	0.986
N10	10446	9564	11408	-0.035	-0.0357	-0.0336	0.978
N11	8183.9	7787	8601	-0.031	-0.0317	-0.0306	0.993

The modulus of unbound layers is a function of the material density, the amount of water present and the level of applied stress, and is generally assumed to be independent of temperature. Figure 6.4 shows the variation of the backcalculated granular base moduli over time for all the sections. This property showed small sensitivity to seasonal effects. This was expected since unbound materials are less affected by changes in temperature. Sections S10, S11 and S12 exhibited slightly lower moduli than S9 while sections N5, N6, N7, N10 and N11 had slightly higher moduli than S9. Table 6.3 exhibits the results of a Tukey-Kramer analysis performed on the modulus of the granular base at a 95% significance level ($\alpha=0.05$). These results indicated that on average all the sections were significantly different from S9 with the exception of N5 and N7.

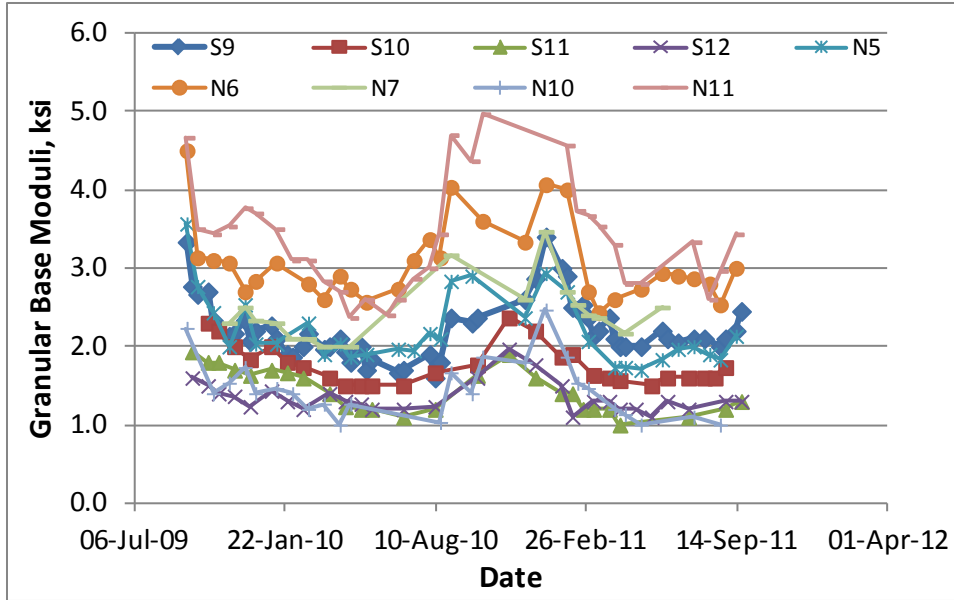


FIGURE 6.4 Backcalculated moduli of the granular base for all sections.

TABLE 6.3 Tukey-Kramer analysis of granular base modulus

Section	Difference of means	SE of Difference	T-Value	P-Value
S10	0.432	0.098	4.43	0.00
S11	0.789	0.100	7.89	0.00
S12	0.875	0.098	8.98	0.00
N5	0.025	0.094	0.26	1.00
N6	-0.836	0.094	-8.87	0.00
N7	-0.219	0.117	-1.88	0.63
N10	0.767	0.101	7.56	0.00
N11	-1.147	0.093	-12.29	0.00

Figure 6.5 shows the variation of the backcalculated subgrade moduli over time for all the sections. This property was slightly sensitive to seasonal effects. This behavior could be explained the variation in stress conditions due to the seasonal variation of the AC layer. At a 95% confidence level, it was determined that sections S10, S11, S12 and N7 exhibited similar moduli compared to section S9 while sections N5, N6, N10 and N11 had significantly higher moduli than S9 (Table 6.4). These differences in modulus could be attributed or explained as an artifact of the backcalculation process. It appears that EVERCALC attributed the increased

deflection at warmer temperatures to slight reductions in subgrade modulus in addition to reductions in AC modulus.

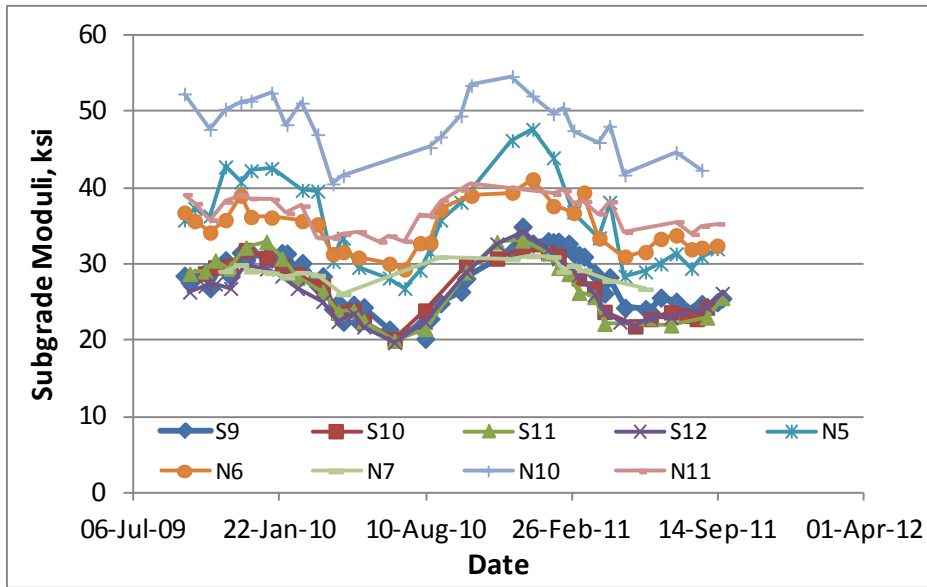


FIGURE 6.5 Backcalculated moduli of the subgrade for all sections.

TABLE 6.4 Tukey-Kramer analysis of subgrade modulus

Section	Difference of means	SE of Difference	T-Value	P-Value
S10	0.759	0.870	0.873	0.99
S11	0.333	0.892	0.374	1.00
S12	1.364	0.870	1.569	0.82
N5	-7.794	0.841	-9.269	0.00
N6	-7.009	0.841	-8.335	0.00
N7	-1.474	1.041	-1.415	0.89
N10	-8.990	0.832	-10.810	0.00
N11	-20.620	0.904	-22.810	0.00

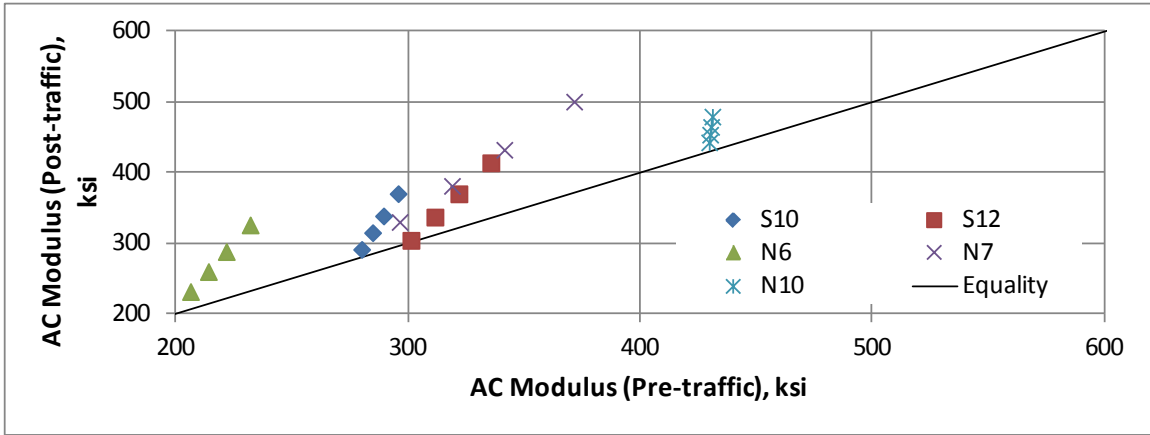
The granular base can be considered as a “thin” base course located beneath “thick” surfacing layers which explained the lower base moduli. In other words, the properties of the granular base are hidden by the high modulus/ thicker layer. In addition, the base modulus may be relatively “low” due to the stress sensitivity of granular materials (14). The use of a stiff layer generally improves the modulus estimate for base/subbase layers. However, an earlier study

performed at the previous Test Track research cycle indicated that the stiff layer analysis was not appropriate because of the higher RMSE values compared to the obtained results without the stiff layer (52).

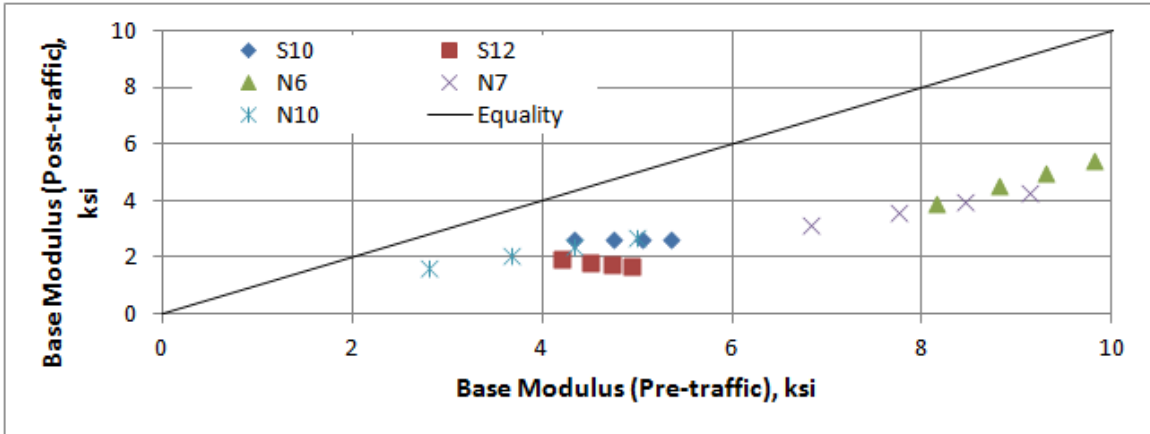
6.2 Indications of Weakening Bond between the AC Layer and the Granular Base Layer

Prior to the application of traffic loads at the Test Track, all the new sections were tested with the FWD device. Backcalculated layer moduli were obtained at 4 load levels (6, 9, 12 and 16 kips) and were defined as pre-traffic layer moduli. These results were compared to matching post-traffic backcalculated layer moduli as shown in Figure 6.6. For the pre-traffic moduli, only five sections had mid-depth temperature data to perform the matching. Post-traffic moduli were obtained from modulus-temperature relationships computed at the same temperature of the pre-traffic results (match in temperature) and then normalized at 6, 9, 12 and 16 kips (match in load level). The results indicated statistically significant differences in terms of the asphalt concrete modulus at a significance level of $\alpha = 0.05$. These differences tended to increase as the load level increase with relative errors ranging from 1% to 35%. The least affected section was N10 which has high RAP contents and stiffer binder. This was shown in Figure 6.a by the smaller deviation of N10 data points from the equality line. Conversely, the most affected section was N7 which has the thinnest AC structure. In terms of the granular base modulus, the opposite was observed with significant differences ranging from 42% to 60% decrease in modulus. This behavior was previously described by Lenngren and Olsson (17). In this case, the results also indicated that the backcalculated modulus of the unbound base was the most affected by the change in friction between layers and the modulus of the subgrade was only marginally affected with differences below 5%. Overall, the results indicated a significant drop in the modulus of the granular base due to the application of traffic loads that consequently affected the bond between the AC and base layers. These results also justified the development of artificial neural networks that

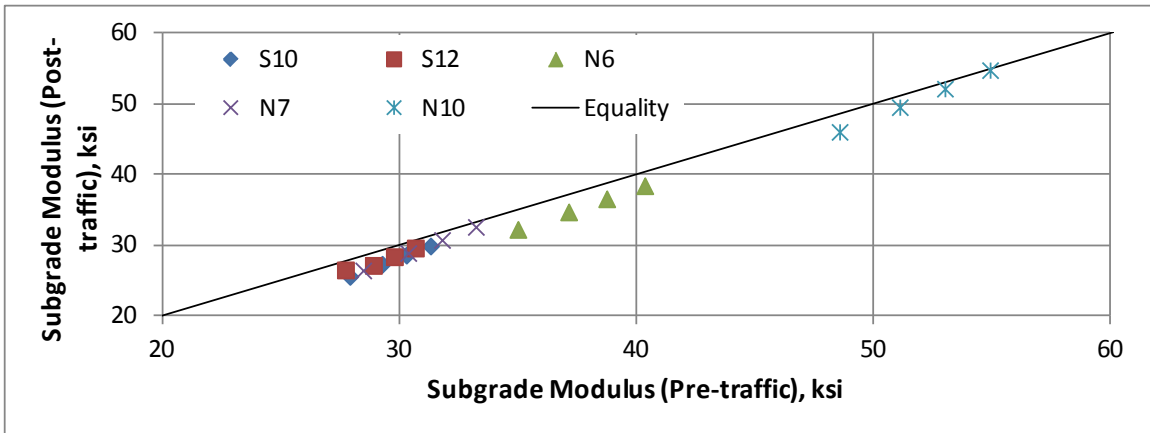
considered a full slip layer interface condition discussed in the following sections of this documents.



a.



b.



c.

FIGURE 6.6 Pre-traffic layer moduli versus post-traffic layer moduli.

6.3 Development of ANN for Selected Sections at the 2009 Test Track

A synthetic database was generated using layered-elastic analysis (LEA) for a three-layered flexible pavement structure. Two customized ANNs were created considering full bond and full slip condition between layers for structural sections built in 2009 with a designed asphalt concrete thickness of 7.0 inches (sections S9, S10, S11, S12, N6, N10 and N11). Table 6.5 shows the range of values used to generate deflection basins. For each ANN, a total of one hundred thousand data points were generated using multiple load levels ranging from 5,000 lb to 20,000 lb. To create each ANN, variables such as deflection basins, layer thicknesses and load were selected as input signals. The target signals were layer moduli (E1, E2 and E3). The outputs (layer moduli) generated by the ANN's using the synthetic inputs were compared against the backcalculated moduli to check for adequacy of the networks. Finally, the FWD test database was used to perform conventional backcalculation and ANN computation of layer moduli.

TABLE 6.5 Artificial database variables

Layer	Moduli Range, ksi	Thickness, in	Poisson Ratio
Asphalt Concrete (E1)	50 - 3000	5.0 - 8.0	0.35
Base (E2)	1 - 100	4.5 - 7.5	0.4
Subgrade (E3)	1 - 100	Infinite	0.45

The learning method used to develop these ANN models was a feed-forward back propagation with the sigmoid function, Equation 6.3, as the transfer function. It was found that the three-layer network with twenty nodes in the two hidden layers was the most appropriate for this dataset. This network configuration was selected by trial and error along with previous experiences found in the literature (18-20). The basic form of the ANN is given by Equations 6.3 through 6.6. For these equations, a single index indicates an array; dual indices represent a matrix with the first letter indicating the values in the row and the second letter indicating the values in the column. The index i represents the input parameters, the index k represents the first hidden

layer, and the j subscript represents the second hidden layer. An illustration of the model and the training process are shown in Figure 6.7.

$$f(T) = \frac{2}{1+e^{-2T}} - 1 \quad \text{Eq. 6.3}$$

$$H_k^1 = B_k^1 + \sum_{i=1}^m W_{ik}^1 P_i \quad \text{Eq. 6.4}$$

$$H_j^2 = f(B_j^2 + \sum_{k=1}^n H_k^1 W_{kj}^2) \quad \text{Eq. 6.5}$$

$$\text{Output} = \text{Ln}(E_1, E_2, E_3) = f(B_0 + \sum_{j=1}^n H_j^2 W_j^3) \quad \text{Eq. 6.6}$$

Where;

T = placeholder variable,

H_k^1 = transferred value of nodes at first hidden layer,

H_j^2 = transferred value of nodes at second hidden layer,

P_i = input variables,

W_{ik}^1 = weight factors for first hidden layer,

W_{kj}^2 = weight factors for the second hidden layer,

W_j^3 = weight factors for the output layer,

B_k^1 = bias factors for first layer,

B_j^2 = bias factors for second layer,

B_0 = bias factor for outer layer,

m = number of nodes in first hidden layer

n = number of nodes in second hidden layer

$\text{Ln}(E_1, E_2, E_3)$ = natural logarithm of the AC, base and subgrade modulus, respectively.

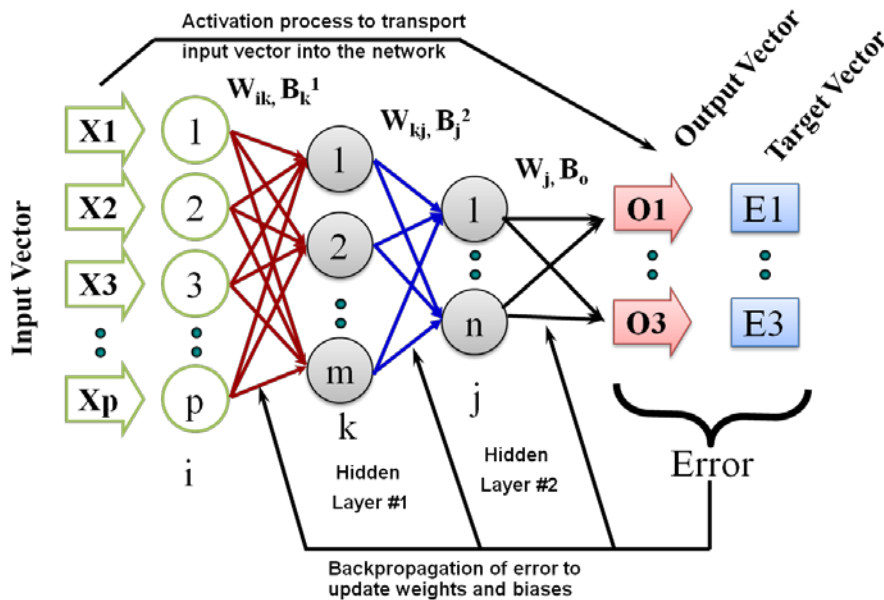


FIGURE 6.7 Schematic of ANN model and training process.

The synthetic deflection basins were used to check the adequacy of the trained ANN's. Since the dataset used for this exercise was synthetic, it was expected to have backcalculated moduli highly correlated to the actual values and with minimum errors. Backcalculated results were obtained using the software EVERCALC 5.0. RMSE values below 1.0% were obtained and statistical parameters such as R^2 values were found to be close to 1.0 as well as minimum Se/Sy values. These results can be seen in Table 6.6 for parameters E1, E2 and E3. Following a similar exercise using ANNs to predict moduli, the results showed that similar R^2 values and Se/Sy values can be obtained for the three parameters using the same synthetic deflection basins. In conclusion, the results suggested that ANN-predicted parameters can be considered equivalent to backcalculated parameters calculated at a level of tolerance below 1.0% and consequently adequate to predict layer moduli.

TABLE 6.6 Comparison of backcalculated and ANN Parameters for Synthetic Database

Parameter	Backcalculated		ANN Predicted – Full Bond		ANN Predicted – Full Slip	
	R ²	Se/Sy	R ²	Se/Sy	R ²	Se/Sy
E1	0.99	0.034	0.99	0.069	0.99	0.057
E2	0.99	0.026	0.99	0.083	0.99	0.071
E3	1.00	0.002	1.00	0.009	1.00	0.010

ANNs were used to estimate the moduli of eight structural sections built in 2009 for the full bond (FB) condition and the full slip (FS) condition. Table 6.7 shows the backcalculated and ANN-predicted layer moduli range for all sections. In general, the predicted moduli from ANN-FB were similar to backcalculated for all three layers. The same trend was observed between ANN-FS predicted moduli and backcalculated for E1 and E3. In the case of E2, the results showed that ANN-FS predicted moduli were more than double the backcalculated ones. These results suggested that the moduli of the granular base was underestimated for considering a full bond condition when applying conventional backcalculation or when predicting moduli with ANN-FB. This also seemed to agree with the results obtained by Lenngren and Olsson (17) which suggested that predicting layer moduli considering air gap or in this case full slip condition could be a more accurate approach. An analysis of the root mean square error was performed to ratify the previous statement.

TABLE 6.7 Range of predicted layer moduli for all sections

Technique	Section	E1, ksi	E2, ksi	E3, ksi
Conventional Backcalculation	S9	134 - 2357	1.0 - 11.2	14 - 42
	S10	122 - 1946	1.0 - 8.1	17 - 38.8
	S11	124 - 2060	1.0 - 7.8	13 - 43.9
	S12	117 - 2829	1.0 - 10.4	14.5 - 40.1
	N6	104 - 2716	1.7 - 13.2	23.1 - 62.5
	N10	172 - 2440	1.0 - 9.8	26.1 - 64.2
	N11	161 - 2173	1.6 - 13.1	28.5 - 52.6
ANN Full Bond	S9	129 - 2519	1.0 - 12.5	12.2 - 38.8
	S10	108 - 2073	1.0 - 7.0	13 - 35.1
	S11	115 - 2190	1.0 - 6.4	10.2 - 41.5
	S12	116 - 2767	1.0 - 9.2	12.6 - 37.1
	N6	135 - 3040	1.1 - 13.4	20.5 - 52.4
	N10	230 - 2536	1.0 - 11.2	17.1 - 54.8
	N11	185 - 2336	1.3 - 13.4	25.1 - 46.6
ANN Full Slip	S9	151 - 2231	1.1 - 26.2	12.1 - 39
	S10	129 - 1817	1.3 - 15.8	14.1 - 36.6
	S11	135 - 1941	1.1 - 13.1	9.1 - 41.7
	S12	144 - 2546	1.1 - 30.6	11.7 - 37.6
	N6	112 - 2626	2.6 - 48.1	22.4 - 53.4
	N10	117 - 2313	1.1 - 35.3	14.9 - 55.7
	N11	159 - 2169	2.6 - 48.6	27.3 - 48.7

Figure 6.8 shows the cumulative distribution plot (CDP) of the RMS error for three different scenarios. CDPs for ANN-FB and ANN-FS showed a significant decrease in the level of error from backcalculated values. In addition, the consideration of a full slip condition yielded even better results. A maximum RMS error of 3.0% was set to determine the amount of data to be used for all the analyses regarding the 2009 Test Track research cycle. Approximately 84% of the backcalculation solutions generated by conventional backcalculation had RMS errors below 3.0%. In the case of ANN-FB method, 88% of the results had RMS errors below 3.0%. Finally, for ANN-FS method, 92% had RMS errors below 3.0%. When the amount of data below 1.0% were considered as an “excellent” match between measured and calculated deflections (14), only 20% were found below 1.0% for backcalculated values, 73% for ANN-FB and 88% for ANN-FS.

These results demonstrated the significant advantage of using ANNs over conventional backcalculation that does not consider a full-slip condition.

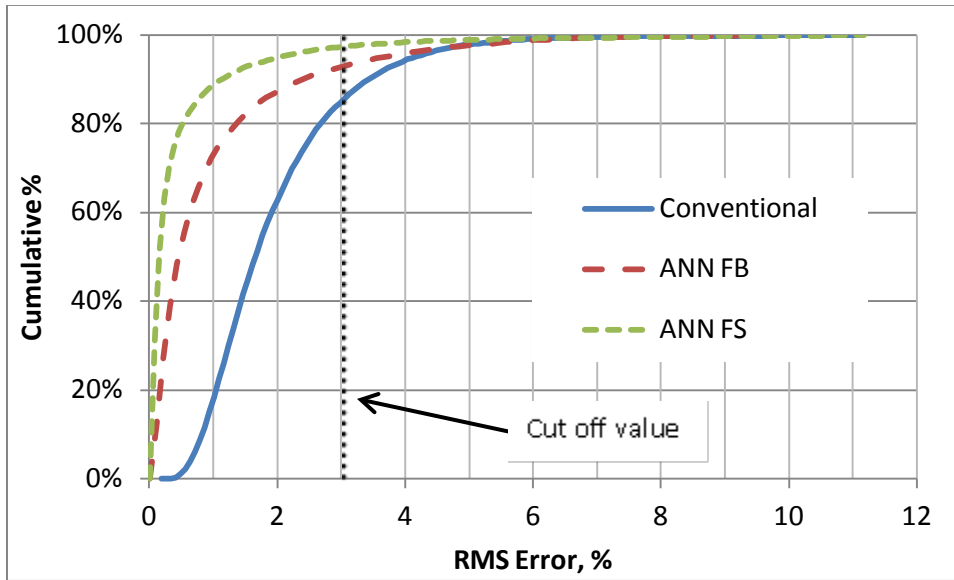


FIGURE 6.8 Cumulative distribution plot for estimated moduli.

Table 6.8 shows an extension of the previous analysis applied to all sections. A significant increase in the amount of data that was considered as “excellent” match between measured and calculated deflections was obtained when using ANNs compared to conventional backcalculation for all sections. The largest increase was observed from conventional backcalculation to ANN-FS for all the sections. Section S10 had the lowest overall increment followed by S11 and N10. These results were attributed to the higher variability observed in the layers moduli due to the higher permanent deformation (rutting) for sections S10 and S11. Rutting is a type of distress that changes the shape of the pavement surface increasing the variability in terms of thickness and density. The amount of data below 3.0% was also increased when using ANN-FB for all sections but S10. However, the increment was significant when using ANN-FS for all sections. In general, the quality of the layer moduli prediction ($RMSE < 1.0\%$) was significantly increased by the use of ANNs and the amount of usable data ($RMSE < 3.0\%$)

was also significantly increased by the consideration of full slip condition between layers (ANN-FS).

TABLE 6.8 Analysis of RMS errors for all sections

RMSE	Section	Percent data below cutoff value		
		Conv. Back.	ANN FB	ANN FS
Below 1%	S9	21.5	76.2	93.2
	S10	22.9	40.9	78.3
	S11	21.9	54.5	79.8
	S12	25.1	71.5	90.9
	N6	14.5	94.6	99.8
	N10	8.28	53.8	65.1
	N11	8.2	92.9	99.9
Below 3%	S9	85.8	94.8	99.2
	S10	89.9	81.3	97.2
	S11	74.7	83.2	95
	S12	76.7	94.6	97.8
	N6	89.7	99.7	99.9
	N10	86.1	86.2	87.6
	N11	92.8	100	100

Based on the results observed in Figure 6.8 and Table 6.8, a difference was expected in the estimated moduli when using ANNs rather than conventional backcalculation. Figure 6.9 shows an example of how the moduli obtained from EVERCALC 5.0 and predicted moduli using ANN-FS are related. The slope of a linear trend-line plotted between backcalculated moduli and ANN moduli was used to quantify the expected difference. For this case, the slope indicated that an overall decrease of 6.0% in the modulus of the AC layer was obtained when using ANN-FS. In this case an R^2 value close to 1.0 indicates that the relationship between variables can be expressed with a linear function.

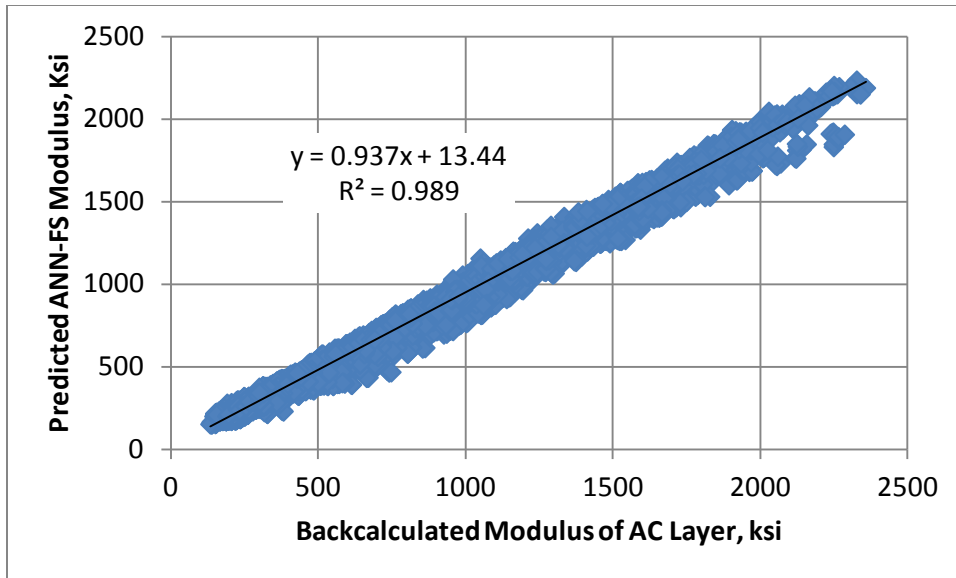


FIGURE 6.9 Backcalculated vs. ANN Predicted E1 of the Control Section (S9).

Table 6.9 shows the slope of a linear function calculated between backcalculated moduli and ANN predicted moduli and its associated R^2 value for each section. These results were used to quantify the expected difference and overall trend. When considering the observed difference for all the sections and for all the layer moduli, the results indicated that an overall decrease in the estimated moduli was obtained for the three layers (from 5.0% to 10.0%) when comparing backcalculated and ANN-FB methods. The largest decrease in modulus was obtained for section S10 followed by S11 in the case of E1. The results also indicated that an overall decrease in the estimated moduli was obtained E1 and E3 when comparing backcalculated and ANN-FS methods. However, a significant increase (overall 234%) was observed in the case of E2. Section N10 was the most affected with an increase in 327%. Although the use of ANNs in full slip condition indicated that the moduli of the granular base can be more than twice the estimated by conventional backcalculation, the results provided lower RMSE values and more realistic moduli for the base. The modulus of the granular base obtained from conventional backcalculation ranged from 1.0 psi to 15.7 psi. The modulus of the granular base obtained from ANN-FS ranged

from 1.1 psi to 48 psi which can be considered as more realistic moduli range and closer to the observed in previous research cycles at the Test Track for the granular base (50-52).

TABLE 6.9 Overall changes in moduli for all sections

ANN	Section	Slope of Back. Mod. Vs ANN Mod.			R ² of Back. Mod. Vs ANN Mod.		
		E1	E2	E3	E1	E2	E3
Full Bond	S9	0.95	0.88	0.93	0.98	0.85	0.85
	S10	0.84	0.97	0.89	0.96	0.65	0.70
	S11	0.85	0.97	0.94	0.97	0.78	0.84
	S12	0.99	0.90	0.87	0.98	0.90	0.81
	N6	1.00	0.85	0.88	0.99	0.91	0.92
	N10	0.91	0.88	0.94	0.97	0.90	0.81
	N11	1.01	1.11	0.89	0.99	0.89	0.88
Average		0.93	0.94	0.90	0.98	0.84	0.83
Full Slip	S9	0.94	2.16	0.94	0.99	0.96	0.94
	S10	0.90	1.90	0.96	0.98	0.93	0.91
	S11	0.91	1.91	0.95	0.98	0.94	0.93
	S12	0.92	2.20	0.95	0.99	0.96	0.93
	N6	0.97	2.59	0.85	1.00	0.90	0.94
	N10	0.98	2.36	1.07	0.99	0.94	0.86
	N11	0.99	3.27	0.84	1.00	0.90	0.89
Average		0.95	2.34	0.94	0.99	0.93	0.91

6.4 General Application of ANNs

In theory, a combination of a high load level and a thin AC layer can produce a similar response than having a low load level with a thick AC layer. This could be considered as a confounding effect in regression analysis because the regression coefficients cannot represent the independent contributions of each independent variable to the prediction of the dependent variable (poor or non-existing correlation). This effect was observed in ANN models with wider range of layer thicknesses compared to the models explained in the previous section of this chapter. Significant errors in the predicted layer moduli along with poor ANN model performance (R² values below 0.3 and high Se/Sy values above 0.7) confirmed the previous statement.

In the previous analysis (Chapter 6, section 6.3), the thickness of the simulated pavement structure was relatively constant and the load was variable. To account for a wider range of thicknesses, it was decided to keep a constant load while the thickness of the AC layer and granular base were variable. A synthetic database was generated using layered-elastic analysis (LEA) for a three-layered flexible pavement structure. ANNs were created considering full bond and full slip condition between layers. Table 6.10 shows the range of values used to generate deflection basins. For each ANN, a total of 100,000 data points were generated using one load level of 9,000 lb \pm 10%. To create each ANN, variables such as deflection basins, layer thicknesses and load were selected as input signals. The target signals were layer moduli (E1, E2 and E3). The outputs (layer moduli) generated by the ANNs using the synthetic inputs were compared against the backcalculated moduli to check for adequacy of the networks. Finally, the FWD test database was used to performed conventional backcalculation and ANN computation of layer moduli.

TABLE 6.10 Artificial database variables

Layer	Moduli Range, ksi	Thickness, in	Poisson Ratio
Asphalt Concrete (E1)	50 - 3000	3.0 - 18.0	0.35
Base (E2)	1 - 100	4.0 - 20	0.40
Subgrade (E3)	1 - 100	Infinite	0.45

Figure 6.10 shows the cumulative distribution plot (CDP) of the RMS error for three different scenarios and for all the sections described in this study. CDPs for ANN-FB and ANN-FS showed a significant decrease in the level of error from backcalculated values. Moreover, the consideration of a full slip condition yielded even better results. A cut off RMS error of 3.0% was set to determine the amount of data to be used for all the analyses regarding the 2009 Test Track cycle. Approximately 85% of the backcalculation solutions generated by conventional backcalculation had RMS errors below 3.0%. In the case of ANN-FB method, 99% of the results had RMS errors below 3.0%. Finally, for ANN-FS method, 99% had RMS errors below 3.0%.

When the amount of data below 1.0% were considered as an “excellent” match between measured and calculated deflections (14), only 12% were found below 1.0% for backcalculated values, 85% for ANN-FB and 85% for ANN-FS. These results demonstrated the significant advantage of using ANNs over conventional backcalculation.

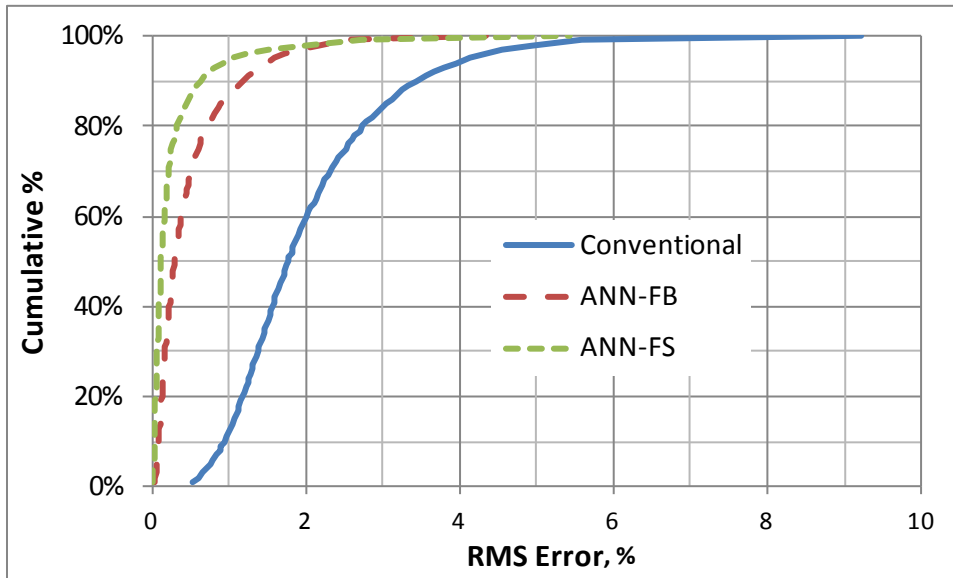


FIGURE 6.10 Cumulative distribution of RMSE for estimated moduli.

Figure 6.11 shows a strong linear relationship between backcalculated layer moduli and predicted moduli from ANN models (full bond – FB and full slip - FS) for the control section. The slope of a linear trend-line was used to quantify the overall expected difference. A slightly lower modulus was predicted for the AC layer (E1) and the subgrade (E3) for both ANN models. On the other hand, the tendency was to obtain higher granular base modulus (E2). As mentioned earlier, these results were significantly higher when using ANN-FS with almost twice the backcalculated moduli. A similar trend was observed for all the sections as shown in Table 6.11. It was found that higher differences in the estimated AC layer and subgrade moduli were associated with the higher RMSE values. For instance, the ANN-FS predicted modulus of the AC layer for N5 was 22% below the backcalculated modulus (on average) and had the highest root mean square error (1.09%). Conversely, sections with low RMSE values had slopes closer to 1.0

and consequently lower differences. Once again, the use of ANNs in full slip condition indicated that the moduli of the granular base can be around twice the estimate from conventional backcalculation, which can provide more realistic moduli for the granular base.

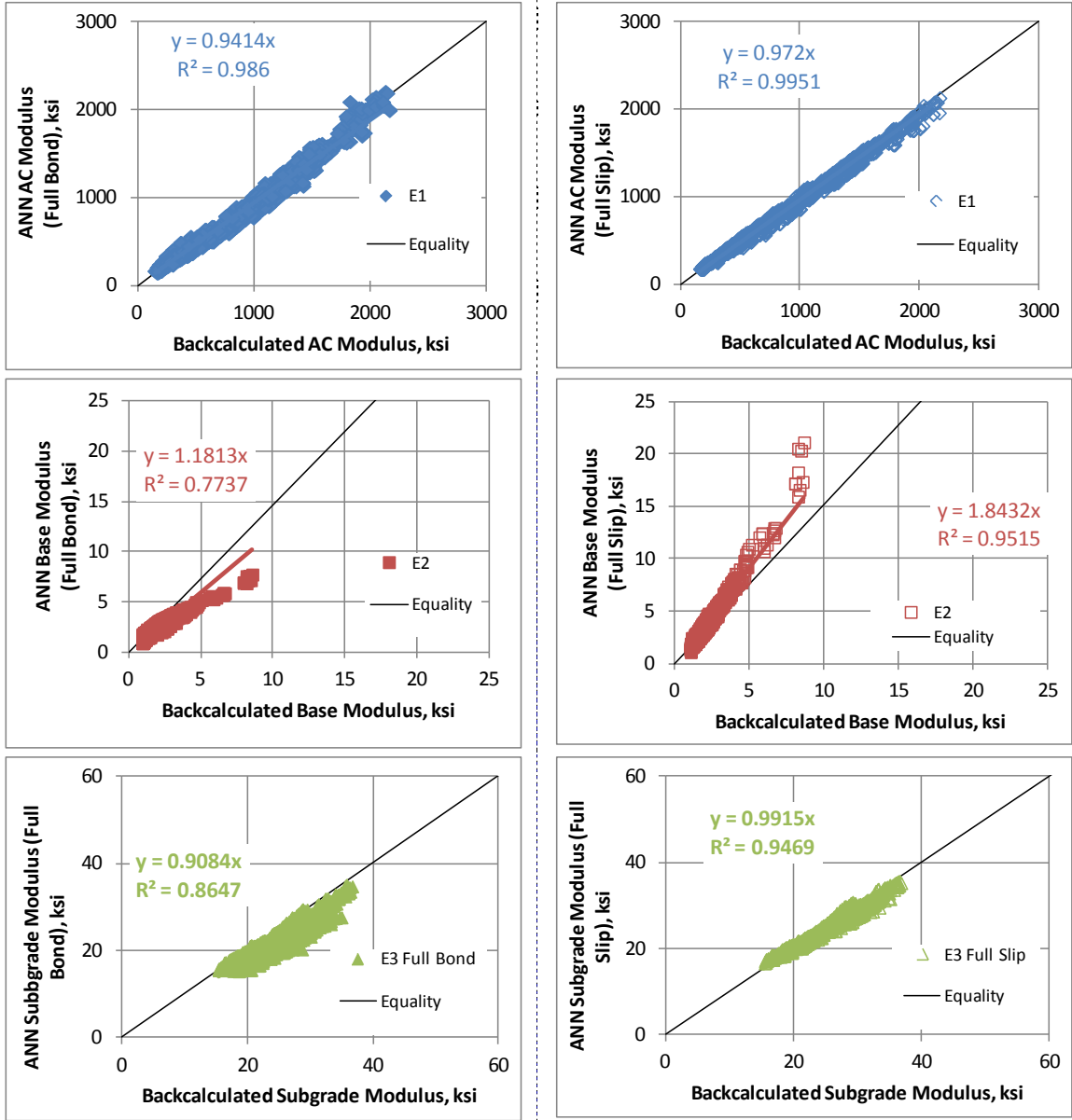


FIGURE 6.11 Backcalculated vs. ANN predicted moduli.

TABLE 6.11 Relationship between backcalculated and ANN predicted moduli

ANN Model	Section	Slope of Back. Mod. Vs. ANN			RMSE, %
		E1	E2	E3	
Full Bond	S9	0.941	1.181	0.908	0.38
	S10	0.913	1.328	0.870	1.05
	S11	0.879	1.277	0.888	0.76
	S12	0.965	1.113	0.904	0.48
	N5	0.971	1.054	0.897	0.45
	N6	0.997	0.996	0.961	0.17
	N7	0.877	1.028	1.005	0.88
	N10	1.003	1.082	0.899	0.75
	N11	1.024	0.979	0.955	0.24
Average		0.952	1.115	0.921	0.57
Full Slip	S9	0.972	1.843	0.992	0.16
	S10	0.942	1.739	0.972	0.35
	S11	0.943	1.763	0.994	0.29
	S12	0.967	1.925	0.979	0.21
	N5	0.784	2.035	0.913	1.09
	N6	1.001	1.909	0.980	0.11
	N7	0.948	1.608	1.040	0.21
	N10	1.024	1.850	0.902	0.96
	N11	1.010	2.074	0.968	0.12
Average		0.955	1.861	0.971	0.39

6.5 Application of ANNs on Low a Volume Roadway

FWD testing was performed in 2012 on a small segment of Lee Road 159 in Auburn, AL. This section was selected by NCAT as an experimental project to investigate different pavement preservation strategies. For this study, this section was selected to further validate the results obtained from a highly controlled facility such as the Test Track and apply these results to typical roadways found in Alabama. The thickness of the asphalt concrete layer was calculated to be 5.75 inches and the thickness of the granular base was estimated to be 6.0 inches. The length of the section was 2500 ft and FWD testing was performed on 51 stations equally distance from each other (every 50 ft). The measured air temperature on the day of the test ranged from 65.1 to 68.4 °F with an average of 66.7 °F while the temperature measured at the surface of the AC layer ranged from 71.9 to 90.5 °F with an average of 85.6 °F.

One of the assumptions behind layered elastic analysis is that each and every layer is infinite horizontally. Therefore, it does not consider any discontinuities in the layer of the pavement. If the load plate is near a crack, the analysis result may have some error. The main distress of this low volume road section was a low to medium severity cracking and therefore higher errors (RMSE), relative to the Test Track sections, were expected. Low severity cracking consisted of few interconnected cracks and was observed close to the center of the left wheel path (LWP). Medium severity cracking consisted of networks of cracks that may have material lightly broken-down along the side of the cracks and was observed mostly on the right wheel path (RWP). Figure 6.12 shows a comparison of layer moduli obtained from backcalculation and the use of ANNs. Measured deflection basins from between wheel paths (BWP) were used for this comparison, specifically the deflection measured directly below the applied load (D0). The observed variability can be attributed to the variability in thickness, the level of distress and differences in material properties. For instance, the modulus of the three layers, more than doubles between some stations.

The average deflection (D0) was 13.46mils with a standard deviation of 2.74mils. In terms of calculated error, the average RMSE from backcalculated moduli was 3.01% (std. dev. = 1.16%) while the average RMSE from ANN moduli was 0.45% (std. dev. = 0.36%). To statistically examine the differences between errors in estimated moduli, a paired t-test indicated that RMSE values from ANN and backcalculation were statistically different ($\alpha = 0.05$).

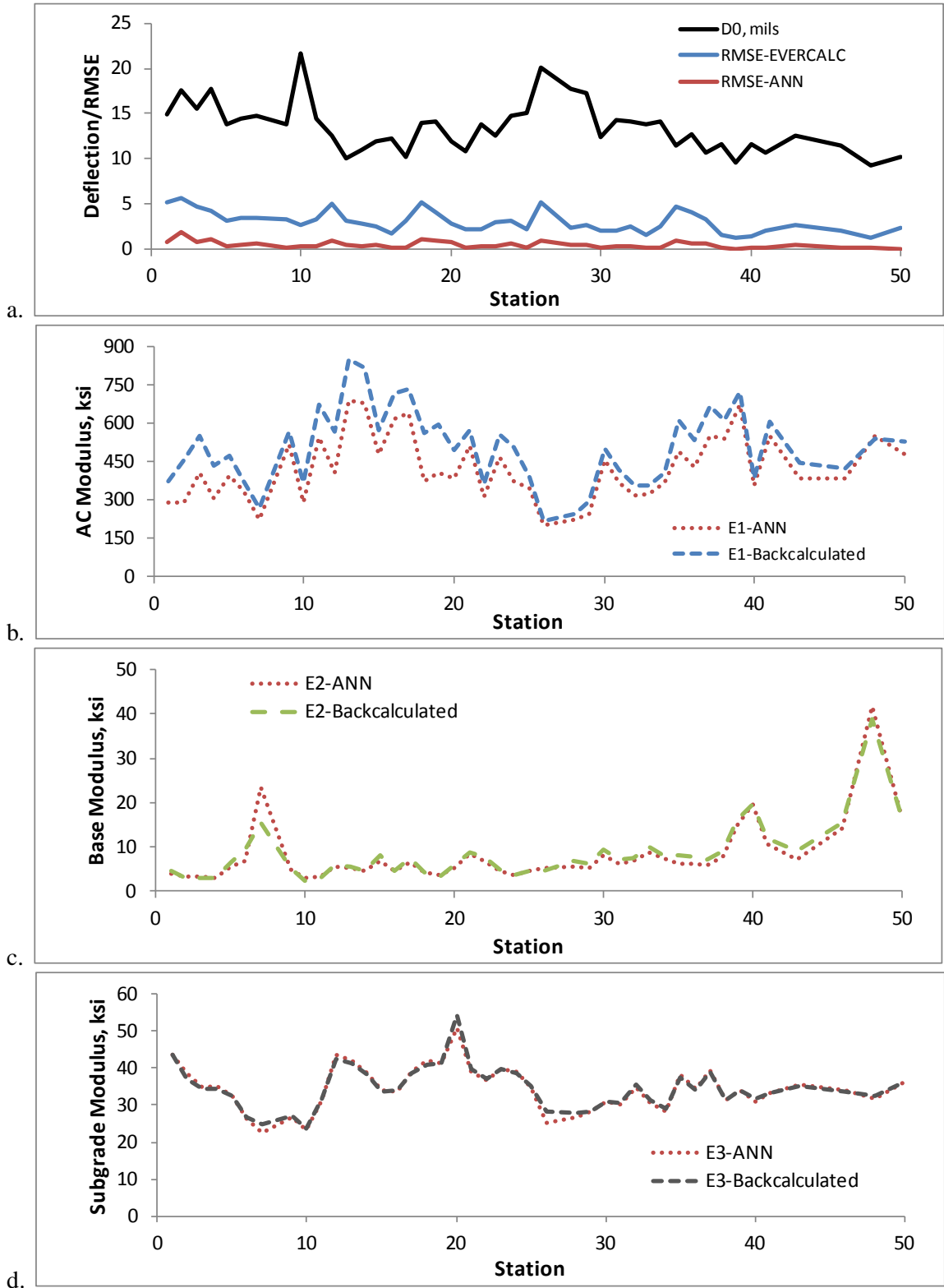


FIGURE 6.12 ANN vs. backcalculated properties (BWP).

A paired t-test indicated that AC moduli from ANN and backcalculation were statistically different ($\alpha = 0.05$). This tendency to overestimate the modulus of the AC layer as the error increases was discussed in Chapter 5 and it was confirmed with these results. Additional paired t-tests indicated that there was no statistical evidence to conclude that the moduli of the granular base and the subgrade were different from the application of ANN models or backcalculation.

The previously-mentioned ANN-Full Slip model was included in this analysis to evaluate the results especially on the granular base. Application of this model produced layer moduli with low errors with an average RMSE of 0.44% (std. dev. = 0.39%). To statistically examine the differences between models in predicted layer moduli a Tukey-Kramer analysis was performed (Figure 6.13). The results indicated that the AC layer moduli (E1) from backcalculation were statistically different, in this case higher than ANN-predicted layer moduli (about 15%). The average modulus of the granular base (E2) from ANN-FS was statistically different (45% higher) and there was no statistical evidence to conclude that moduli of the subgrade were different.

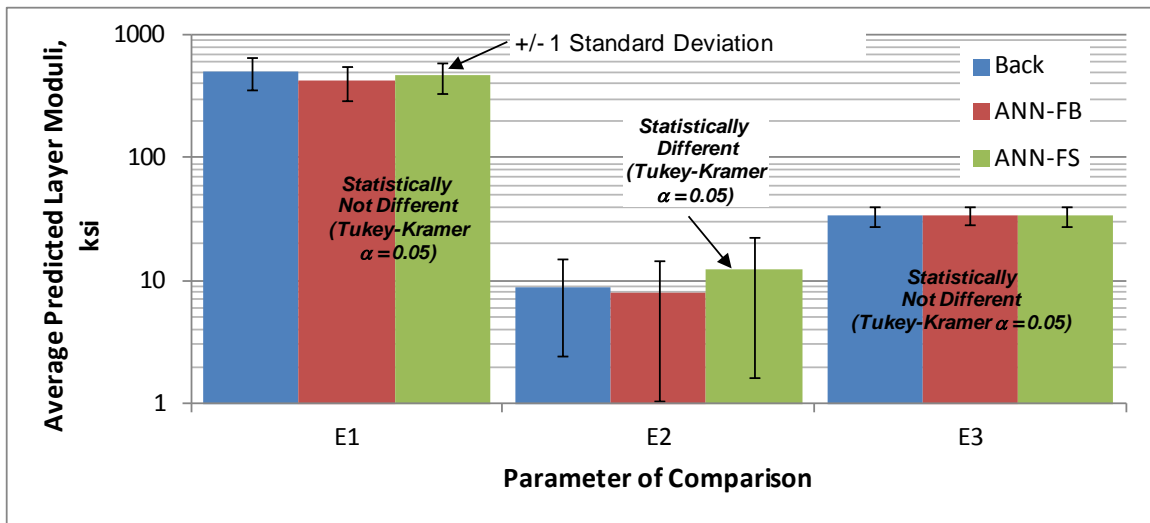


FIGURE 6.13 Comparison of predicted layer moduli from different models.

Deflection testing was also performed on the left and right wheel paths. Overall, lower deflections were observed on the left wheel path along the entire section (Figure 6.14). Therefore; higher moduli were expected for this offset. The average deflection for the three locations LWP,

BWP and RWP were 10.41mils, 13.46mils and 14.41mils, respectively. To statistically examine the differences between locations in measured deflections (D0) a Tukey-Kramer analysis was performed. The results indicated that the following pair locations were statistically different ($\alpha = 0.05$): LWP-BWP and LWP-RWP.

The ANN-FB model was used to predict the results shown in Figure 6.14. Tukey-Kramer analysis performed on predicted ANN layer moduli showed that the AC layer moduli (E1) at the LWP location were statistically different (higher). On the other hand, there was no statistical evidence to state that BWP and RWP had different AC moduli. In terms of the granular base modulus (E2), significant differences were only obtained between LWP and RWP. Despite the small practical difference among locations for the modulus of the subgrade (E3), there were statistically significant differences for all three locations due to the low variability. In general, there was statistical evidence to confirm that the higher moduli of the LWP location can be explained by the lower obtained deflections and the lower severity in the observed distress. The ANN-FS model was also used in this analysis and the results indicated that only the modulus of the granular base was statistically different from the ANN-FB results. On average, the predicted base modulus was 65% higher on the LWP location, 45% on the BWP (as shown in Figure 6.14) and 41% on the RWP.

Once again, the application of ANNs exceeded the performance of the conventional backcalculation process by reducing the RMSE parameter significantly. As mentioned above, low severity cracking was observed close to the center of the lane in the left wheel path (LWP) and medium severity cracking was observed mostly on the right wheel path (RWP). The predicted layer moduli followed the expected trends from the results observed in the field (cracking level) and from measured results (deflections). Overall, the clear advantage of ANNs over backcalculation was further confirmed and validation of ANNs was also achieved.

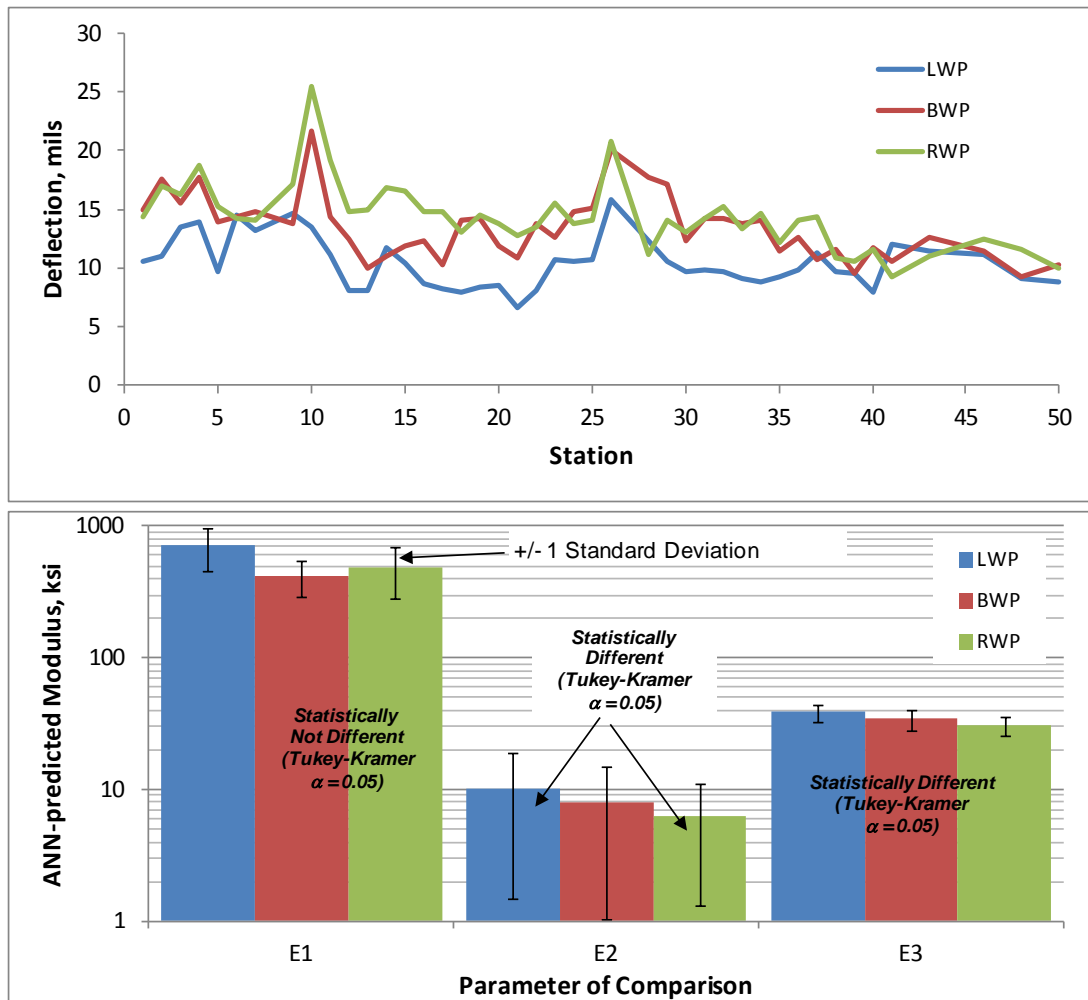


FIGURE 6.14 Comparison of layer moduli at different locations.

6.6 Additional ANN Models

As discussed in the previous chapter, removing the input variable “thickness” to predict pavement responses was, in theory, viable. Several ANN models were created using the same dataset presented in section 6.3 for a load magnitude of 9,000 lb. These models had the variable thickness removed from the analysis. When applying actual data from the Test Track FWD testing database, the results were highly scattered and inconsistent with backcalculated results. Figure 6.15 shows a poor relationship between predicted strain from ANNs with thickness and without thickness. The tendency was to over-predict strains at low levels and under-predict at the upper end of strains. This higher-than-expected variability was attributed to the high variability

observed in measured deflections and to the higher relative importance of the independent variable thickness to predict pavement responses. Further investigation is recommended on this matter to help reduce the gap between theory (chapter 5) and practice.

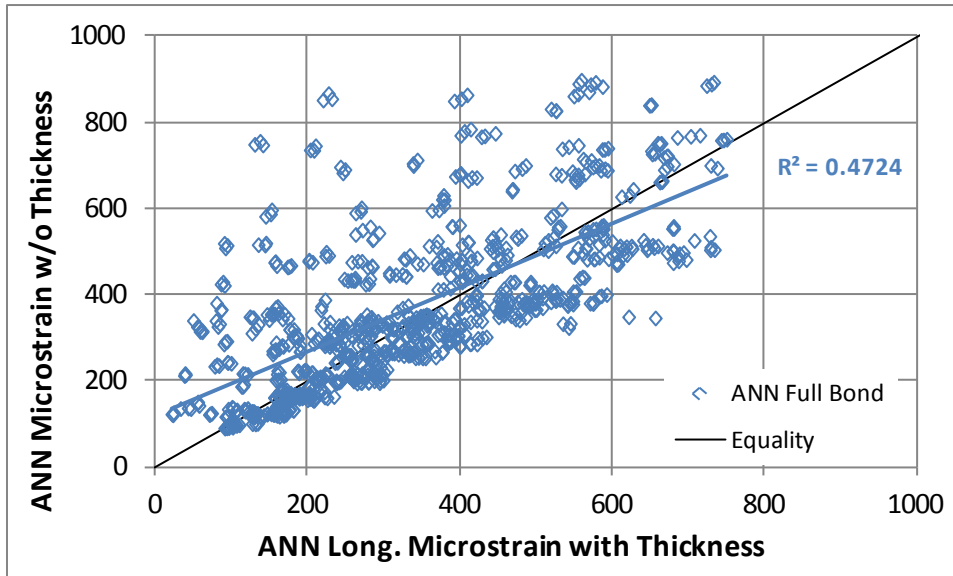


FIGURE 6.15 Predicted strain from ANN model with thickness as input versus predicted strain from ANN model without thickness as input.

Another significant discrepancy between theory and practice was found with ANN models used to predict the thickness of the asphalt concrete layer. Several ANN models were created as an attempt to estimate the AC layer thickness from actual deflections. When applying actual thickness data from the Test Track database, the results were highly scattered and inconsistent with actual thicknesses. Figure 6.16 shows the relationship between predicted and actual AC thickness for all the sections used in this study. In general, the models tended to underestimate the AC layer thickness with standard deviations above 2.0 inches. This higher-than-expected variability was attributed to the high variability observed in measured deflections and to the higher relative importance of the independent variable thickness to predict pavement responses. Further investigation is recommended on this matter to help reduce the gap between theory (Chapter 5) and practice.

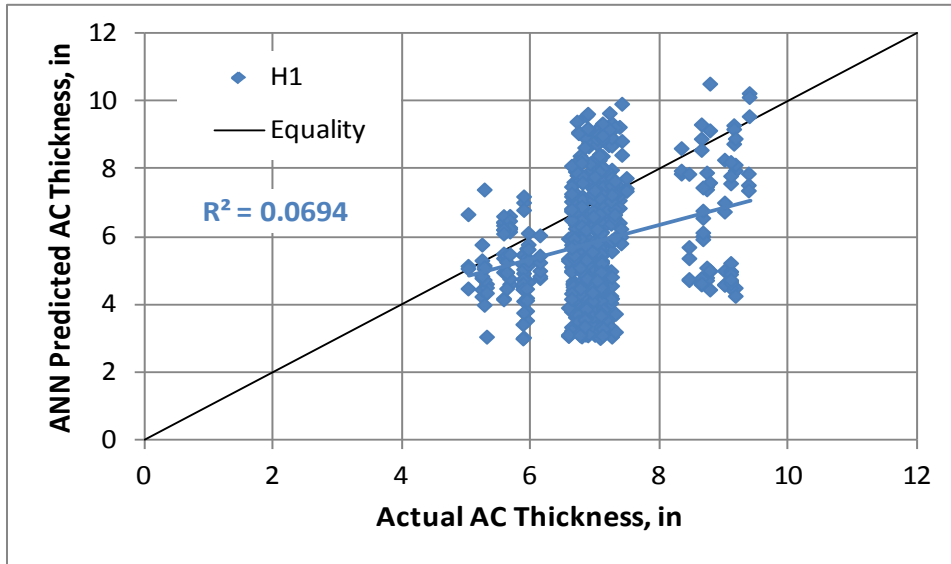


FIGURE 6.16 ANN-predicted versus actual AC thickness.

6.7 Summary

Up to this point, the capability for ANNs to predict pavement layer moduli was first validated on a very specific situation: pavement structures with similar thicknesses with multiple loads. In order to incorporate a typical range of thicknesses the ANN models had to be limited to one load of 9,000 lb due to the confounding interaction between thickness and load. In this case, the capability for ANNs to predict pavement layer moduli was also verified. Further implementation of ANN models was performed on a low volume roadway section. Validation of ANN models was also achieved for this scenario. Overall, the use of ANNs showed a clear advantage over conventional backcalculation by providing layer moduli with significantly lower errors. In addition, the use of ANNs considering full slip condition between layers has proven to be another innovative attempt to create models capable of predicting more realistic layer moduli. Finally, exclusion of the thickness to predict pavement responses from ANN models did not seem viable up to this point. Further investigation was recommended to help explain the differences between results from synthetic and actual data.

CHAPTER SEVEN: DETERMINATION OF EQUIVALENT LOADING PULSE AND STRAIN CORRECTION FACTORS

The loading frequency of the falling weight deflectometer (FWD) impact load of 33 Hz is significantly higher compared to the recommended loading frequency (34, 35) of a vehicle traveling at typical highway speeds (10 Hz). In theory, significantly higher moduli are expected at 33 Hz and consequently lower pavement responses compared to 10 Hz. In other words, the asphalt concrete layer moduli could be overestimated when using FWD test results and conversely the pavement responses could be underestimated. Hence, significant error could result between calculated and measured strain responses under slower speeds when using backcalculated moduli in a mechanistic model.

Prior to evaluating the effect of loading frequencies on pavement responses it was necessary to investigate the effect on the modulus of asphalt concrete mixtures. The difference in modulus calculated at 33 Hz and 10 Hz and the observed trend of nine sections built at the NCAT test track were evaluated and the significance of the difference was quantified. This analysis helped explain the trends and differences observed in pavement responses.

The FWD loading pulse duration was obtained from measured pavement response signals and it was compared to a single axle loading pulse duration traveling at 45 mph. This analysis also helped confirm the significance of the difference between FWD impact loading and traffic loading. Once it was determined the effect of loading type on layer moduli and pulse duration, the *3D-Move* software was used to estimate the speed of a moving load, which in theory should produce an equivalent FWD loading pulse. Finally, pavement responses were calculated at the equivalent FWD speed and at 45 mph to obtain the correction factors.

7.1 Viscoelastic Properties of Asphalt Concrete (AC) Layers

For linear viscoelastic materials such as asphalt concrete mixes, the stress-to-strain relationship under a continuous sinusoidal loading is defined by its complex dynamic modulus (E^*). E^* reflects the time and temperature dependency of AC mixtures. E^* can be defined as the ratio of

stress to strain (σ/ϵ) for an individual mixture at a specific temperature and loading frequency. The modulus of AC mixtures, at all levels of temperature and time rate of loading, is determined from a master curve constructed at a reference temperature (i.e. 70 °F). Master curves are constructed using the principle of time-temperature superposition. The *2002 Design Guide: Design of New and Rehabilitated Pavement Structures*, developed under NCHRP Project 1-37A (4) provides, in detail, the procedures needed to create master curves.

All the dynamic modulus testing was performed according to AASHTO TP62 (53) and master curves were created for all the mixtures (three lifts) for each structural section. Once a master curve has been created the dynamic modulus can be computed at any temperature and frequency. An effective dynamic modulus ($E_{\text{effective}}$) of three-layer pavement can also be calculated using Equation 7.1 (11, 54-55). An effective modulus is a mathematical combination of the individual layer E^* that has been used to compared against backcalculated AC modulus.

$$E_{\text{effective}} = \left[\frac{c_1(h_1 \sqrt[3]{E_1} + h_2 \sqrt[3]{E_2} + h_3 \sqrt[3]{E_3})}{h_1 + h_2 + h_3} \right]^3 \quad \text{Eq. 7.1}$$

Where;

E_1 , E_2 and E_3 = dynamic modulus of top layer, intermediate and base layer,

h_1 , h_2 , and h_3 = the thickness of respective layers.

C_1 = correction factor (0.8 to 0.9) used to obtain better agreement with exact theory of elasticity (54-55). The value of correction factors depend on the layer thicknesses, modular ratios, Poisson ratios and the number of layers in pavement structure. In the present study correction factor was taken as 0.85 (midpoint of range).

Figure 7.1 shows a comparison of effective E^* values computed from master curves for all the AC mixtures used in the 2009 Test Track experiment. The $E_{\text{effective}}$ of the control section was used as baseline and the relative difference between that baseline and the $E_{\text{effective}}$ from another mixture was the parameter of comparison. These values were calculated at four temperatures (40, 70, 100 and 130°F) and at two frequencies (10 and 33 Hz). These two

frequencies were used to represent highway speeds (10 Hz) and the FWD test frequency (33 Hz) as shown in the literature (33-35). This analysis showed which sections had higher, similar and lower moduli compared to the control section. Sections S10 and S11 had lower modulus at any temperature while sections N5, N6, N10 and N11 had higher modulus at any temperature. On the other hand, sections S12 and N7 had slightly higher modulus at any temperature but at 130°F. Overall, N10 had the highest AC modulus and S11 the lowest and the same trend was observed at both frequencies 10 Hz and 33 Hz. Moreover, these results were later used to help explain the effect of temperature and frequency on the differences and trends obtained in pavement responses at operational highway speeds (10 Hz) and equivalent FWD speed (33 Hz).

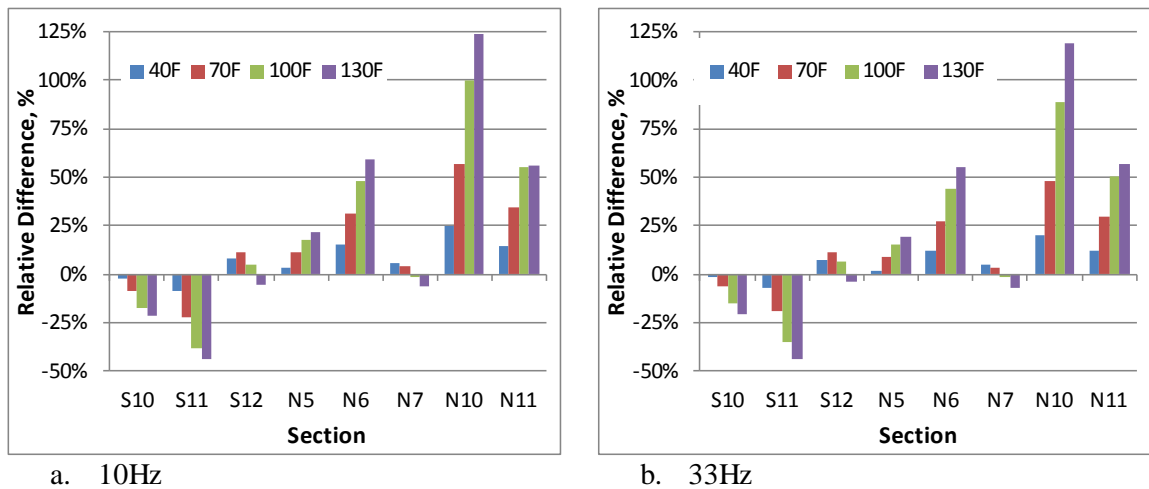


FIGURE 7.1 Dynamic modulus relative differences from the control section at 10 and 33 Hz.

Figure 7.2 shows the relative difference in effective modulus calculated at 10 and 33 Hz as function of temperature. Higher dynamic moduli were calculated at a frequency of 33 Hz than at 10 Hz. A significant increase of the relative difference in effective modulus as the temperature increases was observed for all sections. Additionally, the mean difference in effective modulus considering all the sections was found to be 164 ksi and it was significant at a confidence level of 95% ($\alpha = 0.05$, paired t-test). With respect to the control section, S10 and S11 had higher relative differences which corresponded to lower effective modulus. Sections N5, N6, N10 and N11 had

lower relative differences which matched the respective higher effective modulus. Sections S12 and N7 showed similar results and were closer to the results obtained for S9. Based on these results, a higher relative difference in pavement responses are expected for sections with lower relative difference in effective modulus and the opposite apply for sections with higher relative difference in effective modulus.

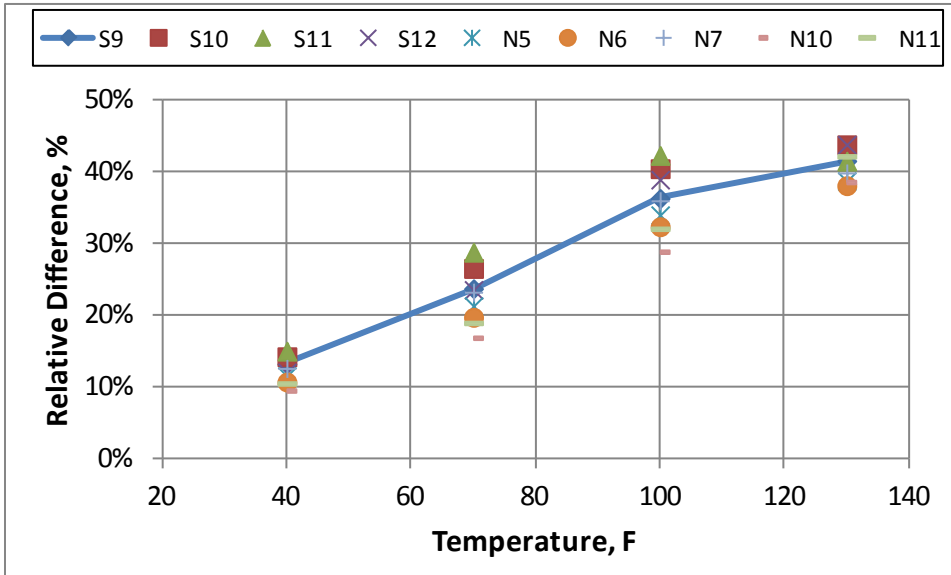


FIGURE 7.2 Relative differences between dynamic moduli at 10 and 33 Hz.

Backcalculated AC moduli were compared to calculated effective modulus at 10 and 33 Hz and at selected (matching) temperatures contained within the range of measured AC mid-depth temperatures for all sections. Figure 7.3 shows that the effective modulus calculated at 33 Hz was closer to the backcalculated with an average deviation of 5.6% (below the equality line). A two sample t-test ($\alpha=0.05$, two tails) found no significant differences between backcalculated and effective modulus calculated at 33 Hz ($p\text{-value} = 0.0601$). On the other hand, the backcalculated modulus was underestimated by about 18.4% when the effective modulus was calculated at 10 Hz. A two sample t-test ($\alpha=0.05$, two tails) found statistically-significant differences between backcalculated and effective modulus calculated at 10 Hz ($p\text{-value} = 0.0327$). The variability of the backcalculated AC moduli was responsible for the scattered results shown

in Figure 7.3. These results not only exhibited the significant difference between effective moduli at 10 Hz and backcalculated moduli, but also suggested a potential error in the prediction of pavement responses when using backcalculated moduli to represent moduli at highway speeds (about 10 Hz). Therefore, the need to quantify the potential error to correctly predict pavement responses became more evident for this study. This analysis not only suggested that the choice of 33 Hz to match E^* to FWD results can be appropriate but also questioned the ability for the FWD to match traffic loads at operational highway speeds.

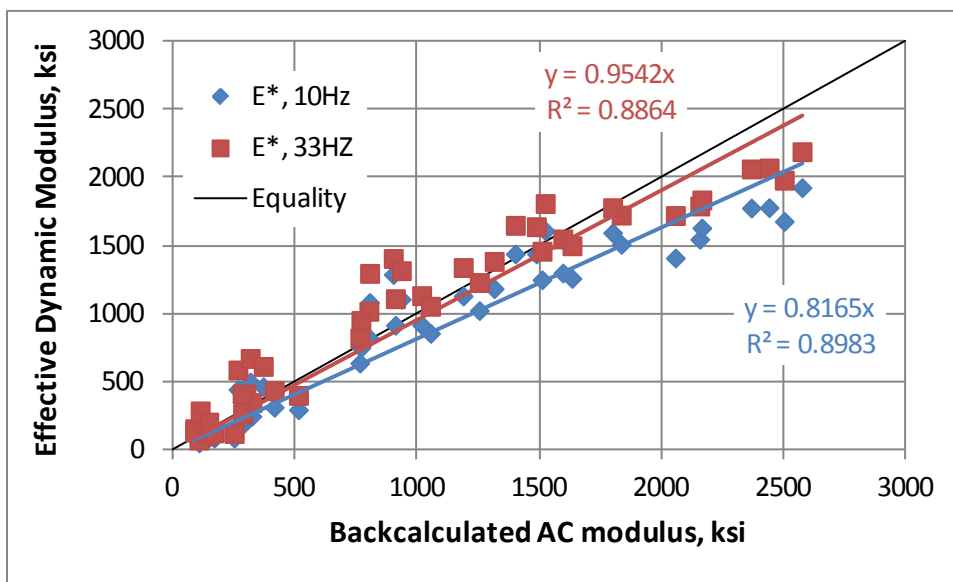


FIGURE 7.3 Backcalculated AC modulus versus $E_{\text{effective}}$.

7.2 FWD Loading Pulse from Instrumented Pavements

Field data for this investigation were generated in August 2009. FWD testing was performed on every single piece of instrumentation (asphalt gauges and pressure plates) to quantify the in-place gauge variability. Response signals were taken for three repetitions of the FWD at four load levels (6, 9, 12 and 16 Kip) but only the data generated at a load of 9 kip were used in this study because this is the load level close to the equivalent single axle load (ESAL). Measured response traces provided not only the magnitude of the strain or stress but also the pulse duration. Stress traces from a pressure sensor located at the bottom of the AC layer were used to calculate the

pulse duration from FWD testing. Figure 7.4 shows a comparison between a measured stress pulse resulting from an FWD impact load and the simulated stress pulse from a moving load with a speed of 130 mph for the control section S9. The simulated stress pulse is an example of the output that was obtained from the software 3D-Move for a single moving load of 9 kip as an attempt to reproduce the measured FWD signal. The pulse duration was measured from the point where the signal starts deviating from the base line to the point where it returns to the base line.

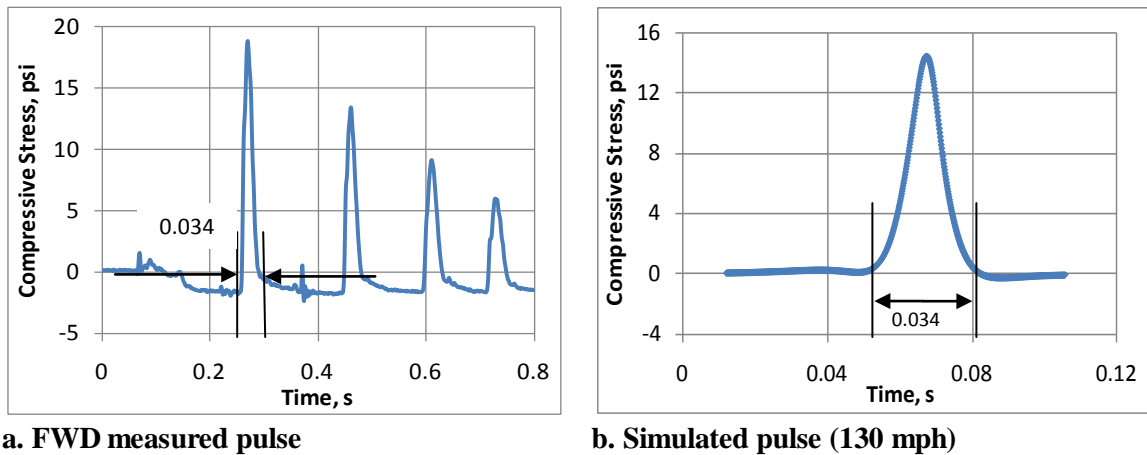


FIGURE 7.4 Measured versus simulated FWD loading pulse.

Table 7.1 shows the measured pulse duration obtained from different instrumentation devices from the FWD 9 kip load and from a single axle dual-tire load moving an average speed of 45 mph for section S9. All the signals were recorded at the same temperature (115 °F) but a month passed between FWD testing and single axle loading. Pulse durations for FWD loading were consistent among gauges varying from 30 to 38 milliseconds (ms). Pulse durations for single axle load were significantly longer than FWD pulse durations. The results were 2 to 3 times larger for the cases of the transverse strain pulse (T) and the base plate stress pulse (B). For the longitudinal strain pulse (L) and subgrade stress pulse (Sg) the results were at least 3 times greater than FWD pulse durations. Such discrepancies suggest that the loading frequency of FWD loading should be similar to that of vehicle loading at a significantly higher speed. Table 7.2

shows the measured pulse duration obtained for the remaining sections. These results were acquired at different dates because it was desired to have comparable results in terms of temperature. The results followed the same trend observed for section S9 with longer pulse durations under traffic than FWD loading.

TABLE 7.1 Pulse durations on different gauges, Section S9

Gauge Type	Pulse Duration, ms	
	FWD	Single Axle
Longitudinal (L)	33 - 37	137 - 146
Transverse (T)	30 - 35	94 - 103
Base Plate (B)	32 - 38	94 - 96
Subgrade Plate (Sg)	33 - 38	106 - 119

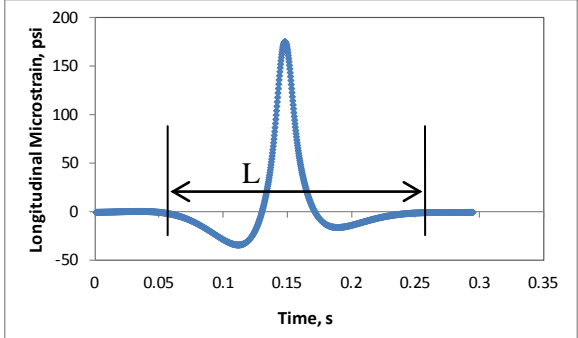
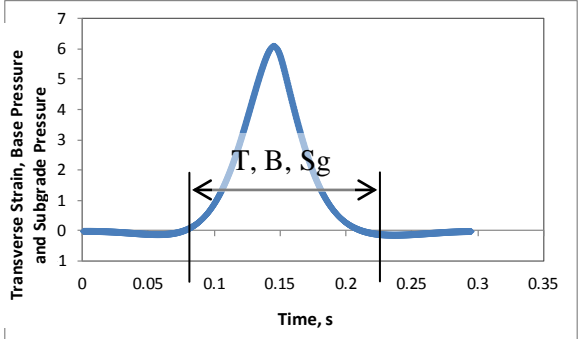



TABLE 7.2 Pulse durations on different gauges, remaining sections

Section	Date	Pulse duration, ms			
		L	T	B	Sg
S10	5/27/2010	136	127	97	126
S11	5/27/2010	134	133	103	122
S12	9/22/2010	139	104	90	104
N5	10/28/2010	235	205	197	203
N6	9/15/2009	194	158	149	153
N7	11/3/2009	142	111	108	128
N10	10/21/2009	177	168	140	151
N11	5/26/2011	159	146	128	NA

Figure 7.5 shows a comparison among pulse durations under different loading frequencies: FWD loading and single axle loading at variable speed. The data for the variable speed loading were generated in May, 2010 at an average temperature of 113 °F (2 degrees lower than FWD testing). Stress traces from the pressure sensor in section S9 located at the bottom of the AC layer were used to calculate the pulse duration. For a truck driven at a speed of 41 mph, the pulse duration of the single axle load was about three times longer than the FWD loading, about 3.4 times longer for a truck driven at a speed of 33 mph, 4.7 times longer for 24 mph and 6.7 times longer for a truck driven at a speed of 16 mph. These results indicate that even more caution is needed when using predicted pavement layer moduli in mechanistic analysis as the operational speed is decreased below 45 mph.

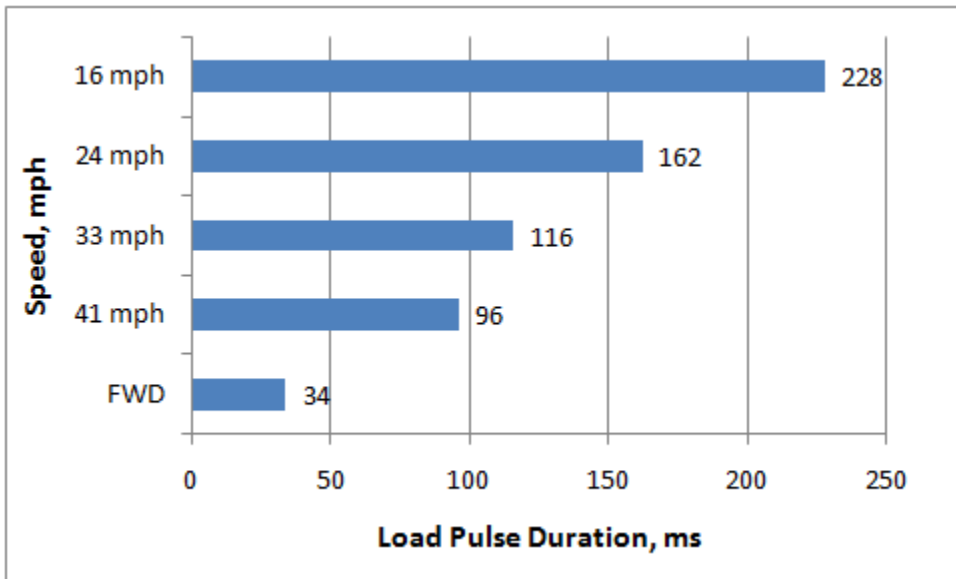


FIGURE 7.5 Pulse duration under different loading speeds.

7.3 Determination of Equivalent Loading Pulse and Equivalent Loading Speed

To determine the speed which may produce a loading pulse equivalent to the FWD impact load, a single circular load with a magnitude of 9 kips and a radius of 5.91 inches was modeled in 3D-Move. This load configuration is normally used in mechanistic analysis to represent a typical

FWD load. Different speeds starting at 25 mph were modeled to determine an equivalent loading pulse. Figure 7.6 provides an example of the effects of temperature and vehicle speed/frequency on loading pulse duration for a simulated FWD load (section S9). This figure shows how the simulated loading pulse duration for section S9 decreases as the simulated single circular load speed increases. Higher pulse durations were obtained at lower temperatures and the reduction in simulated loading pulse with the increase in vehicle speed seems much more significant for lower temperatures. Higher pulse durations are expected for mixtures with higher modulus (lower temperature) since the stress is distributed in a wider area, while lower pulse durations are expected for mixtures with lower modulus (higher temperature) because of the more concentrated stress distribution. The target pulse duration for S9 was within 0.032 and 0.038 seconds at 115 °F. The simulated curve 115F reached the target range at a speed of 130 mph.

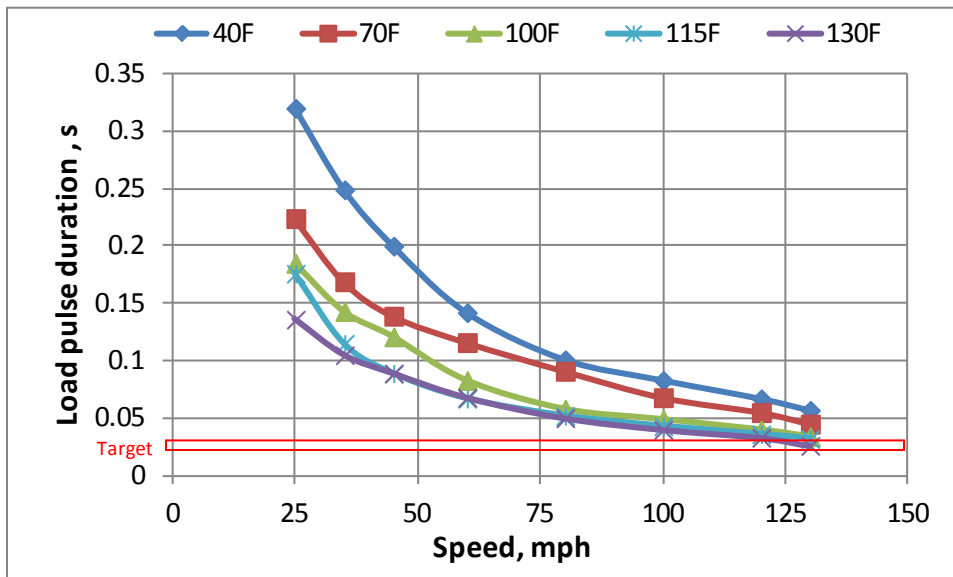


FIGURE 7.6 Influence of vehicle speed on pulse duration – Control Section S9.

Table 7.3 shows the range of loading pulse durations from FWD tests performed on pressure sensors along with recorded mid-depth temperature and the equivalent speed that produced pulse durations within the measured range. The measured pulse duration ranged from

0.030 to 0.055 seconds and the measured mid-depth temperature during the FWD tests ranged from 75 to 120 °F. The speed of a moving load that produces a loading pulse equivalent to the loading pulse produced by the FWD was determined to be over 120 mph.

The differences in measured pulse durations and resulting equivalent speeds can be explained by the effect of mid-depth temperature and total AC thickness has on the modulus of the AC. It was expected that an increase in the pulse duration would result from a decrease in pavement temperature and with an increase in AC thickness (39). The thicker AC layer and lower temperature obtained for sections N5, N6, N10 and N11 with respect to S9 explained the higher measured pulse durations and higher equivalent speeds. For the case of N5, a combination of lower temperature and thicker AC layer resulted in the highest pulse duration/equivalent speed. In the case of N7, the lower temperature and thinner AC layer resulted in similar pulse duration/equivalent speed than S9. In the case of sections S10 and S11, the lower simulated speed can be attributed to the softer asphalt concrete layer compared to S9 and the contrary can be applied in the case of S12 with higher AC layer moduli.

TABLE 7.3 Determination of moving load speed at equivalent loading pulse

Section	Pulse duration range, ms	Temperature, °F	Backcalculated AC Modulus at Measured Temperature, ksi	Equivalent Speed, mph	Pulse at Equivalent Speed, ms
S9	32 - 38	115	181.5	130	34
S10	35 - 39	120	180.4	120	36
S11	34 - 37	115	173.1	120	35
S12	28 - 32	118	241.1	145	30
N5	50 - 55	75	748.8	150	53
N6	42 - 48	80	555.7	140	45
N7	37 - 43	83	771.6	130	38
N10	37 - 43	86	514.9	145	41
N11	28 - 31	91	487.3	145	30

7.4 Simulated Temperature and Speed Effects

A typical single axle dual-tire configuration with a total axle load of 10.4 kips (5.2 kips per tire) was modeled in *3D-Move*. This load was the average single axle load from the Test Track truck

fleet. A uniform circular tire-pavement interaction stress distribution of 100 psi was also used. Figure 7.7 shows the influence of vehicle speed on longitudinal tensile microstrain located at the bottom of the AC layer for section S9. Speeds ranging from 15 to 130 mph were used to generate this plot. A significant reduction in the strain magnitude as the speed increases was obtained for speeds ranging between 15 and 60 mph. The results also showed that the reduction in the simulated strain response with vehicle speed was much more significant for pavements at higher temperature. Similar trends in pavement strain for a variety of speeds and temperatures were observed for measured strains at the Test Track from two different studies (56, 57). Figure 7.8 shows the influence of vehicle speed on compressive stress calculated at the top of the granular base and at the top of the subgrade for section S9. A significant reduction in the stress level and loading pulse as the speed increases was obtained for lower speeds and higher temperatures.

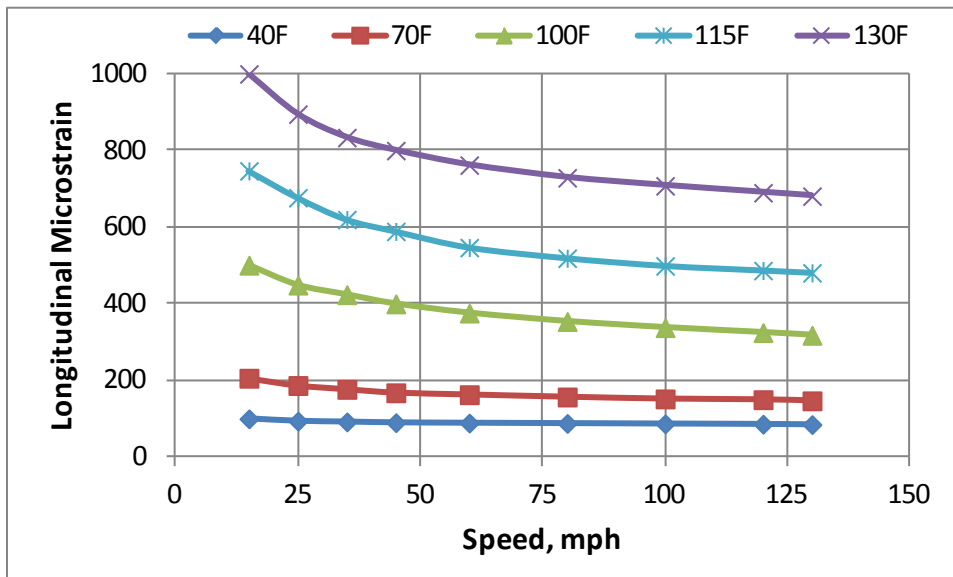


FIGURE 7.7 Influence of vehicle speed on simulated longitudinal microstrain – Control Section S9.

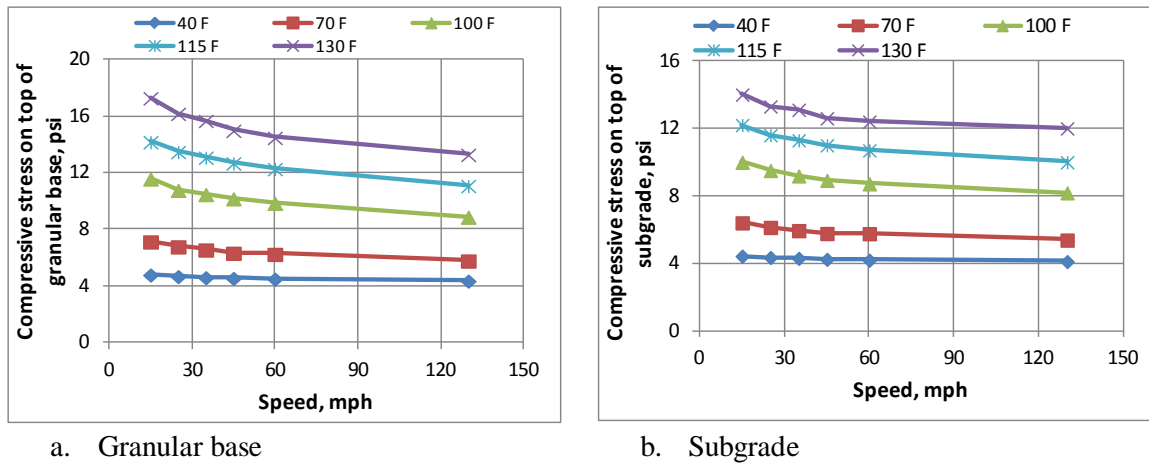


FIGURE 7.8 Influence of vehicle speed on simulated compressive stress – Control Section S9.

Figure 7.9 shows a comparison in longitudinal microstrain for all sections versus S9. Pavement responses were compared at 5 different temperatures (40, 70, 100, 115 and 130 °F) and at 5 different operating speeds (15, 25, 35, 45 and 60 mph). Compared to section S9, sections S10, S11 and N7 exhibited higher strains along the entire range of temperatures and speeds. Higher strain levels were expected for sections S10 and S11 due to the lower AC layer moduli. In the case of N7, the higher strain levels were explained by the significantly thinner AC layer (about 2 inches thinner) with respect to S9. Section S12 showed slightly lower strains at lower temperatures/higher speeds and similar strains at higher temperatures/lower speeds than S9. Lower strain levels were expected for section S12 due to the higher AC modulus; however, the observed behavior could be explained by the thinner structure (AC + base) placed on top of the subgrade (about 1 inch thinner). Sections N6 and N10 exhibited lower strains at lower temperatures/higher speeds but similar strains at higher temperatures/lower speeds. As expected, sections N5 and N10 exhibited lower strains along the entire range of temperatures and speeds. Lower strain levels were expected for sections N5, N6, N10 and N11 due to the higher AC moduli and thicker AC layer for N5.

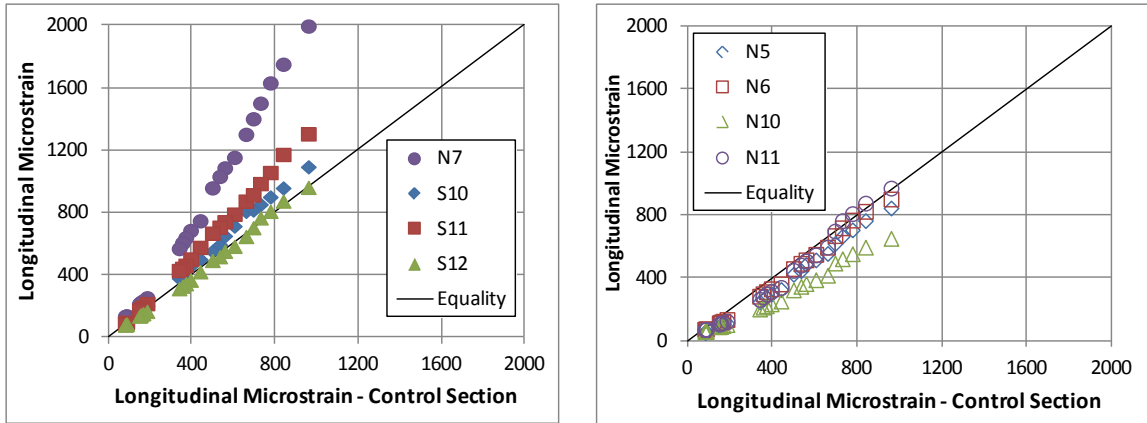


FIGURE 7.9 Simulated longitudinal microstrain – All sections versus S9.

Figure 7.10 shows a comparison in terms of compressive stress for all sections versus S9. Compared to section S9, section N7 exhibited higher stresses along the entire range of temperatures and speeds. Higher stress levels were expected for N7 due to the thinner AC layer (about 2 inches thinner) with respect to S9. Sections S10, S11 and S12 exhibited similar stresses at lower temperatures/higher speeds and higher stresses at higher temperatures/lower speeds. Section N5 showed lowest stress levels along the entire range of temperature and speed due to the thicker AC layer. Lower stress levels were also expected for sections N6, N10 and N11 due to the higher AC moduli compared to S9.

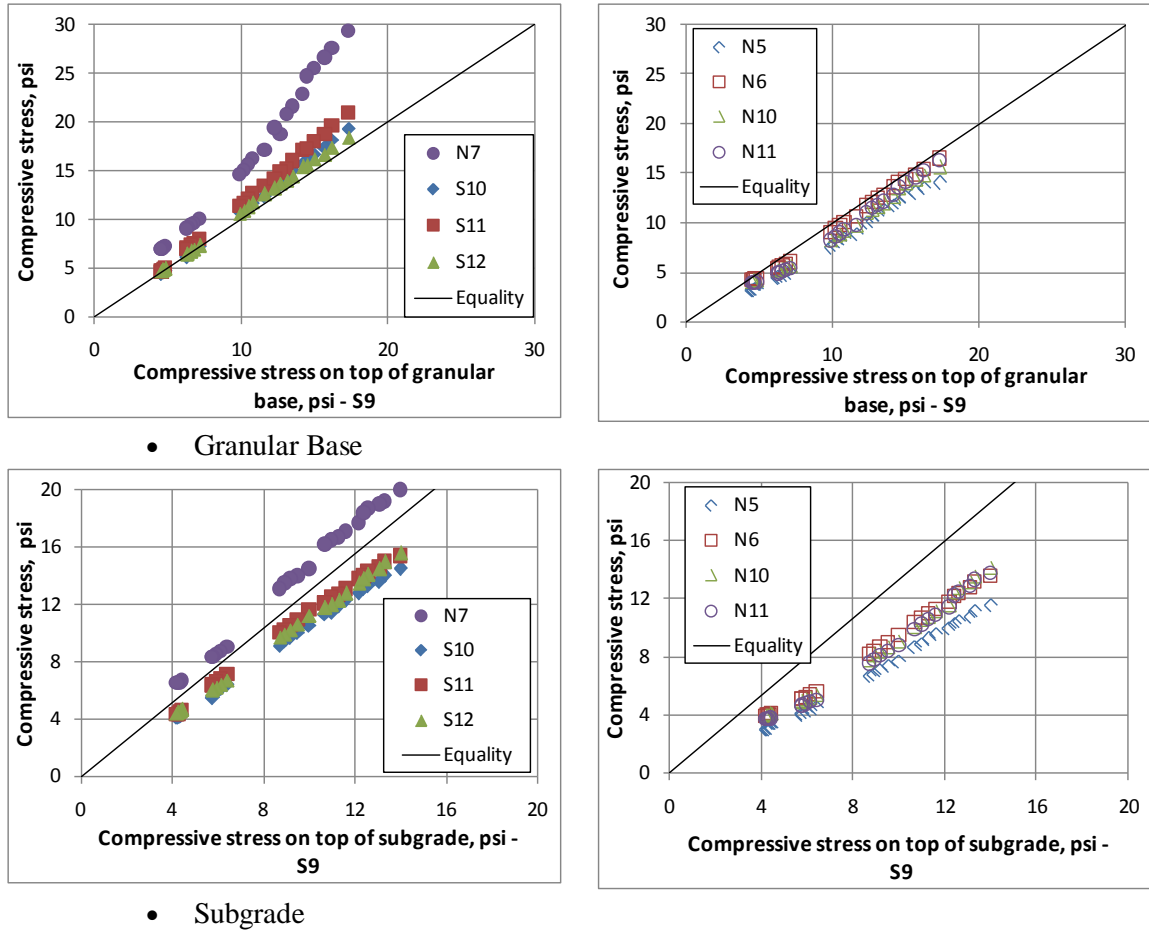


FIGURE 7.10 Simulated compressive stress – All sections versus S9.

7.5 Determination of Correction Factors

Correction factors were determined for three pavement responses: horizontal longitudinal strain computed at the bottom of the AC layer, vertical compressive stress computed at the top of the granular base and compressive stress computed at the top of the subgrade. Correction factors were defined as the difference between the calculated pavement response at the desired operational speed (in this study 45 mph) and the calculated pavement response at the equivalent FWD speed. The mean difference in strain levels or the mean of the strain correction factors considering all the sections was found to be 59.96 microstrain and it was significant at a confidence level of 95% ($\alpha = 0.05$, paired t-test). Figure 7.11 illustrates the strong relationship between longitudinal strain correction factors and temperature of the AC layer. Sections N7 and

N10 had the highest and lowest correction factor curves respectively. This trend was also obtained for the respective strain levels (Figure 7.9). These strong relationships allowed the application of correction factors for any temperature within the evaluated temperature range (40 – 130 °F). An exponential function (Equation 7.2) was found to be the best fit for all the cases and the corresponding coefficients are shown in Table 7.4. The coefficient k_1 is an indication of the level of absolute difference between strains computed at FWD speed and 45 mph. As expected higher correction factor levels were obtained for S10 and S11 due to the higher relative difference in effective dynamic modulus. Sections N5, N6, N7 and S12 exhibited intermediate levels while N10 and N11 showed significantly lower levels compared to the control section.

$$\text{Correction Factor} = k_1 e^{k_2 T} \quad \text{Eq. 7.2}$$

Where;

T = Mid-depth AC temperature, °F

k_1 and k_2 are regression coefficients

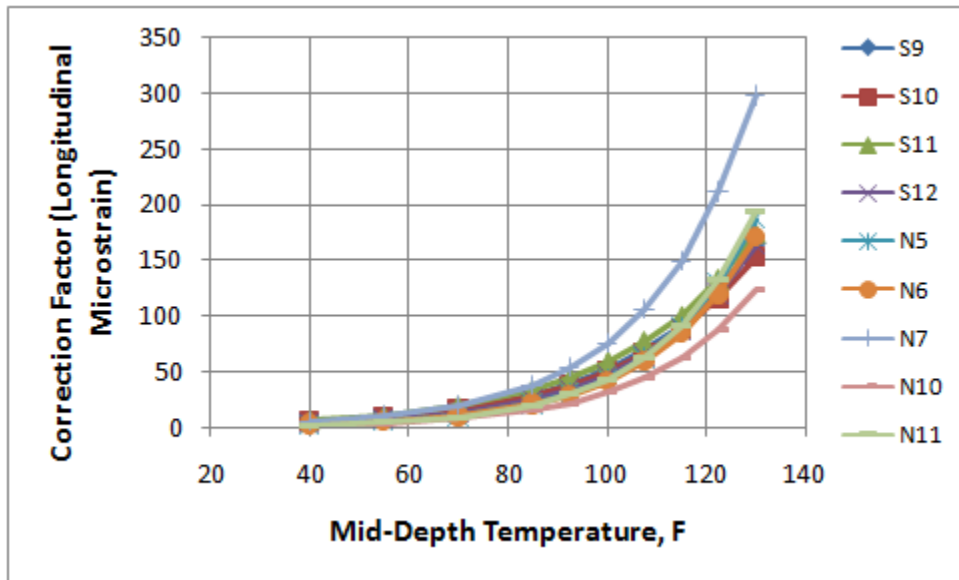


FIGURE 7.11 Relationship between strain correction factors and temperature.

TABLE 7.4 Equation coefficients for strain correction factors

Section	k₁	k₂	R²
S9	1.0753	0.0387	0.995
S10	1.2078	0.0372	0.998
S11	1.5129	0.0365	0.999
S12	0.6798	0.0422	0.991
N5	0.3239	0.0489	0.986
N6	0.3643	0.0473	0.982
N7	0.7784	0.0457	0.992
N10	0.3065	0.0462	0.979
N11	0.2801	0.0503	0.975

The mean difference in base stress levels or the mean of the stress correction factors considering all the sections was found to be 1.087 psi and it was significant at a confidence level of 95% ($\alpha = 0.05$, pair t-test). Figure 7.12 illustrates the strong relationship between the compressive stress correction factors of the granular base and temperature. Sections N7 and N5 had the highest and lowest correction factor curves respectively. This trend was also obtained for the respective strain levels (Figure 7.10). An exponential function was found to be the best fit for all the cases and the corresponding coefficients are shown in Table 7.5. In this case, slightly higher correction factor levels were obtained for S10, S11 and S12 while N10 and N11 showed significantly lower levels compared to the control section as expected.

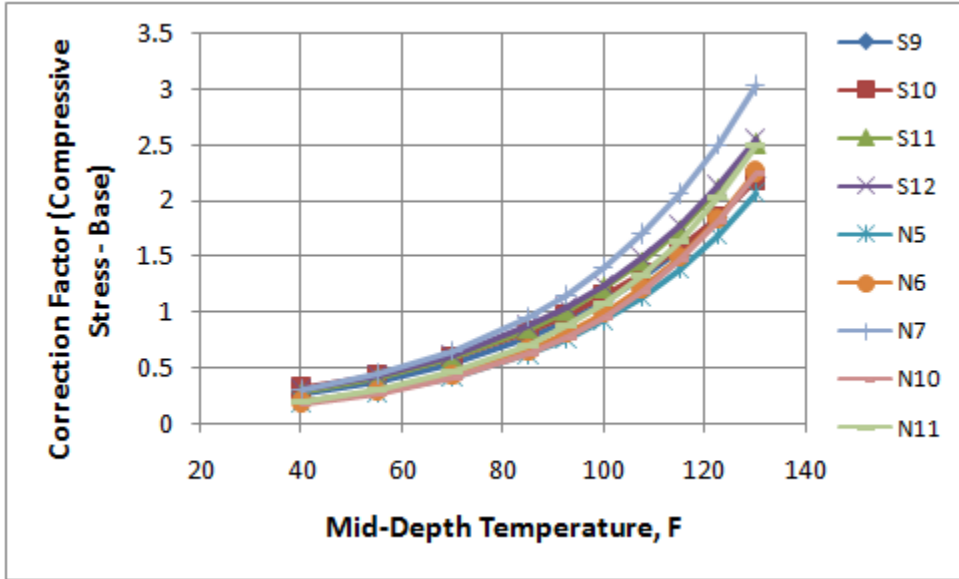


FIGURE 7.12 Relationship between stress (base) correction factors and temperature.

TABLE 7.5 Equation coefficients for stress (base) correction factors

Section	k_1	k_2	R^2
S9	0.1031	0.0236	0.996
S10	0.1317	0.0216	0.999
S11	0.1066	0.0243	0.998
S12	0.1141	0.0239	0.997
N5	0.0635	0.0268	0.996
N6	0.0632	0.0275	0.992
N7	0.1072	0.0257	0.995
N10	0.0552	0.0285	0.989
N11	0.0646	0.0281	0.992

The mean difference in subgrade stress levels or the mean of the stress correction factors considering all the sections was found to be 0.622 psi and it was significant at a confidence level of 95% ($\alpha = 0.05$, pair t-test). Figure 7.13 illustrates the relationship between the compressive stress correction factors of the subgrade and temperature. At this point, stress correction factors were found to be less sensitive to changes in temperature for all section but N10 and N11. An exponential function was found to be the best fit for all the cases and the corresponding coefficients are shown in Table 7.6. In this case, slightly higher correction factor levels were

obtained for S11, S12 and N5; however, the curve of N5 matched the S9 curve. On the other hand N10 and N11 showed significantly lower levels compared to the control section as expected; however, higher slopes provided higher correction factors at higher temperatures. Sections N10 and N11 had thinner structures placed on top of the subgrade and therefore stress levels were expected to be higher.

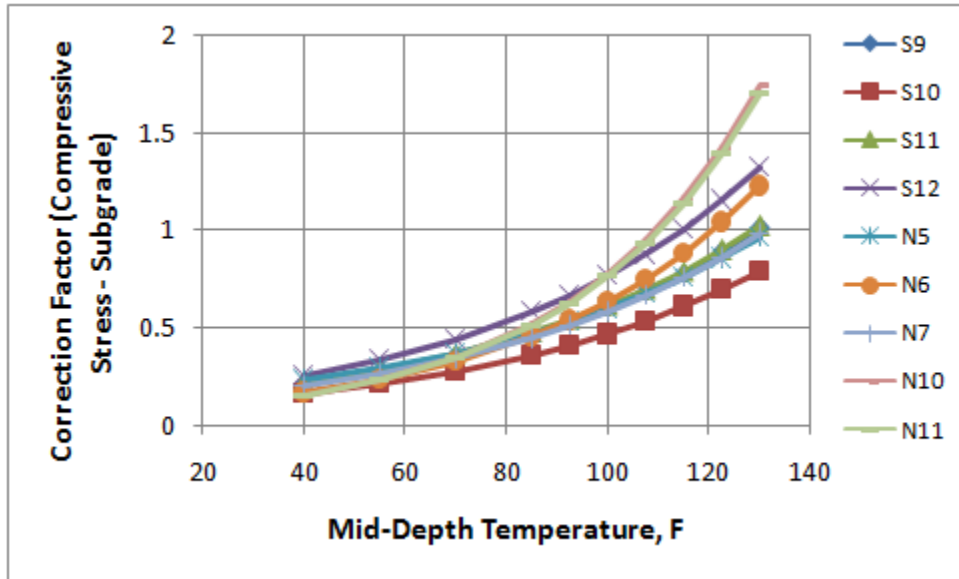


FIGURE 7.13 Relationship between stress (subgrade) correction factors and temperature.

TABLE 7.6 Equation coefficients for stress (subgrade) correction factors

Section	k_1	k_2	R^2
S9	0.1081	0.0172	0.999
S10	0.0805	0.0176	0.999
S11	0.1135	0.0169	0.999
S12	0.1243	0.0182	0.999
N5	0.1223	0.0159	0.999
N6	0.0703	0.022	0.997
N7	0.1012	0.0175	0.999
N10	0.0534	0.0268	0.991
N11	0.053	0.0267	0.993

7.6 Measured Pavement Responses

Previous studies at the Test Track (58, 59) developed strain-temperature relationships based on the mid-depth temperature. To remain consistent with the previous research, the mid-depth temperature was once again used to develop new strain-temperature relationships. For each test section, the strain was expressed as a function of mid-depth temperature using Equation 6.2. A positive relationship between temperature and AC strain was expected because as the temperature in a pavement structure increases the measured strain also increases (58, 59).

$$\text{Strain} = k_1 e^{k_2 T} \quad \text{Eq. 7.3}$$

Where:

T = Mid-depth AC temperature, °F

k_1, k_2 = Regression coefficients.

Figure 7.14 illustrates the strong relationship between mid-depth asphalt concrete (AC) temperature and measured strain responses for section S9. An exponential function was found to be the best fit for all sections and Table 7.7 exhibits the respective equation coefficients and R^2 values.

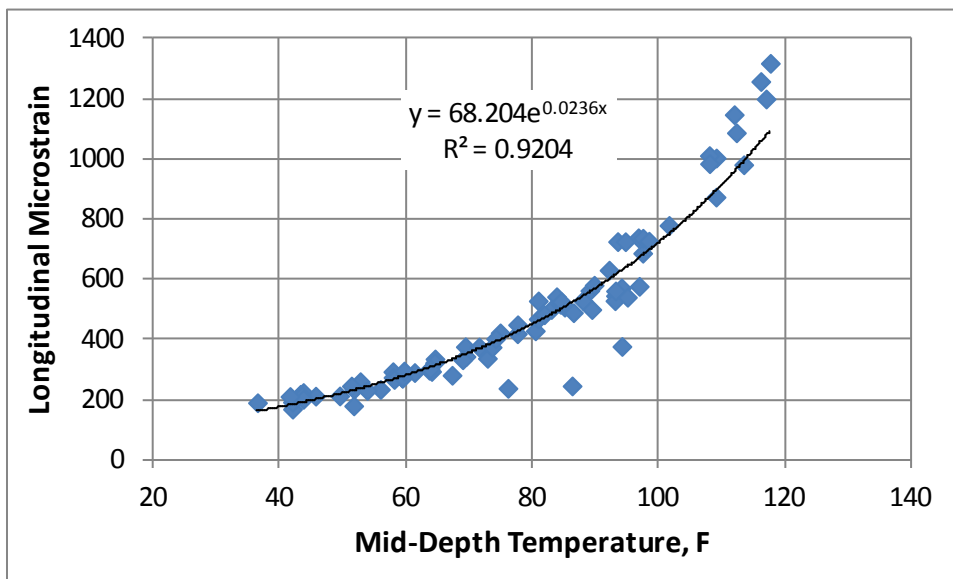


FIGURE 7.14 Measured longitudinal microstrain section S9.

To determine if the response-temperature relationships were statistically similar among the sections, 95% confidence intervals were obtained on the intercepts (k_1) and slopes (k_2). At a 95% confidence level there was no evidence that the regression coefficients of all sections were statistically different from the control with the exception of N5. It was expected that thicker sections should have lower strain levels. Strain levels were represented by the coefficient k_1 . As expected, N5 had a lower k_1 coefficient than S9. The k_2 coefficients represented the rate of strain increase with temperature. Pavements with higher k_2 coefficients were considered more susceptible to temperature changes. Section N11 was statistically less sensitive to temperature changes while N5 was more sensitive to temperature changes than S9.

TABLE 7.7 Strain equation coefficients

Section	k_1	k_1 Lower 95%	k_1 Upper 95%	k_2	k_2 Lower 95%	k_2 Upper 95%	R²
S9	68.97	57.27	80.18	0.0236	0.0220	0.0251	0.920
S10	53.49	49.85	57.41	0.0257	0.0248	0.0265	0.977
S11	53.28	46.20	61.46	0.0255	0.0236	0.0273	0.928
S12	71.29	57.26	88.76	0.0217	0.0191	0.0243	0.771
N5	35.73	32.57	39.20	0.0275	0.0263	0.0286	0.970
N6	65.96	60.40	72.03	0.0251	0.0240	0.0261	0.963
N7	42.99	27.52	67.16	0.0289	0.0229	0.0349	0.607
N10	64.47	52.52	79.13	0.0199	0.0173	0.0225	0.883
N11	73.24	66.90	80.17	0.0185	0.0175	0.0196	0.961

Figure 7.15 illustrates the strong relationship between mid-depth asphalt concrete (AC) temperature and measured compressive stress on top of the granular base for all the sections. An exponential function was found to be the best fit for all sections and Table 7.8 exhibits the respective equation coefficients and R² values for all sections. It was determined that at a 95% confidence level the k_1 coefficients of S10, N5 and N7 were statistically different from the control. The significantly lower k_1 coefficient for S10 was not expected and it was attributed to gauge malfunction. As expected, N5 had lower k_1 coefficient due to the thicker AC layer than S9 and N7 had a higher k_1 coefficient due to the thinner AC layer. Statistically lower k_2 coefficients

than the control section were found for sections S12, N7, N10 and N11 while section S10 exhibited higher susceptibility to changes in temperature than the control section.

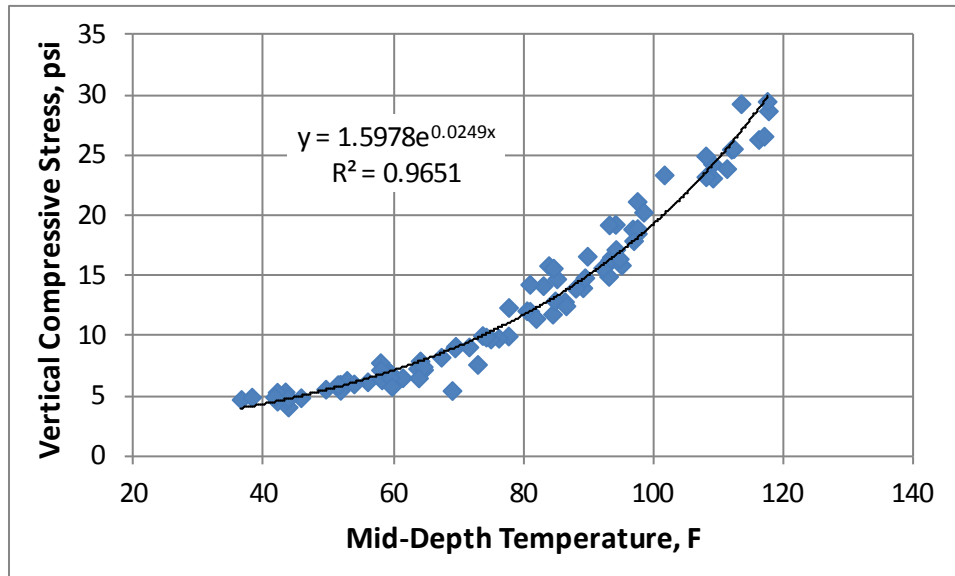


FIGURE 7.15 Measured compressive stress on top of granular base.

TABLE 7.8 Base stress equation coefficients

Section	k_1	k_1 Lower 95%	k_1 Upper 95%	k_2	k_2 Lower 95%	k_2 Upper 95%	R^2
S9	1.598	1.472	1.734	0.0246	0.0239	0.0259	0.965
S10	0.711	0.647	0.781	0.0288	0.0277	0.0300	0.967
S11	1.461	1.334	1.600	0.0254	0.0243	0.0266	0.968
S12	1.553	1.441	1.674	0.0226	0.0217	0.0235	0.969
N5	0.998	0.931	1.070	0.0262	0.0253	0.0270	0.981
N6	1.618	1.517	1.725	0.0252	0.0244	0.0260	0.980
N7	3.482	3.000	4.042	0.0197	0.0178	0.0215	0.863
N10	1.265	1.157	1.382	0.0219	0.0208	0.0229	0.951
N11	1.611	1.450	1.790	0.0218	0.0205	0.0230	0.961

Figure 7.16 illustrates the strong relationship between mid-depth asphalt concrete (AC) temperature and measured compressive stress on top of the subgrade for all the sections. An exponential function was found to be the best fit for all sections. Table 7.9 exhibits the respective equation coefficients and R^2 values for all sections. At a 95% confidence level there was no evidence that the regression coefficients of all sections were statistically different from the

control with the exception of N5 and N7. As expected, N5 had a lower k_1 coefficient (lower compressive stresses) due to the thicker AC layer than S9 and on the contrary N7 had a higher k_1 coefficient due to the thinner AC layer than S9. The k_2 coefficients represented the rate of strain increase with temperature. Pavements with higher k_2 coefficients were considered more susceptible to temperature changes. Only sections N7 and N10 were statistically less sensitive to temperature changes than the control section.

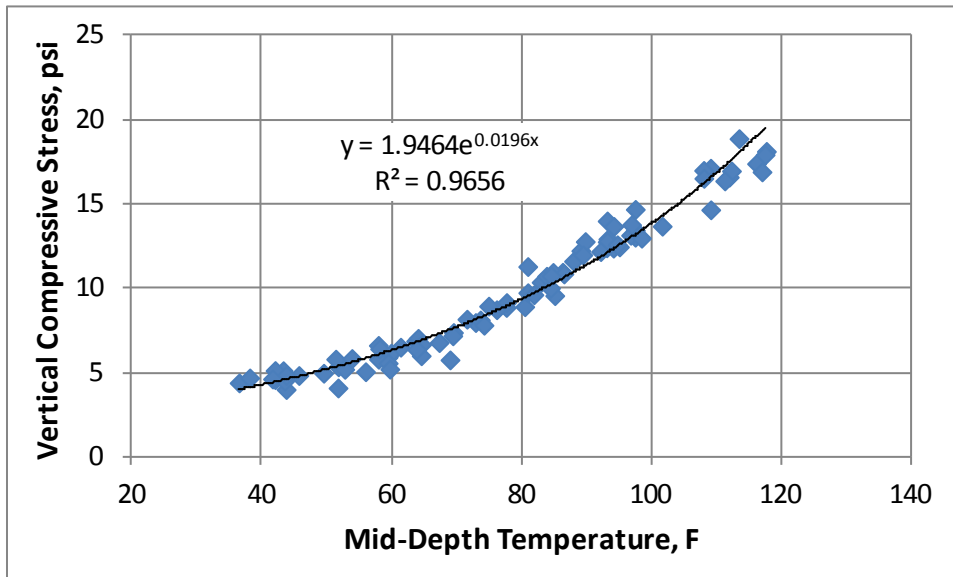


FIGURE 7.16 Measured compressive stress on top of subgrade.

TABLE 7.9 Subgrade stress equation coefficients

Section	k_1	k_1 Lower 95%	k_1 Upper 95%	k_2	k_2 Lower 95%	k_2 Upper 95%	R^2
S9	1.946	1.825	2.075	0.0196	0.0188	0.0204	0.966
S10	1.816	1.725	1.912	0.0204	0.0198	0.0210	0.980
S11	1.722	1.620	1.830	0.0200	0.0193	0.0208	0.976
S12	1.803	1.719	1.890	0.0188	0.0183	0.0194	0.982
N5	1.382	1.306	1.462	0.0203	0.0196	0.0209	0.979
N6	2.113	1.994	2.238	0.0197	0.0190	0.0204	0.974
N7	4.504	3.993	4.538	0.0119	0.0120	0.0136	0.855
N10	2.085	1.858	2.338	0.0136	0.0122	0.0150	0.818
N11	1.877	1.630	2.161	0.0191	0.0175	0.0207	0.927

7.7 Predicted Versus Measured Critical Responses

Backcalculated layer moduli were used to compute pavement responses under a single axle load assuming a full bond interaction between layers. ANN-predicted moduli were used to compute pavement responses assuming a full slip interaction between layers. In the second case, the AC layer was divided into the three original (as built) layers (Figure 7.17). Layered-elastic analysis was utilized to calculate all pavement responses from backcalculated and ANN-predicted layer moduli. The measured strain-temperature equations shown previously were developed using the strain amplitude measured from inflection to peak. A similar approach was followed using layered-elastic theory to calculate the strain amplitude for a single axle load. A predicted strain had to be matched to the mid-depth temperature recorded during FWD testing at a given date and section. Best fit curves between predicted strain and mid-depth temperature were obtained for each section.

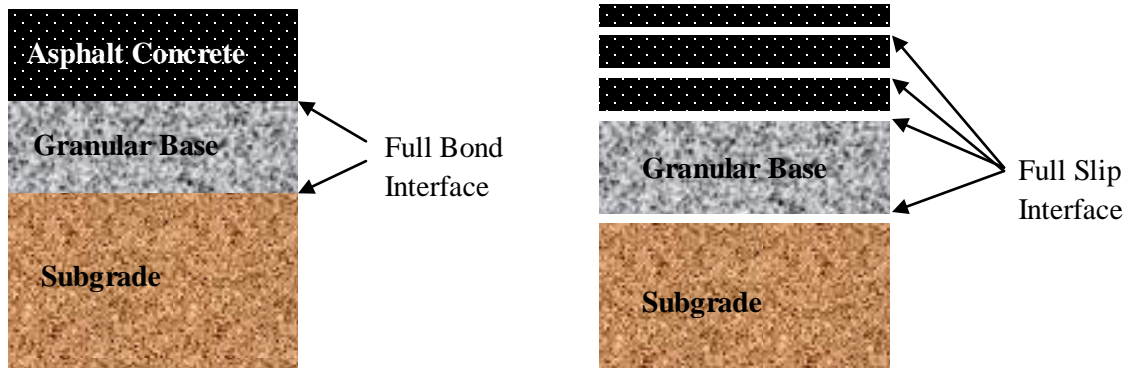


FIGURE 7.17 Modeled layer interface conditions.

Figure 7.18 shows the strong relationship between temperature and calculated longitudinal microstrain for section S9 in full bond and full slip conditions. Higher strain levels were expected when considering full slip interaction between consecutive layers (for all five layers). When full bond is specified during the analysis process, the pavement acts as one

cohesive structure (stronger), but when full slip is specified, the pavement behaves as independent structures stacked on each other (weaker structure).

An exponential function was found to be the best fit for all sections and Table 7.10 exhibits the respective equation coefficients and R^2 values. To determine if the response-temperature relationships were statistically similar among the sections, hypothesis tests were performed on the intercepts (k_1) and slopes (k_2). At a 95% confidence level there was no evidence that the regression coefficients of all sections were statistically different from the control with the exception of N5 and N7. It was expected that thicker sections should have lower strain levels. Strain levels were represented by the coefficient k_1 . As expected, N5 had lower k_1 coefficients and N7 had higher k_1 coefficients for all cases (FB and FS). The k_2 coefficients represented the rate of strain increase with temperature. Pavements with higher k_2 coefficients were considered more susceptible to temperature changes. Only section N7 was statistically less sensitive to temperature changes.

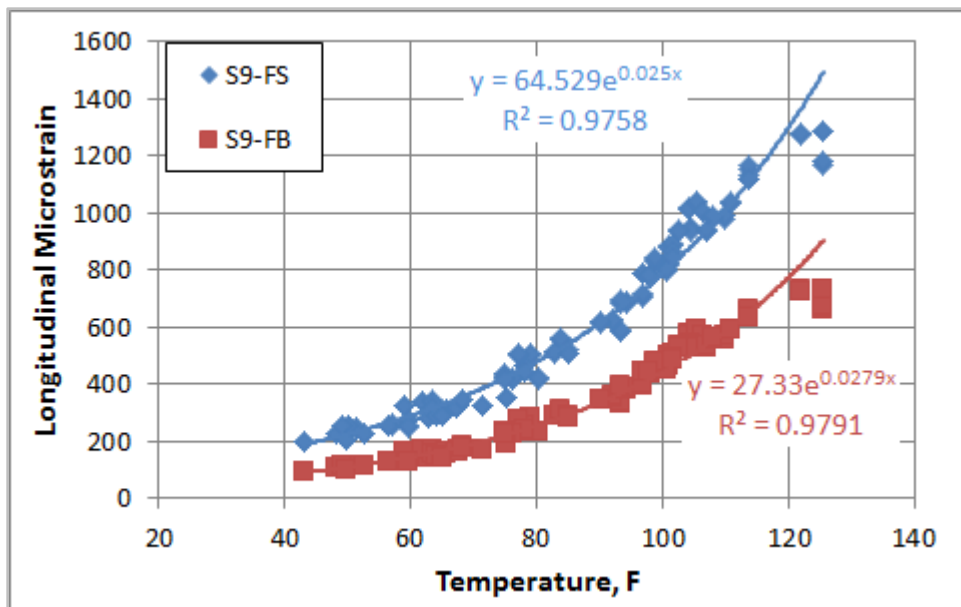


FIGURE 7.18 Calculated microstrain versus temperature - S9.

TABLE 7.10 Equation coefficients for calculated microstrain

Section	Full Slip Condition			Full Bond Condition		
	k_1	k_2	R^2	k_1	k_2	R^2
S9	64.529	0.025	0.976	27.33	0.0279	0.979
S10	78.823	0.0234	0.974	37.715	0.0245	0.974
S11	60.15	0.0276	0.968	28.432	0.0287	0.969
S12	66.003	0.0245	0.973	28.83	0.0256	0.974
N5	28.982	0.0283	0.981	11.243	0.0337	0.984
N6	66.938	0.0237	0.987	20.349	0.0305	0.989
N7	238.61	0.0142	0.957	60.855	0.0196	0.983
N10	36.691	0.0291	0.973	17.312	0.0301	0.974
N11	45.718	0.025	0.986	24.158	0.0257	0.989

A direct comparison of measured and computed pavement responses was not possible due to the differences in test/measurement conditions such as: different date, temperature and traffic (load). However, indirect comparisons were performed. Figure 7.19 shows the cumulative distribution curves of the measured and computed longitudinal microstrain (full bond and full slip condition) for all sections. Underestimation of the strains was obtained when full bond was specified during the analysis process and when full slip is specified, the opposite (overestimation) was obtained. The lower strain levels obtained when considering full bond condition can be partially explained by the higher speed/frequency of the backcalculated properties as discussed earlier in this chapter. Figure 7.18 also suggests that assuming either a full bond or a full slip conditions are extreme cases and that the true layer interface condition has to be somewhere in between.

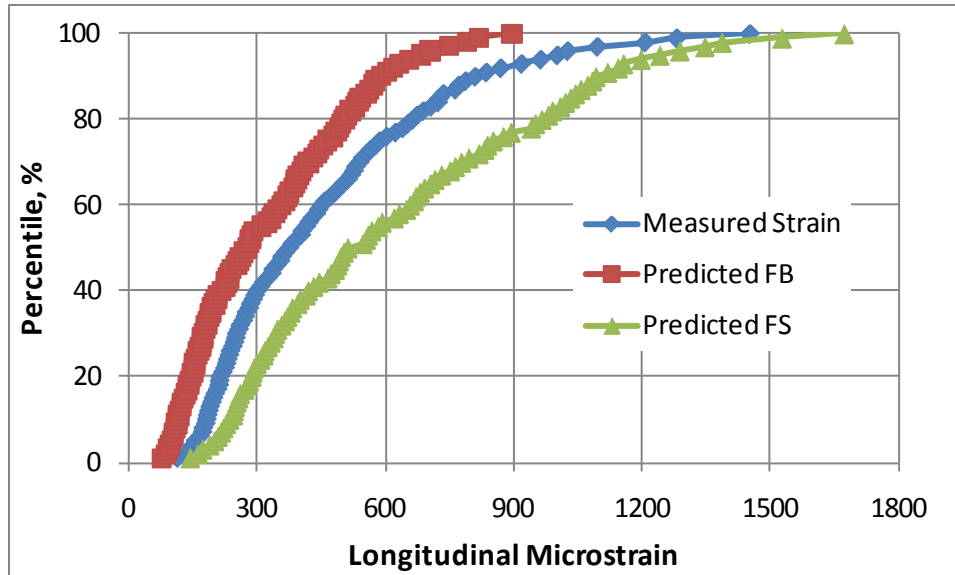


FIGURE 7.19 Comparison between measured and calculated microstrain.

Figure 7.20 shows a comparison between measured strains and computed strains from the equations shown in Table 7.10. The slope of the curves showed in Figure 7.19 was used as a measure of equivalency between predicted and measured strain levels. The deviation from a slope of 1.0 (perfect equivalency between groups) provides a percentage of predicted values above or below the expected ones. On average, the tendency was to overestimate strain responses by 7% for the full slip (FS) scenario and underestimate strain responses by 43% for the full bond (FB) scenario. In addition, it was found that 69% of the FS points were above the equality line while 84% of the FB points were below the equality line. This indicated that the use of FS condition could predict strains closer to the measured ones. However, predicted strains from both scenarios were influenced by the higher speed/frequency of the FWD tests. The current backcalculation process utilizes layered elastic models that do not take into account viscoelastic effects; therefore, this can also help explain the poor match between predicted and measured strains.

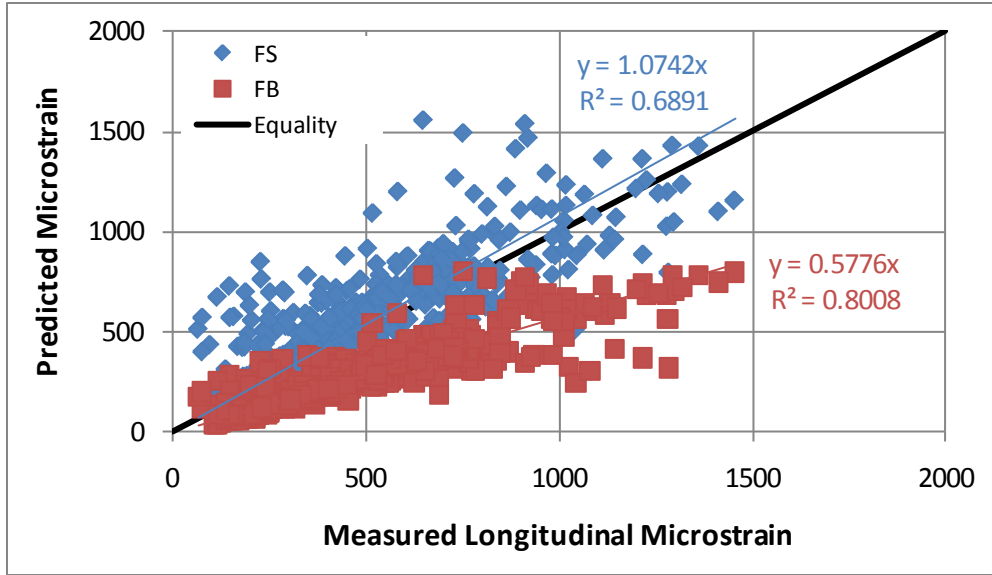


FIGURE 7.20 Measured versus predicted longitudinal microstrain.

Figure 7.21 shows the strong relationship between temperature and calculated compressive stress (granular base) for section S9 in full bond and full slip conditions. Higher stress levels were expected when considering full slip interaction (weaker structure) between consecutive layers. In this case, either a straight line or an exponential function was found to be the best fit for all sections; however, an exponential function was used since most relationships appeared to follow that trend. Table 7.11 exhibits the respective equation coefficients and R^2 values for all sections. It was determined that at a 95% confidence level there was no evidence that the equation coefficients of all sections were statistically different from the control except for N5 in full bond condition. As expected, N5 had a lower k_1 coefficient due to the thicker AC layer; however, a higher k_2 coefficient indicated higher susceptibility to temperature changes.

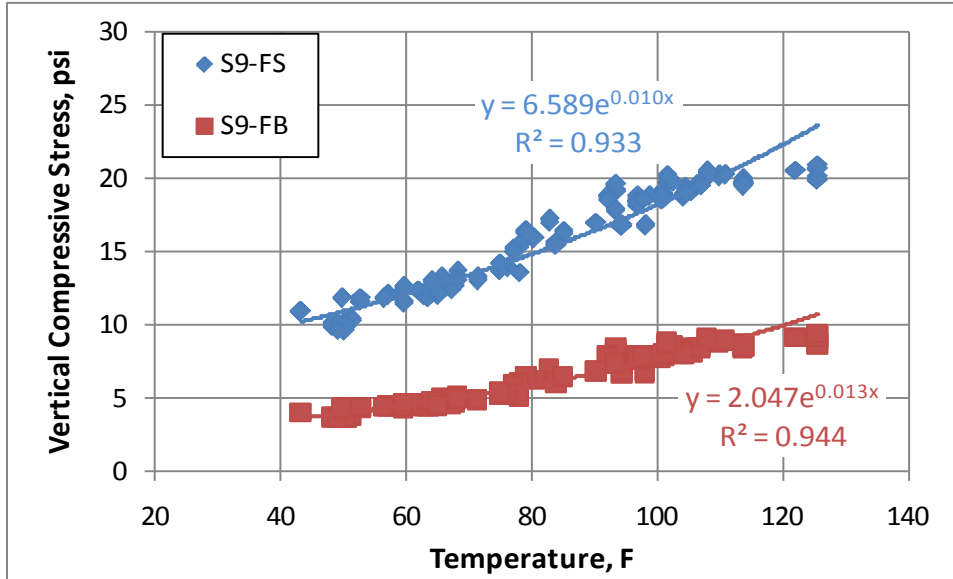


FIGURE 7.21 Calculated compressive stress section S9 (Base).

TABLE 7.11 Equation coefficients for calculated stress (Base)

Section	Full Slip Condition			Full Bond Condition		
	k_1	k_2	R^2	k_1	k_2	R^2
S9	6.589	0.0102	0.933	2.0472	0.0132	0.944
S10	6.995	0.0086	0.958	2.037	0.012	0.965
S11	6.357	0.0093	0.932	1.8828	0.0124	0.935
S12	6.253	0.0094	0.955	1.795	0.0128	0.959
N5	2.215	0.0191	0.907	1.1579	0.0173	0.929
N6	5.742	0.0133	0.938	1.906	0.0162	0.950
N7	7.771	0.011	0.926	3.5387	0.0107	0.938
N10	6.887	0.009	0.925	2.0453	0.0126	0.933
N11	8.294	0.0089	0.951	2.4607	0.0129	0.959

Figure 7.22 shows the cumulative distribution curves of the measured and computed compressive stress located at the top of the granular base (full bond and full slip condition) for all sections. Underestimation of the stresses was obtained when full bond was specified during the analysis process and when full slip is specified overestimation was obtained for about 90% of the data points. The remaining 10% of stress underestimation took place at high end of the measured stresses (over 24 psi). The lower stress levels obtained when considering full bond condition can

be partially explained by the higher speed/frequency of the backcalculated properties and the lower susceptibility of predicted stresses to changes in temperature.

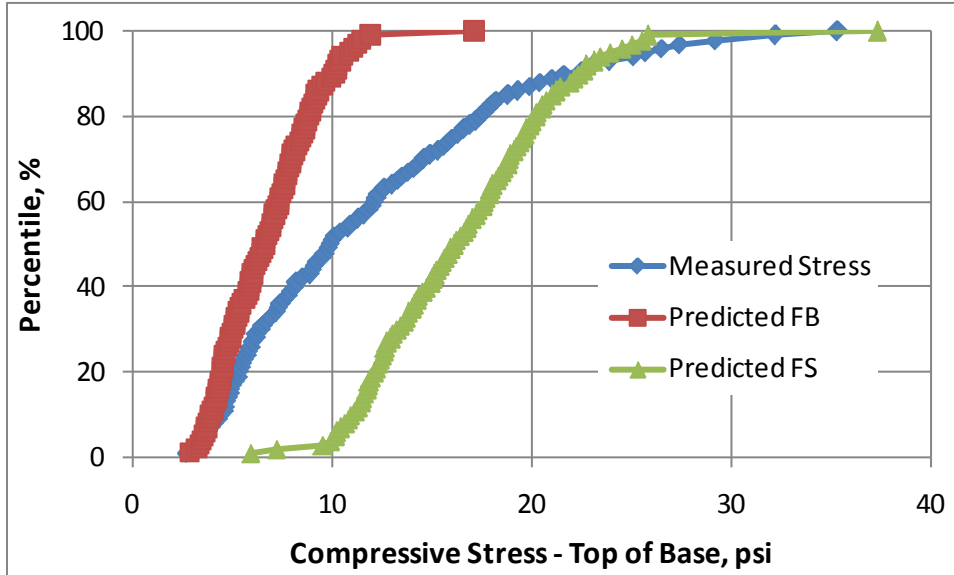


FIGURE 7.22 Comparison between measured and calculated stress (Base).

Figure 7.23 shows a comparison between measured and computed base stresses from the equations shown in Table 7.11. In this case, the intercept of the both linear equations were statistically significant and this was explained by the lower sensitivity of predicted stresses to react to small changes in temperature. On average, the tendency was to overestimate stress responses by 78% (percent of points above equality line) for the full slip (FS) scenario and underestimate stress responses by 82% (percent of points below equality line) for the full bond (FB) scenario.

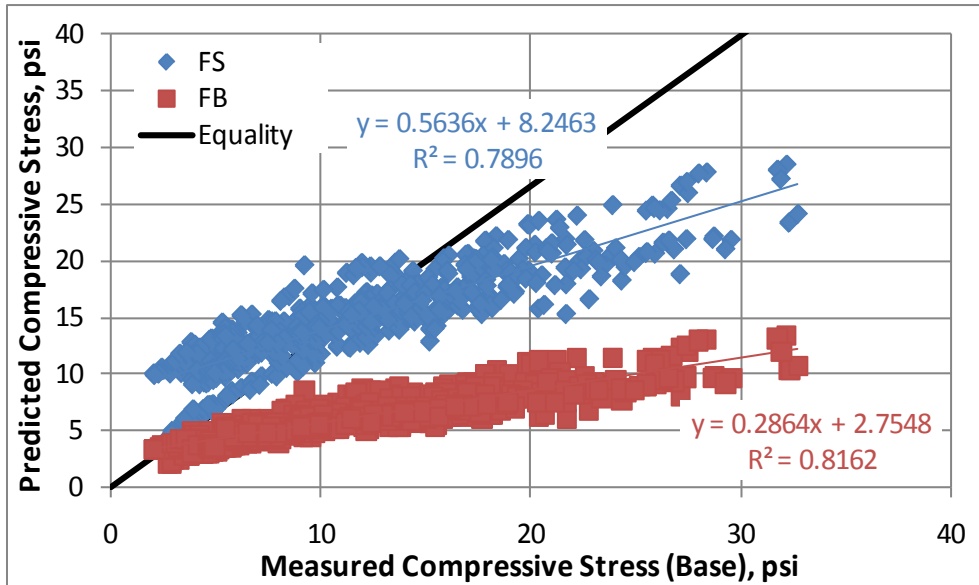


FIGURE 7.23 Measured versus predicted compressive stress (Base).

Figure 7.24 shows the strong relationship between temperature and calculated compressive stress (subgrade) for section S9 in full bond and full slip conditions. Once again, higher stress levels were expected when considering full slip interaction (weaker structure) between consecutive layers. An exponential function was found to be the best fit for all sections. Table 7.12 exhibits the respective equation coefficients and R^2 values for all sections. It was determined that at a 95% confidence level there was no evidence that the equation coefficients of all sections were statistically different from the control except for N5 in full bond condition. Also for this case, N5 had a lower k_1 coefficient due to the thicker AC layer and a higher k_2 coefficient indicated higher susceptibility to temperature changes.

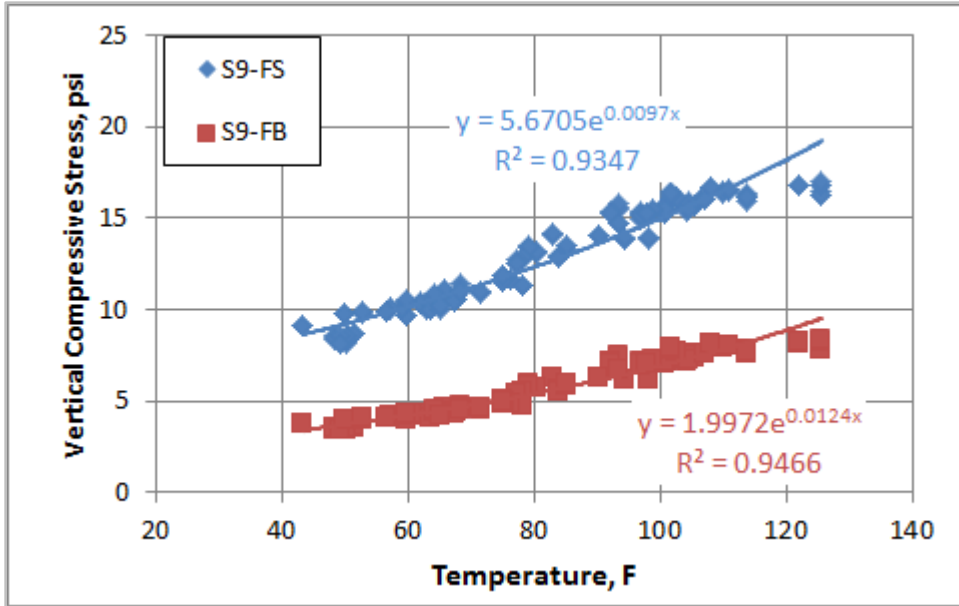


FIGURE 7.24 Calculated compressive stress section S9 (Subgrade).

TABLE 7.12 Equation coefficients for calculated stress (Subgrade)

Section	Full Slip Condition			Full Bond Condition		
	k_1	k_2	R^2	k_1	k_2	R^2
S9	5.6705	0.0097	0.934	1.9972	0.0124	0.946
S10	6.0849	0.0078	0.956	1.9855	0.0112	0.965
S11	5.5974	0.0087	0.934	1.8378	0.0118	0.936
S12	5.5634	0.009	0.956	1.7695	0.0123	0.959
N5	1.9266	0.0188	0.907	1.1524	0.0164	0.931
N6	4.9408	0.0129	0.941	1.8738	0.0154	0.954
N7	6.401	0.011	0.930	3.421	0.0102	0.942
N10	6.1607	0.0088	0.928	2.018	0.0124	0.935
N11	7.2468	0.0086	0.957	2.3838	0.0125	0.964

Figure 7.25 shows the cumulative distribution curves of the measured and computed subgrade compressive stress (full bond and full slip condition) for all sections. Underestimation of the stresses was obtained when full bond was specified during the analysis process and when full slip is specified overestimation was obtained. The lower stress levels obtained when considering full bond condition can be partially explained by the higher speed/frequency of the

backcalculated properties and the lower susceptibility of predicted stresses to changes in temperature.

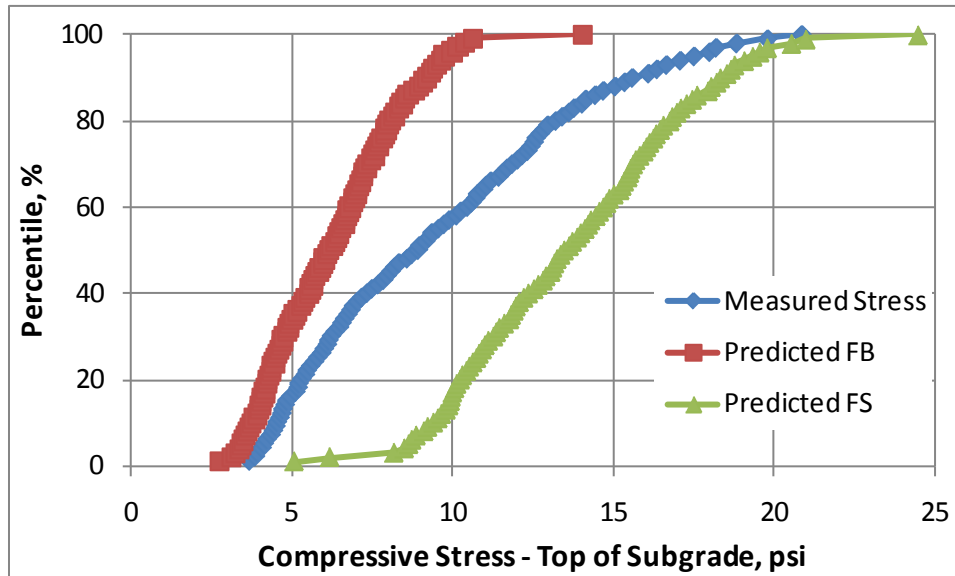


FIGURE 7.25 Comparison between measured and calculated stress (Base).

Figure 7.26 shows a comparison between measured and computed subgrade stresses from the equations shown in Table 7.12. The intercept of the both linear equations were also statistically significant and this was explained by the lower sensitivity of predicted stresses to react to small changes in temperature. The results showed that the tendency was to overestimate stress responses by 94% (percent of points above equality line) for the full slip (FS) scenario and underestimate stress responses by 86% (percent of points below equality line) for the full bond (FB) scenario.

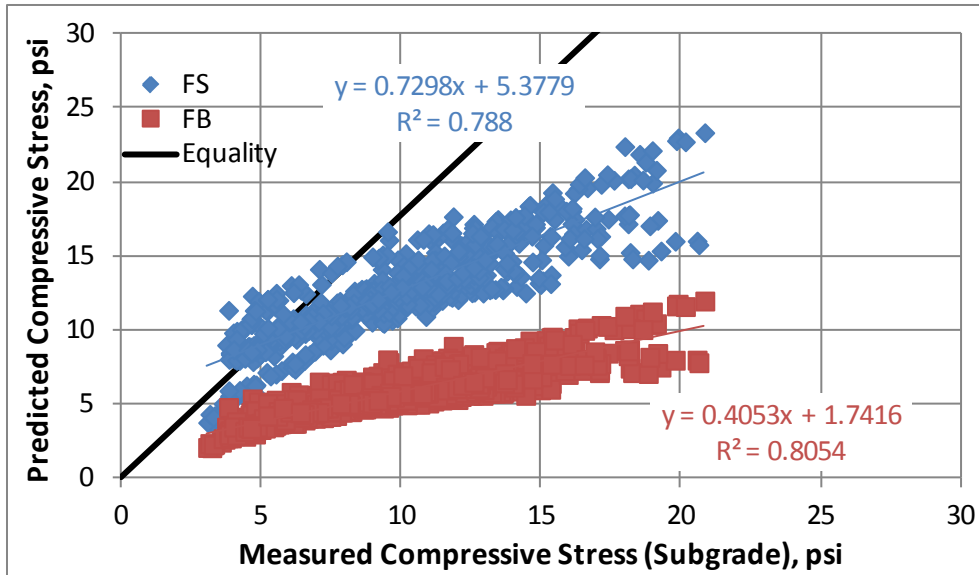


FIGURE 7.26 Measured versus predicted compressive stress (Subgrade).

7.8 Application of Correction Factors

Correction factors were obtained from the assumption that all the layers had a full bond interface. Therefore, these factors can only be applied to the predicted responses that also considered a full bond condition. The results obtained up to this point indicated that predicted pavement responses assuming full bond condition tended to underestimate measured responses. It was also expected that the application of the correction factors increased the level of pavement responses in order to predict more accurate results. On the other hand, if the software utilized in this study (*3D-Move*) had the capability to simulate full slip conditions between layers, this should provide correction factors that in theory should also increase the level of pavement responses.

Figure 7.27 shows an example of the application of correction factors on longitudinal strains. The curve of measured longitudinal microstrain versus temperature was significantly above the curve of predicted microstrain using backcalculated AC moduli. This second curve was adjusted by correction factors providing a new curve closer to the measured one. The difference between measured and predicted strains was significantly higher (average of 42%) even for the corrected curve which had an average difference of 35.5%. These results were obtained from the

slope of the predicted versus measured strain levels curves. The closer the slope of these curves to 1.0 the closer the predicted values are to the measured ones. Table 7.13 shows the analyses performed to evaluate the effect of the correction factors. The slopes of predicted versus measured strains curves were approached to 1.0 by an average of 12%. The average absolute error (AAE) was also computed to evaluate the effect of the correction factors. On average, an AAE of 42.7% was obtained for all sections. Once the correction factors were applied, the error was reduced by 10.8%. The most affected section by the application of the correction factors was N11 which had the highest change in slope (14.8%) and the highest change in AAE (16.9%).

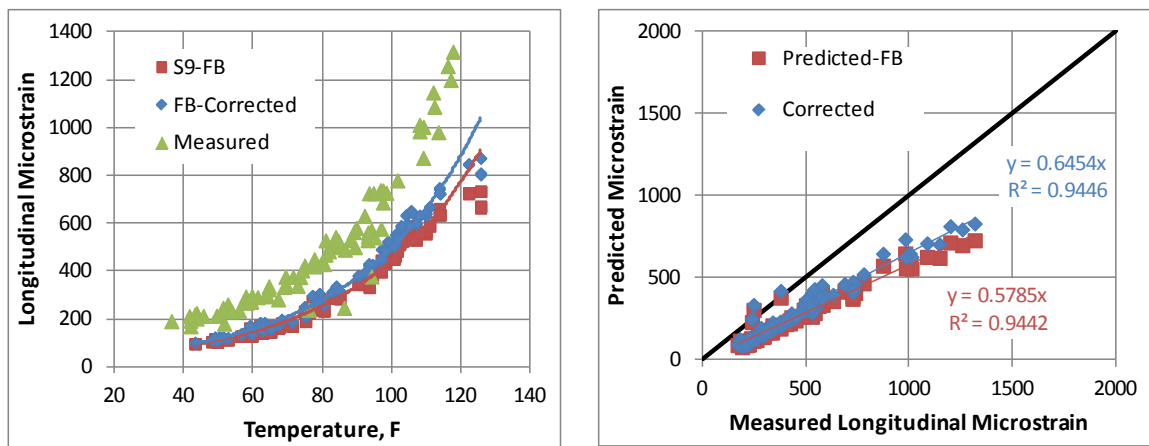


FIGURE 7.27 Example of the application of strain correction factors.

TABLE 7.13 Application of strain correction factors

Section	Slope	Slope corr.	% Change in Slope	AAE	AAE FB corr.	% Change in AAE
S9	0.578	0.645	11.7%	43.7%	38.9%	11.0%
S10	0.618	0.692	12.0%	35.5%	29.7%	16.4%
S11	0.692	0.769	11.1%	33.3%	27.9%	16.1%
S12	0.558	0.634	13.6%	43.1%	38.9%	9.6%
N5	0.583	0.664	13.9%	47.6%	42.0%	11.7%
N6	0.522	0.575	10.2%	52.0%	48.5%	6.7%
N7	0.492	0.560	13.9%	43.7%	42.0%	4.0%
N10	0.671	0.730	8.8%	40.0%	36.4%	9.0%
N11	0.661	0.759	14.8%	39.4%	32.8%	16.9%
ALL	0.577	0.647	12.2%	42.7%	38.1%	10.8%

Figure 7.28 shows an example of the application of correction factors on compressive stress. The curve of measured stress versus temperature was significantly above the curve of predicted microstrain using backcalculated AC moduli. This second curve was adjusted by correction factors providing a new curve closer to the measured one. The error between measured and predicted stresses was significantly higher (AAE = 18.2%) even for the corrected curve with an average difference of (15.8%). In this case, the errors were found to be greater at higher stresses due to the poor ability of the layer elastic analysis to predict the sensitivity of stresses as function of temperature (Tables 7.11 and 7.12). Table 7.14 shows the analyses performed to evaluate the effect of the base stress correction factors. On average, an AAE of 39.7% was obtained for all sections. Once the application factors were applied the error was reduced in 13.1%. The most affected section by the application of the correction factors was N11 which had the highest change in AAE (22.8%). However, N10 had the lowest error (AAE = 15.8%) after applying the respective correction.

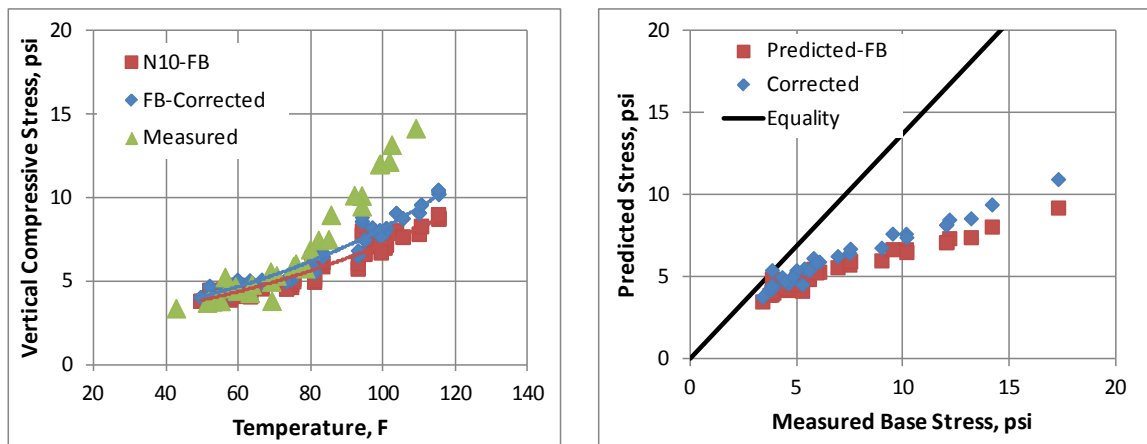


FIGURE 7.28 Example of the application of stress correction factors.

TABLE 7.14 Application of base stress correction factors

Section	AAE	AAE Corr.	% Change in AAE
S9	46.0%	40.2%	12.7%
S10	32.5%	31.4%	3.3%
S11	49.3%	42.6%	13.6%
S12	45.5%	37.3%	18.0%
N5	41.4%	34.7%	16.2%
N6	40.7%	35.9%	11.6%
N7	45.6%	40.9%	10.2%
N10	18.5%	15.8%	14.8%
N11	25.2%	19.5%	22.8%
ALL	39.7%	34.5%	13.1%

Table 7.15 shows the results of the analyses performed on the subgrade stress correction factors. On average, an AAE of 37.1% was obtained for all sections. Once the correction factors were applied the error was reduced by 12.4%. The most affected section by the application of the correction factors was N10 which had the highest change in AAE (29.4%) and the lowest error (AAE = 9.4%) after applying the respective correction.

TABLE 7.15 Application of subgrade stress correction factors

Section	AAE	AAE Corr.	% Change in AAE
S9	40.2%	37.0%	7.9%
S10	45.9%	42.3%	7.8%
S11	41.1%	35.8%	12.8%
S12	40.8%	34.3%	16.1%
N5	38.3%	32.0%	16.4%
N6	36.5%	32.5%	11.0%
N7	33.3%	30.0%	9.9%
N10	13.3%	9.4%	29.4%
N11	26.2%	20.8%	20.8%
ALL	37.1%	32.5%	12.4%

Overall, the use of correction factors helped reduce the gap between predicted and measured pavement responses. However, these factors were applied on structures that were

modeled with full bond layer interface. The development of correction factors and the prediction of pavement responses from non-destructive testing should be considered an intermediate condition between full bond and full slip. In addition, a viscoelastic analysis of asphalt concrete mixtures combined with nonlinearity properties of unbound material could show better agreement with measured tensile strains and compressive stresses. For instance, the ratio of the inflection point over the strain amplitude ranged from 10% to 60%. In the case of simulated strains at 45 mph (*3D-Move*) the same ratio was found between 11% and 22%, significantly lower than the measured results. This could be explained by the use of linear elastic properties (only option in *3D-Move*) for the base and subgrade materials.

Additional analysis of the effect of pavement instrumentation on pavement responses could also help explain these observed differences. Asphalt strain gauge installation procedures have typically used hot mix sieved through a 4.75mm screen, hand placed over the gauges and hand compacted prior to roller compaction which has led to a high gauge survival rate. However, this process introduces finer mix in the immediate vicinity of the gauge which could theoretically yield lower moduli and higher strains. It should also be noted that all of the pressure cells were installed in each respective layer within a bed of fine, uniformly graded material which protected the cells from puncture or other damage from the sharp, coarse fractured particles that compose the base layer. Because of the low density/low modulus bedding material, there is the possibility of higher pressures to be measured.

7.9 Summary

Significant differences in dynamic modulus can be expected between 10 and 33 Hz at any temperature. Moreover, these differences tend to increase with an increase in temperature. As suggested in the literature, dynamic moduli calculated at 33 Hz cannot match the backcalculated AC moduli. Hence, a significant error was expected from calculated pavement responses with respect to measured ones. This pattern was also confirmed by the comparison of load pulse

durations between FWD loading and a single axle load. For example, a truck driven at a speed of 41 mph had a load pulse duration about three times longer than the FWD loading. It was determined that the speed of a moving load that produces a loading pulse equivalent to the loading pulse produced by the FWD has to be over 120 mph for the studied conditions. Correction factors were then obtained as the difference between the calculated pavement response at the desired operational speed (in this study 45 mph) and the calculated pavement response at the equivalent FWD speed. An analysis of measured versus predicted pavement responses indicated and confirmed that significant errors can be obtained from using high speed/high frequency backcalculated moduli to predict highway speed pavement responses. Finally, the use of correction factors helped reduce the gap between predicted and measured pavement responses. However, these factors were applied on structures which in theory had full bond layer interface. The development of correction factors and the prediction of pavement responses from non-destructive testing should consider an intermediate condition between full bond and full slip.

CHAPTER EIGHT: CONCLUSIONS AND RECOMMENDATIONS

8.1 Summary of Findings

This dissertation investigated the use of advanced techniques to obtain pavement material properties from non-destructive testing. In the mechanistic-empirical (M-E) flexible pavement design framework, characterization of material properties is a key element to predict pavement responses and consequently remaining life of a pavement structure. To meet the objectives of this study, a literature review was first completed. This review was focused on current backcalculation techniques used for characterization of material properties and the use of Artificial Neural Networks (ANNs) for similar purposes. The effects of time and temperature dependency properties of asphalt concrete mixtures on pavement responses within a non-destructive testing prospective were also reviewed. The body of this investigation included two main studies related to advance material characterization techniques. The first one was focused on the application of ANNs as an alternative procedure to conventional backcalculation. The second one, also related to non-destructive testing, was focused on the correction of predicted responses from high frequency/speed load to represent typical operational vehicle speeds.

8.1.1 Application of ANNs

Artificial Neural Networks were created to perform forward calculations of pavement layer moduli and critical responses from non-destructive testing information. Synthetic databases were created using a modified version of the software PerRoad (LEA-based software) for a three layer flexible pavement. These databases included layer moduli, deflection basins, critical pavement responses and layer thicknesses.

An analysis of the conventional backcalculation process was performed to investigate the non-uniqueness of backcalculated results when setting different initial conditions. The software EVERCALC 5.0 was used to analyze the effect of the level of tolerance, calculated by means of the root mean square error (RMSE), on estimated pavement layer moduli. Three different levels

of tolerance: 0.1%, 1.0% and 3.0% were analyzed. The results indicated that the conventional backcalculation process used to estimate layer moduli can be considered sensitive to seed values such as setting the level of tolerance. The results also indicated that the backcalculation process tended to overestimate the modulus of the top layer (asphalt concrete layer) and underestimate the modulus of the granular base. On the other hand, even at a set tolerance level as high as 3.0% the results in terms of subgrade modulus were little or not affected.

The back-propagation algorithm was used as a learning algorithm to be applied on multilayer feed-forward networks. A synthetic database was generated using LEA for a three layered flexible pavement structure. Inputs for the ANN's were deflection basins, layer thicknesses and load. The targets were layer moduli and critical pavement responses. An additional dataset was used to test the accuracy of the ANN and the results were compared to the outcomes obtained using EVERCALC. The results indicated that ANN-predicted layer moduli can be equivalent to backcalculated parameters calculated at a level of tolerance as low as 0.1%. The results also suggest that the thickness of the asphalt concrete pavement could be estimated with an acceptable level of accuracy. In addition, obtaining the backcalculated moduli can be time consuming. The process can last from minutes to hours depending on the size of the dataset and the required level of tolerance. When using ANNs, obtaining the layer moduli would take only a few seconds, which can be very useful for agencies and researchers that may be dealing with relatively large data sets spanning years of testing.

Validation of the ANN models was performed using the Test Track FWD database and a selected section of the Lee Road 159 dataset. The capability for ANNs to predict pavement layer moduli was first validated on a very specific situation: pavement structures with similar thicknesses with multiple loads. In order to incorporate a typical range of thicknesses the ANN models had to be limited to one load of 9,000 lb due to the confounding interaction between thickness and load. In this case, the capability for ANNs to predict pavement layer moduli was also verified. Further implementation of ANN models was performed on a low volume roadway

section (Lee Road 159). Validation of ANN models was also achieved for this scenario. Overall, the use of ANNs showed a clear advantage over conventional backcalculation by providing layer moduli with significantly lower errors. In addition, the use of ANNs considering full slip condition between layers has proven to be another innovative attempt to create models capable of predicting more realistic layer moduli. Finally, exclusion of the thickness to predict pavement responses from ANN models did not seem viable up to this point. Further investigation was recommended to help explain the differences between results from synthetic and actual thickness.

8.1.2 Correction Factors for the High Frequency/High Speed FWD Pavement Responses to Typical Operating Speed Responses

The falling weight deflectometer (FWD) loading pulse duration was obtained from measured pavement response signals. FWD tests were performed on nine structural sections containing embedded instrumentation that were built in 2009 at the Test Track. These sections had well-characterized material properties (E^* from lab tests and backcalculated moduli for granular base and subgrade). The signal measured from a pressure plate was used to calculate the loading pulse. FWD stress and strain pulses followed a haversine waveform with distinguishable termination points. Stress pulses due to moving loads produced a waveform very similar to the pulse from FWD testing and therefore it was used in the analysis. The measured pulse ranged from 0.030 to 0.050 seconds and the measured mid-depth temperature during the FWD tests ranged from 75 to 120°F. Measured stress pulse durations from trucks moving at 45 mph were found to be two to three times greater than the measured FWD pulse durations at the same temperature.

The mechanistic analysis software *3D-Move* was used to model a single uniform moving load of 9000 lb with radius of 5.91 inches. The speed of that moving load that produces a loading pulse equivalent to the loading pulse produced by the FWD was determined to be over 120 mph. To find correction factors, a dual tire load of 10,000 lb (5,000 lb/tire) was also simulated using *3D-Move* to compute critical strain responses that were calculated at 6 different speeds (15, 25,

35, 45, 60 mph and at the equivalent FWD speed) and at 5 different temperatures (40, 70, 100, 115 and 130°F). Correction factors were calculated as the relative difference between the simulated responses from the Test Track operating speed of 45 mph and at simulated responses from the equivalent FWD speed. Finally, these factors were applied on simulated strain responses obtained from actual backcalculated moduli and compared to measured strain responses from the embedded instrumentation. The application of these correction factors helped close the observed gap between simulated and measured strain responses.

8.2 Conclusions

Based upon the research conducted in this dissertation, the following conclusions can be made concerning the application of ANNs used to characterize material properties.

1. The conventional backcalculation process used to estimate layer moduli can be considered sensitive to the level of tolerance. In the case of the asphalt concrete modulus and granular base modulus, a significant increase in variability can be expected when changing the level of tolerance from 0.1% to 1.0% and from 1.0% to 3.0%.
2. Contrary to backcalculation, ANNs do not depend on seed values and the ANN-predicted layer moduli can be equivalent to backcalculated parameters calculated at an RMSE level of tolerance as low as 0.1%.
3. Based on the use of synthetic databases, the layer moduli and pavement responses can still be estimated with the application of ANN when only deflections are used as inputs (no layer thicknesses are input). However, more scattered results with higher relative errors can be expected for this type of analysis.
4. Significant differences can be obtained between actual and predicted layer moduli when the actual condition of the asphalt layer interface(s) is full slip and the simulated conditions are full bond between layers.

5. The capability for ANNs to predict pavement layer moduli was validated using multiple load levels and full slip condition as a layer interaction. This presented a clear advantage over previous studies that have been focused on one load level and full bond conditions.
6. The use of ANNs considering full slip condition has proven to be another innovative attempt to create models capable of predicting more realistic layer moduli, especially for the granular base.
7. Overall, the use of ANNs presented a clear advantage over conventional backcalculation. While backcalculated properties can be obtained from a couple of minutes to an hour, with ANN the same results are always obtained in a couple of seconds. In addition, a significant reduction in the root mean square error can be expected when using ANNs compared to backcalculation.

Based upon the research conducted in this dissertation, the following conclusions can be made concerning the use of correction factors for the high frequency/high speed FWD pavement responses to typical operating speed responses

1. Significant differences between moduli at 33Hz and 10Hz mean significant differences in pavement responses between FWD and highway speeds. Moreover, these differences tend to increase with an increase in temperature.
2. Significant differences between load pulse duration from FWD and a single axle load of truck traveling at 45 mph were obtained. Single axle load pulse durations were three times longer than the FWD durations.
3. It was determined that the speed of a moving load that produces a loading pulse equivalent to the loading pulse produced by the FWD has to be over a 120 mph for the studied conditions.
4. An analysis of measured versus predicted pavement responses indicated and confirmed that significant errors can be obtained from using high speed/high frequency backcalculated moduli to predict highway speed pavement responses. Therefore, correction factors should be

- applied on pavement responses from backcalculated moduli to represent highway speed loads.
5. For the conditions and scenarios evaluated in this study, correction factors helped close the gap between measured and predicted pavement responses.

8.3 Recommendations

Layered-elastic properties of the different layers of flexible pavements are obtained using conventional backcalculation. Layered-elastic properties were also utilized in this study to generate and train ANNs. In reality, material properties are more complex and may require the application of more complex algorithms such as finite element analysis that can be time consuming. Future investigation should be able to incorporate more complex properties (non-linear properties of unbound materials and viscoelastic properties of asphaltic materials) to create new and even more advanced ANNs.

It is recommended that more research be conducted in developing correction factors to account for the significant difference between FWD loading and traffic loading. The correction factors developed were based upon limited data (nine sections with similar thicknesses); therefore, they should be provisionally implemented until further research validates their accuracy.

The exclusion of the thickness to predict pavement responses from ANN models did not seem viable up to this point. Further investigation is recommended to help explain the differences between results from synthetic (theory) and actual (field) data.

Further research should be conducted to help explain the differences between measured and predicted pavement responses of the studied sections. A viscoelastic analysis of asphalt concrete mixtures combined with nonlinearity properties of unbound material could show better agreement with measured tensile strains and compressive stresses.

REFERENCES

1. Meier, R. W., and G. J. Rix. "Backcalculation of Flexible Pavement Moduli Using Artificial Neural Networks". In Transportation Research Record 1448, TRB, National Research Council, Washington, D.C., 1995, pp. 75–82.
2. Meier, R., Alexander, D., and Freeman, R. "Using Artificial Neural Networks as a Forward Approach to Backcalculation." Transportation Research Record, Washington, D.C., 1997. 1570, pp. 126-133.
3. Ferregut C., Abdallah I, Melchor O, and Nazarian S., "Artificial Neural Network-Based Methodologies for Rational Assessment of Remaining Life of Existing Pavements". Center for Highway Materials Research, The University of Texas at El Paso. Texas Department of Transportation, April 1999.
4. Eres Consultants Division. "Guide for Mechanistic-Empirical Pavement Design of New and Rehabilitated Pavement Structures; Appendix CC-3, Updated Traffic Frequency Calculation for Asphalt Layers", Final Document, NCHRP 1-37A, 2003.
5. Winters, B.C., "The PACCAR Pavement Test Section - Instrumentation and Validation," Master's thesis, Department of Civil Engineering, University of Washington, Seattle, Washington, March 1993.
6. Priddy K.L., Keller. P. E., "Artificial neural networks: an introduction". SPIE-The International Society of Photo-Optical Instrumentation Engineer. Washington, 2005.
7. Asphalt Research Consortium webpage. <http://www.arc.unr.edu/Software.html>. Date Accessed 03-20-2011.
8. Siddharthan, R.V., Krishnamenon, N., and Sebaaly, P.E., "Pavement Response Evaluation using Finite-Layer Approach," Transportation Research Record No. 1709, TRB, 2000, pp. 43-49.
9. Shahin, M.Y., "Pavement Management for Airport, Roads and Parking Lots", New York, Chapman & Hall, 1994.

10. "8000 FWD Test System; Owners' manual, version 1.7, Dynatest, Denmark, 2002.
11. Huang, Y.H. "Pavement Analysis and Design". 1st Ed., Prentice Hall, Upper River Saddle, N.J., 1993.
12. Ulliditz, P., and Stubstad, R. N., "Analytical-Empirical Evaluation Using the Falling Weight Deflectometer." Transportation Research Board, TRB, ed., Washington, D.C. 1985.
13. Pavement Tools Consortium. "Pavement Interactive Guide: Pavement Evaluation". <http://training.ce.washington.edu/PGI/>. Date accessed: January, 10th 2011.
14. Everseries User's Guide. "Pavement Analysis Computer Software and Case Studies", Washington State Department of Transportation, Olympia, Washington. 2005.
15. Ulliditz, P., "Modelling Flexible Pavement Response and Performance", Technical University of Denmark, Polyteknisk Forlag.
16. Romanoschi S.A. and Metcalf J.B., "Errors in Pavement Layer Moduli Backcalculation due to Improper Modeling of the Layer Interface Condition". Proceedings, Transportation Research Board, TRB 2003 Annual Meeting CD-ROM.
17. Lenngren C. A., Olsson J., "Enhanced Backcalculation Techniques for Assessing Highway Structural Properties", International Symposium (NDT-CE 2003) Non-Destructive Testing in Civil Engineering, 2003.
18. Ceylan, H., Guclu, A., Tutumluer, E., and Thompson, M. R., "Backcalculation of fulldepth asphalt pavement layer moduli considering nonlinear stress-dependent subgrade behavior," The International Journal of Pavement Engineering, Vol. 6, No. 3, pp. 171-182.
19. Tutumluer E., Pekcan O. and Ghaboussi J., "Nondestructive Pavement Evaluation Using Finite Element Analysis Based Soft Computing Models". USDOT Region V Regional University Transportation Center Final Report. NEXTRANS Project No 010IY01. October, 2009.

20. Gopalakrishnan, K., and Thompson, M.R., "Characterization of NAPTF subgrade soils for mechanistic-based analysis and design of airport flexible pavements." *International Journal of Pavement Engineering*, 8(4), 2007, pp. 307-321.
21. Lawrence J., "Introduction to Neural Networks - Design, Theory and Applications". California Scientific Software Press, Nevada City. 1993.
22. Chatti, K, Kim, TK., "Effect of Frequency-dependent Asphalt Concrete Layer Moduli on Pavement Response". Symposium on Nondestructive Testing of Pavements and Backcalculation of Moduli: Third Volume. American Society for Testing and Materials. Seattle, Washington, 1999.
23. Hoffman, M. S., and Thompson, M. R., "Comparative Study of Selected Nondestructive Testing Devices," Record 852, Transportation Research Board, 1982, pp. 32-41.
24. Jianfeng Q., "Predicting Flexible Pavement Structural Response Using Falling Weight Deflectometer Deflections". M.S. Thesis. Ohio University, Ohio. June, 2010.
25. Siddharthan, R.V., Krishnamenon, N., El-Mously, M., and Sebaaly, P.E., "Investigation of Tire Contact Stress Distributions on Pavement Response," *Journal of Transportation Engineering*, ASCE, Vol. 128(2), March/April, 2002, pp. 136-144.
26. Siddharthan, R.V., El-Mously, M., Krishnamenon, N., and Sebaaly, P.E., "Validation of a Pavement Response Model using Full-Scale Field Tests," *International Journal in Pavement Engineering*, Vol. 3(2), 2002, pp. 85-93.
27. Siddharthan, R.V., Yao J. and Sebaaly, P.E., "Field Verification of Moving Load Model for Pavement Response". Transportation Research Record No. 1540, TRR, 1998, pp. 125-131.
28. Kim J.," General Viscoelastic Solutions for Multilayered Systems Subjected to Static and Moving Loads", *Journal of Materials in Civil Engineering / Volume 23 / Issue 7* , 2010.
29. Elseifi, M. A., Al-Qadi, I. L., Loulizi, A., "Viscoelastic Modeling and Field Validation of Flexible Pavements *Journal of Engineering Mechanics*", ASCE. February 2006.

30. Thompson, M. R., S. H. Carpenter, B. J. Dempsey, and R. B. Elliot. "Independent Review of the Recommended Mechanistic–Empirical Design Guide and Software". NCHRP Project 1-40A. Transportation Research Board of the National Academies, Washington, D.C., 2006.
31. Al-Qadi I. L., Elseifi M. A., Yoo P. J., Dessouky S. H., Gibson N., Harman T., D'Angelo J., Petros K., "Accuracy of Current Complex Modulus Selection Procedure from Vehicular Load Pulse: NCHRP Project 1-37A Mechanistic-Empirical Pavement Design Guide". Transportation Research Record: Journal of the Transportation Research Board. Volume 2087, 2009.
32. Jacobs, M. M. J., P. C. Hopman, and A. A. A. Molenaar. "Application of Fracture Mechanics Principles to Analyze Cracking in Asphalt Concrete". Journal of the Association of Asphalt Paving Technologists, Vol. 65, 1996, pp. 1–28.
33. Kim, Y. R., and Y. C. Lee. "Interrelationships Among Stiffnesses of Asphalt–Aggregate Mixtures". Journal of the Association of Asphalt Paving Technologists, Vol. 64, 1995, pp. 575–600.
34. Bonaquist, R. F., W. Stump III, and D. W. Christensen. "NCHRP Report 513: Simple Performance Tester for Superpave Mix Design: First- Article Development and Evaluation". Transportation Research Board of the National Academies, Washington, D.C., 2003.
35. Witczak, M. W., K. Kaloush, T. Peillinen, M. El-Basyouny, and H. Von Quintus. "NCHRP Report 465: Simple Performance Test for Superpave Mix Design". Transportation Research Board of the National Academies, Washington, D.C., 2002.
36. Loulizi, A., I.L. Al-Qadi, S. Lahouar, and T.E. Freeman. "Measurement of Vertical Compressive Stress Pulse in Flexible Pavements: Representation for Dynamic Loading Tests". In Transportation Research Record: Journal of the Transportation Research Board No. 1816, TRB, National Research Council, Washington D.C., 2002, pp 125-136.

37. Garcia, G., and M.R. Thompson. "Strain and Pulse Duration Considerations for Extended Hot Mix Asphalt Pavement Design". Proceedings of the 87th Annual Meeting of the Transportation Research Board, Washington, D.C., 2008.
38. Robbins, M.M., "An Investigation Into Dynamic Modulus Of Hot-Mix Asphalt And Its Contributing Factors". M.S. Thesis. Auburn University. Auburn, AL. May, 2009.
39. MathWorks, Inc., "Neural Networks Toolbox™ 2 User's Guide". Natick, MA, 2010.
40. Brown, E., L. Cooley, D. Hanson, C. Lynn, B. Powell, B. Prowell, and D. Watson. "NCAT Test Track Design, Construction, and Performance," NCAT Report 2002-12. National Center for Asphalt Technology, Auburn University, 2002.
41. <http://www.warmmixasphalt.com/WmaTechnologies.aspx>
42. Timm, D. H. "Design, Construction and Instrumentation of the 2006 Test Track Structural Study". Draft report. National Center for Asphalt Technology, Auburn University, Ala., 2008.
43. Timm, D. H., A. L. Priest, and T. V. McEwen. "Design and Instrumentation of the Structural Pavement Experiment at the NCAT Test Track". Report No. 04-01. National Center for Asphalt Technology, Auburn University, Ala., 2004.
44. Timm, D., "Design, Construction and Instrumentation of the 2006 Test Track Structural Study". National Center for Asphalt Technology: NCAT Report 09-01, February 2009.
45. ASTM D4694.96, Standard Test Method for Deflections with a Falling Weight Type Impulse Load Device, Annual Book of ASTM Standards 2005, Vol. 04.03, West Conshohocken, Pa., 2005.
46. Schmalzer, P. "Long-Term Pavement Performance Program Manual for Falling Weight Deflectometer Measurements", Version 4.1, Federal Highway Administration, McLean, Va. 2006.
47. Bush, A.J. and D.R. Alexander. "Pavement Evaluation Using Deflection Basin Measurements and Layered Theory." Transportation Research Record: Journal of the Transportation

- Research Board No. 1022. TRB, National Research Council, Washington D.C., 1985. pp. 16-28.
48. Parker, F. "Estimation of Paving Materials Design Moduli from Falling Weight Deflectometer Measurements." *Transportation Research Record: Journal of the Transportation Research Board*, No. 1293: TRB, National Research Council, Washington, D.C., 1991, pp. 42-51.
49. Irwin, L.H. "Backcalculation: An Overview and Perspective." *Proceedings of the Pavement Evaluation Conference*. Roanoke, VA. 2002.
50. Timm D., R. West, A. Priest, B. Powell, I. Selvaraj, J. Zhang, and R. Brown. "Phase II NCAT Test Track Results". NCAT Report 06-05, National Center for Asphalt Technology, Auburn University, 2006.
51. Willis R., D. Timm, R. West, B. Powell, M. Robbins, A. Taylor, A. Smit, N. Tran, M. Heitzman and A. Bianchini. "Phase III NCAT Test Track Findings". NCAT Report 09-08, National Center for Asphalt Technology, Auburn University, 2009.
52. Taylor A. and Timm, D.H., "Mechanistic Characterization of Resilient Moduli of Unbonded Pavement Layer Materials". Report No. 09-06, National Center for Asphalt Technology: Auburn University, 2009.
53. AASHTO TP 79. "Standard Method of Test for Determining the Dynamic Modulus and Flow Number for Hot Mix Asphalt (HMA) Using the Asphalt Mixture Performance Tester (AMPT)". American Association of State Highway Transportation Officials, 2009.
54. Lu, Q., Ullidtz, P., Basheer, I., Ghuzlan, K., and Signore, J.M. CalBack: Enhancing Caltrans Mechanistic-Empirical Pavement Design Process with New Back-Calculation Software. *Journal of Transportation Engineering*, Vol. 135, No.7, 2009, pp. 479-488.

55. Ullidtz, P. Modeling Flexible Pavement Response and Performance. Narayana Press, Odder, Denmark, 1998, pp. 38-43.
56. Robbins, M.M. and D.H. Timm, "Temperature and Velocity Effects on a Flexible Perpetual Pavement," 3rd International Conference on Accelerated Pavement Testing, Madrid, Spain, 2008.
57. Ellison, A. and D. Timm, "Speed and Temperature Effects on Full-Scale Pavement Responses in Non-Conventional Flexible Pavements ," Proceedings, T&DI Congress 2011: Integrated Transportation and Development for a Better Tomorrow, Proceedings of the First T&DI Congress 2011, American Society of Civil Engineers, Chicago, IL, 2011, pp. 824-833.
58. Priest, A.L. and D. Timm "Methodology and Calibration of Fatigue Transfer Functions for Mechanistic-Empirical Flexible Pavement Design," NCAT Report 06-03, National Center for Asphalt Technology, Auburn University, 2006.
59. Willis, J.R., Timm D.H., "Field-Based Strain Thresholds for Flexible Perpetual Pavement Design," Report No. 09-08, National Center for Asphalt Technology, Auburn University, 2009.